Rochester Institute of Technology
RIT Scholar Works

2009

Propellant tank pressurization modeling for a hybrid rocket

Margaret Mary Fernandez

Follow this and additional works at: http://scholarworks.rit.edu/theses

Propellant Tank Pressurization Modeling for a Hybrid Rocket

by

Margaret Mary Fernandez

A thesis submitted in partial fulfillment of the requirements for the

Master of Science
in
Mechanical Engineering.

Approved by:

Dr. Steven Weinstein
Department of Chemical Engineering
Thesis Advisor

_____

Dr. Amitabha Ghosh
Department of Mechanical Engineering
Thesis Committee

_____

Dr. Satish Kandlikar
Department of Mechanical Engineering
Thesis Committee

_____

Dr. Edward Hensel
Department of Mechanical Engineering
Department Representative

_____

Gregory G. Zilliac
NASA Ames Research Center – Moffet Field, CA
NASA Guest Member

Department of Mechanical Engineering
Kate Gleason College of Engineering

Rochester Institute of Technology
Rochester, NY 14623

August 2009

Permission for Thesis Reproduction

I, Margaret Mary Fernandez, hereby grant permission to the Wallace Memorial Library of the Rochester Institute of Technology to reproduce my thesis entitled *Propellant Tank Pressurization Modeling for a Hybrid Rocket* in whole or in part. Any reproduction will not be for commercial use or profit.

_____   _____

Margaret Mary Fernandez   August 21, 2009

ABSTRACT

Hybrid rockets are currently being examined as a simpler and safer alternative to solid and liquid rocket propulsion. A basic hybrid rocket oxidizer delivery system utilizes the self-pressurizing nature of a liquid oxidizer at ambient temperatures in conjunction with a non-condensable pressurant to provide a high oxidizer tank pressure that drives liquid oxidizer flow to the combustion chamber. In this study, the oxidizer fluid is nitrous oxide since it produces high vapor pressures at ambient temperatures, and helium is the pressurant. The goal of this thesis is to model the pressure draining history of the oxidizer tank to within ± 5% accuracy.

Previous studies of the self-pressurization processes in a propellant tank have focused on long-term cryogenic storage applications where the primary concern is heat leaking into the tank, causing unwanted pressure increases that result in propellant loss through necessary venting. Results of these cryogenic studies have been used to justify the inclusion of heat and mass transfer resistances in propellant tank models in order to be sufficiently accurate. However, these cryogenic studies were performed under conditions of very low vapor pressures and temperatures, and it is not clear that the conclusions drawn from such studies are valid for self-pressurization under ambient temperature conditions. Thus, the validity of simpler thermodynamically-based models has not been considered for self-pressurizing, draining tanks under high pressure conditions.

In this study, two models are developed, both assuming thermodynamic equilibrium states at every point in time throughout draining. The first model assumes the P-V-T behavior of the nitrous oxide/helium mixture follows the ideal gas law; the second model assumes that the mixture adheres to the non-ideal Peng-Robinson equation-of-state. Both models are compared to experimental data from pure nitrous oxide draining tests, published in G. Zilliac & M. Karabeyoglu (*Modeling of Propellant Tank Pressurization*, AIAA 2005-3549, 41st AIAA/ASME/ASEE Joint Propulsion Conference). Sensitivity studies have been performed in order to determine the effect of experimental error on the time-dependent flow from the tank and to assess the behavior of the models near physical extremes, such as high or low initial nitrous oxide fill-levels. Theoretical draining histories for the Peregrine hybrid sounding rocket (a joint effort between NASA Ames Research Center and Stanford

University), soon to be launched from NASA Wallops Flight Facility, have also been examined.

A variety of comparisons with available experimental data, theoretical sensitivity studies, and theoretical launch data demonstrates that the non-ideal draining model provides favorable agreement. The additional complexity introduced by a non-ideal equation-of-state is necessary due to the high pressures encountered in the tank during draining. Sensitivity studies reveal that small deviations in the initial temperature, initial fill-level, or the discharge coefficient can produce nearly 5% errors in liquid drain time, demonstrating the need for accurately measured model inputs and suggesting sources of error in experimental design. It is found that despite the highly nonlinear nature of the draining process, the liquid flow rate from the tank remains reasonably constant, which is a highly desirable characteristic of a rocket oxidizer delivery system. The study provides a proposal for a new set of experiments necessary to assess and refine the theoretical models to allow for design and scale-up of hybrid rocket oxidizer delivery systems.

to Todd, Mom, and Katie

<u>ACKNOWLEDGMENTS</u>

TABLE OF CONTENTS

Appendices

LIST OF FIGURES

LIST OF TABLES

NOMENCLATURE

$A_{injector}$ = total injector area $\left[m^2 \right]$

C_D = discharge coefficient $\left[-- \right]$

$\overline{C}_{P_T}$ = specific heat capacity at constant pressure of the oxidizer tank $\left[\dfrac{J}{kg \cdot K} \right]$

$\hat{C}_{P_{1g}}^*$ = ideal molar heat capacity at constant pressure of pressurant gas $\left[\dfrac{J}{kmol \cdot K} \right]$

$\hat{C}_{P_{2l}}^*$ = ideal molar heat capacity at constant pressure of oxidizer liquid $\left[\dfrac{J}{kmol \cdot K} \right]$

$\hat{C}_{P_{2v}}^*$ = ideal molar heat capacity at constant pressure of oxidizer vapor $\left[\dfrac{J}{kmol \cdot K} \right]$

$\hat{C}_{V_{1O}}$ = molar heat capacity at constant volume of pressurant gas $\left[\dfrac{J}{kmol \cdot K} \right]$

$\hat{C}_{V_{2l}}$ = molar heat capacity at constant volume of oxidizer liquid $\left[\dfrac{J}{kmol \cdot K} \right]$

$\hat{C}_{V_{2v}}$ = molar heat capacity at constant volume of oxidizer vapor $\left[\dfrac{J}{kmol \cdot K} \right]$

$\hat{H}_g$ = molar enthalpy of gaseous oxidizer and pressurant mixture $\left[\dfrac{J}{kmol} \right]$

$\hat{H}_{g,excess}$ = excess molar enthalpy of gaseous oxidizer and pressurant mixture $\left[\dfrac{J}{kmol} \right]$

$\overline{H}_T$ = specific enthalpy of oxidizer tank $\left[\dfrac{J}{kg} \right]$

$\hat{H}_{1g}^*$ = ideal molar enthalpy of pressurant gas $\left[\dfrac{J}{kmol} \right]$

$\hat{H}_{2l}$ = molar enthalpy of oxidizer liquid $\left[\dfrac{J}{kmol} \right]$

$\hat{H}_{2l}^*$ = ideal molar enthalpy of oxidizer liquid $\left[\dfrac{J}{kmol} \right]$

$\hat{H}_{2l,excess}$ = excess molar enthalpy of oxidizer liquid $\left[\dfrac{J}{kmol}\right]$

$\hat{H}_{2v}$ = molar enthalpy of oxidizer vapor $\left[\dfrac{J}{kmol}\right]$

$\hat{H}_{2v}^{*}$ = ideal molar enthalpy of oxidizer vapor $\left[\dfrac{J}{kmol}\right]$

m_T = oxidizer tank mass $[kg]$

$(MW)_2$ = molecular weight of oxidizer $\left[\dfrac{kg}{kmol}\right]$

n_g = moles of gas phase oxidizer and pressurant mixture $[kmol]$

n_{1_o} = moles of pressurant gas $[kmol]$

$\dot{n}_{2,drain}$ = molar flow rate of oxidizer liquid out of tank exit $\left[\dfrac{kmol}{s}\right]$

$\dot{n}_{2,evap}$ = molar flow rate of oxidizer liquid into gas due to evaporation $\left[\dfrac{kmol}{s}\right]$

n_{2l} = moles of oxidizer liquid $[kmol]$

n_{2l_o} = initial moles of oxidizer liquid prior to drain $[kmol]$

n_{2T} = total moles of nitrous oxide loaded into tank prior to drain $[kmol]$

n_{2v} = moles of oxidizer vapor $[kmol]$

n_{2v_o} = initial moles of oxidizer vapor prior to drain $[kmol]$

P = total pressure in tank $[Pa]$

P_C = critical pressure $[Pa]$

P_e = exit pressure (combustion chamber pressure) $[Pa]$

P_2^{*} = vapor pressure of oxidizer at a given temperature $[Pa]$

$\dot{Q}_g$ = heat transferred from gas phase to liquid phase through interface $\left[\dfrac{J}{s}\right]$

$\dot{Q}_{2l}$ $\quad=$ heat transferred from liquid phase to gas phase through interface $\left[\dfrac{J}{s}\right]$

R $\quad=$ universal gas constant $\left[\dfrac{J}{kmol \cdot K}\right]$

T $\quad=$ temperature in tank $[K]$

t $\quad=$ time $[s]$

T_C $\quad=$ critical temperature $[K]$

T_o $\quad=$ initial temperature in tank prior to drain $[K]$

$\hat{U}_g$ $\quad=$ molar internal energy of gas phase oxidizer and pressurant mixture $\left[\dfrac{J}{kmol}\right]$

$\overline{U}_T$ $\quad=$ specific internal energy of oxidizer tank $\left[\dfrac{J}{kg}\right]$

$\hat{U}_{1o}$ $\quad=$ molar internal energy of pressurant gas $\left[\dfrac{J}{kmol}\right]$

$\hat{U}_{2l}$ $\quad=$ molar internal energy of oxidizer liquid $\left[\dfrac{J}{kmol}\right]$

$\hat{U}_{2v}$ $\quad=$ molar internal energy of oxidizer vapor $\left[\dfrac{J}{kmol}\right]$

V $\quad=$ oxidizer tank volume $[m^3]$

V_g $\quad=$ gas phase volume $[m^3]$

V_l $\quad=$ liquid phase volume $[m^3]$

$\hat{V}_g$ $\quad=$ molar volume of gas phase $\left[\dfrac{m^3}{kmol}\right]$

$\hat{V}_{2l}$ $\quad=$ molar volume of oxidizer liquid $\left[\dfrac{m^3}{kmol}\right]$

$\hat{V}_{2v}$ $\quad=$ molar volume of oxidizer vapor $\left[\dfrac{m^3}{kmol}\right]$

ω $\quad=$ acentric factor $[--]$

y_2 = mole fraction of oxidizer in gas phase $[--]$

Z_g = compressibility of oxidizer and pressurant gas mixture $[--]$

Z_{2l} = compressibility of oxidizer liquid $[--]$

$\Delta \hat{H}_{2v}$ = molar heat of vaporization of oxidizer $\left[\dfrac{J}{kmol} \right]$

ϕ_{2l} = fugacity coefficient of oxidizer liquid $[--]$

ϕ_{2v} = fugacity coefficient of oxidizer and pressurant gas mixture $[--]$

CHAPTER 1

BACKGROUND AND GOAL OF THE THESIS

Hybrid rocket propulsion systems (referred to as "hybrids" throughout this thesis) are generally viewed as promising alternatives to conventional rockets, but their use has not been fully accepted. Hybrids show potential because they are capable of producing a comparable thrust to both liquid and solid rocket engines. Yet, they are safer than solid rockets because the oxidizer and fuel are not intimately mixed and, moreover, cannot mix since they are in different phases; this eliminates the danger of unintended ignition. Hybrids often utilize a self-pressurizing propellant delivery system in which the liquid oxidizer in a storage tank vaporizes at ambient temperatures, generating high pressures that drive liquid flow to the combustion chamber. Nitrous oxide is a particularly sensible oxidizer in such a delivery system because its critical temperature is so close to ambient temperatures. This greatly simplifies the rocket design since complex pumps and plumbing are not required in the delivery system. By contrast, liquid rockets typically utilize cryogenic oxidizers and fuels requiring sophisticated cooling systems and more complex plumbing. Like liquid rockets, hybrid rockets can be throttled, providing an element of precise combustion control.
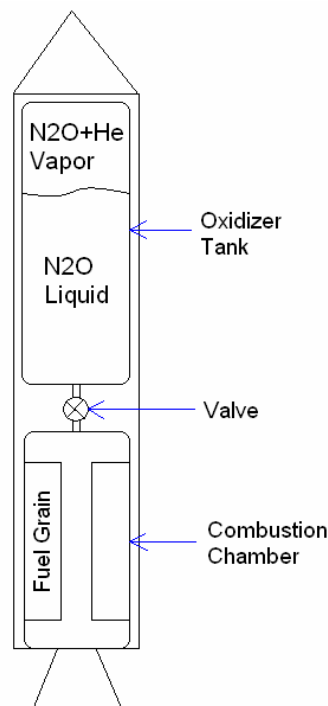
Figure 1.1: Hybrid Rocket with Basic Propellant Delivery System

Hybrids are on the verge of widespread use for rocket propulsion. However, the technology has not yet proven itself as being suitable for use in critical manned and unmanned missions carried out by NASA. Currently, Ames Research Center (NASA Ames) and Stanford University are jointly conducting research on hybrid performance in order to assess its candidacy for use as a sounding rocket. Wallops Flight Facility (NASA Wallops, part of NASA Goddard Space Flight Center) is a launch facility that has an active sounding rocket program and is interested in using new hybrid technology if it proves to be as effective as its current solid stage sounding rockets. Currently, a large-scale hybrid sounding rocket called Peregrine is being developed by NASA Ames and Stanford to be launched from NASA Wallops. The work presented in this thesis has been supported jointly by NASA Ames and NASA Wallops; it is a further attempt to assess hybrid rocket potential for use in NASA missions.

One of the main difficulties in designing hybrid rockets is the lack of predictive models for hybrid performance that have been published compared with those for solid and liquid rockets. Such models would be useful in interpreting experimental data, designing further experiments, and scaling-up or modifying rocket designs in new geometries. When a pressure-fed propellant delivery system is used, hybrid combustion performance is dependent on the pressure of the oxidizer tank. Hybrids often use a volatile (i.e., "self-pressurizing") oxidizer such as nitrous oxide in conjunction with a non-condensable pressurant such as helium. Inside the oxidizer tank, liquid oxidizer and vaporized oxidizer maintain the pressure in the tank. The internal energy, and thus the temperature, of the tank decreases as liquid oxidizer drains since energy exits the tank with the flow. Additionally, some of the liquid in the tank evaporates, maintaining a high pressure in the tank. However, the strong dependence of vapor pressure on temperature yields tank pressures that decrease with time. One of the goals of this study is to examine how this pressure variation affects the oxidizer flow rate out of the tank. If the oxidizer flow varies appreciably, then the rate of combustion and resulting thrust generated downstream will vary substantially. Significant flow rate variations would make self-pressurizing delivery prohibitive without additional control systems to compensate, diminishing the intended simplicity of the original system.

While the main focus of the research at NASA Ames and Stanford University is the combustion behavior in hybrid rockets, they have also modeled the oxidizer tank

pressurization process and draining. Part of this work has been published by Zilliac and Karabeyoglu (2005) and is the starting point for this thesis. One of the key deficiencies of this prior model is a large, semi-empirically determined parameter required for the theory to agree with experiment. Furthermore, relatively complex physics has been incorporated into the model, but the underlying justification for this sophistication has not been systematically examined. Thus, this model may not be able to extrapolate beyond existing designs.

The goal of this work is to produce an improved model that is accurate enough for engineering design and scale-up. The desired accuracy requested by G. Zilliac, a collaborator on this study, is to model the tank pressure draining history to within $\pm$ 5%. Two models of the oxidizer tank pressurization processes are developed, one based on the ideal gas law and associated equilibrium assumptions, and the second utilizing a non-ideal equation-of-state with appropriate equilibrium complexity. The latter model is motivated by the high pressures in the tank which likely invalidate the ideal assumptions of the first model. The assumptions used in building these models are clearly stated and can thus be critically assessed. The model inputs are material parameters that are tabulated and/or correlated in engineering handbooks; there are no free parameters requiring empirical fitting. The models developed in this work are compared with experiments provided by NASA Ames. The results of this comparison, an assessment of the viability of self-pressurized tank delivery, and a discussion of future work motivated by this study are provided.

CHAPTER 2

LITERATURE REVIEW

2-1   Overview

       The physical configuration of the pressure-driven propellant delivery system considered in this thesis is a tank filled with high-pressure oxidizer and a non-condensable pressurant that drains through a feedline to a combustion chamber at a lower pressure. As will be seen in Chapter 3, this thesis contains two models, both of which assume thermodynamic equilibrium states (pressure and temperature are uniform everywhere) at each instant in time as the oxidizer tank drains. This type of model, as well as any model in the cited literature that uses this assumption, will be referred to as an equilibrium model; note that previous literature also refers to such models as "homogeneous" or "thermodynamic" models. Equilibrium models are commonly found in literature published in the 1960s, likely due to the limitations on computational power that the differential forms of the conservation equations and CFD-based models require. However, the mathematical simplicity of equilibrium models still makes them attractive to researchers today, as evidenced by locating these models in more recent literature. Many previous models have incorporated heat and mass transfer resistances, but the motivation for this increased complexity has not been well-established for the hybrid configuration focused on in this work.

       The equilibrium assumption used in the current work is not intended to represent the precise physical state of the oxidizer tank contents; heat and mass transfer gradients are always present in real physical systems during self-pressurization. However, it is believed that the draining behavior of the tank may be modeled accurately enough by a simple equilibrium model. In addition, it is worthwhile to consider a simple model, validate or disprove it, and then continue to add complexity until the desired degree of agreement between theory and experiment is achieved. A more complex model may not be needed to achieve the desired accuracy. Additionally, lack of agreement between theory and experiment can provide insight to the legitimacy of the set of assumptions used in the simple model should a deviation be unacceptable.

2-2   Literature Relevant to Current Study

The pressurization behavior of rocket oxidizers and fuels has been well-studied and documented in the literature. In fact, the vast majority of the literature cited in this chapter is connected with NASA and its space programs.

Equilibrium models have been moderately utilized in previous literature. Eleven of the twelve references found containing an equilibrium model state that their purpose was *not* to model the physical state of the system (Abdalla, Frysinger, & Andracchio, 1965; Aydelott, 1967a; Aydelott, 1967b; Aydelott & Spuckler, 1969; Barsi & Kassemi, 2007; Barsi, Kassemi, Panzarella, & Alexander, 2005; Hasan, Lin, & Van Dresar, 1991; Liebenberg & Edeskuty, 1965; Otto, 1966; Panzarella & Kassemi, 2003; Van Dresar, Lin, & Hasan, 1992). Rather, equilibrium models were used as a limiting case, often in conjunction with one or two other bounding models. For example, many of the 1960s references cited above use an equilibrium model and a "surface-evaporation" model to bound the measured behavior of the system. The equilibrium model provides the lower limit on the rate of pressure-rise in a *closed* fuel tank for a given heat flux input. The surface evaporation model, used as the upper limit, assumes that all the heat absorbed is used to evaporate liquid to maintain the vapor at the saturation temperature corresponding to the final system pressure; the liquid phase temperature remains constant at the initial saturation temperature corresponding to the initial tank pressure. Liebenberg & Edeskuty (1965) and Otto (1966) include a similar upper limiting case in addition to an equilibrium model, where all the energy is absorbed by the vapor only with no mass transfer between the phases. In fact, it is stated explicitly by Aydelott (1967a,b) that an equilibrium model cannot correctly predict the rate of pressure rise in a closed liquid hydrogen system with heat input because the temperature of the vapor phase increases at a faster rate than the liquid phase. The references cited above that were published after the 1960s compare their experimental or other computational results to an equilibrium model only, illustrating the effects of thermal stratification on the pressure history of the tank contents for a given heat flux. In the above-cited literature, several different variables were studied, including the effects of normal- and zero-gravity, heat flux, tank size, tank geometry, fill level, mixing, and heating configuration (top heating, bottom heating, or uniform heating), for a *closed* liquid hydrogen tank with a given heat flux into the tank.

Some general findings regarding these equilibrium models include the following. Note that these equilibrium models use tabulated or correlated properties that have been published, not properties predicted by non-ideal equations-of-state (Sandler, 2006) such as what is used in this work. Earlier literature has found that equilibrium models predict a slower pressure-rise rate versus time compared with experiment for a given heat flux. The rate of pressure-rise can be more than three times the equilibrium rate for smaller tanks (4.89 m^3) (Hasan, Lin, & Van Dresar, 1991; Van Dresar, Lin, & Hasan, 1992) and can be as much as ten times the equilibrium rate for larger tanks (50,000 gallons) (Hasan, Lin, & Van Dresar, 1991; Liebenberg & Edeskuty, 1965; Van Dresar, Lin, & Hasan, 1992). This earlier literature also shows that equilibrium model predictions are closer to experimental pressure-rise rates for low heat fluxes but deviates at higher heat fluxes. However, later literature shows that for a closed tank with a constant incoming heat flux over a period of time, the final rate of pressure rise as a function of time is very close to that predicted by the equilibrium model for both low and high heat fluxes. However, this agreement is observed only after an initial transient which ultimately makes the pressures predicted by the equilibrium model different from that observed both in experiment and more sophisticated models. (Panzarella & Kassemi, 2003; Barsi, Kassemi, Panzarella, & Alexander, 2005; Barsi & Kassemi, 2007). Previous literature also reveals that, under normal gravity conditions, the pressure-rise rate is highly affected by the location of heat addition, where the highest rate is seen in the case where heat is added to the vapor phase.

Only one equilibrium model in the recent literature has been identified that uses an equilibrium model as an approximation of actual physics. Lin, Van Dresar, & Hasan (2004) discuss the relevance of an equilibrium model because it produces the lowest pressure attainable in a system for a given heat flux into the tank. As discussed later in this chapter, this behavior is desirable in cryogenic applications. In this article (Lin, Van Dresar, & Hasan, 2004), the tank propellant is mixed in order to reduce the effects of temperature gradients in the liquid and gas phases. Thus, it is shown that an equilibrium model can provide suitable accuracy for a well-mixed, homogeneous system.

Apart from the equilibrium model literature cited above, most of the literature on rocket propellant delivery systems consists of heat and mass transfer models that focus on the effects of thermal stratification on propellant self-pressurization (Arnett & Millhiser, 1965;

Arnett & Voth, 1972; Barakat, 1965; Bornhorst & Hatsopoulos, 1967; Clark & Barakat, 1965; Grayson, 1995; Grayson, Watts, & Jurns, 1997; Greer, 1999; Holt, Majumdar, Steadman, & Hedayat, 2000; Majumdar & Steadman, 2001; Nein & Thompson, 1965; Zilliac & Karabeyoglu, 2005). There are a large number of publications in this field, including an entire conference on pressurization and stratification in cryogenic fuel or oxidizer tanks (Conference on Propellant Tank Pressurization and Stratification, January 1965, Marshall Space Flight Center). A significant number of these models were published around the same time as the equilibrium models, back in the 1960s. Zilliac and Karabeyoglu (2005) noted that the work of Morey & Traxler (Ring, Ed., 1964) is a common foundation for heat and mass transfer models of propellant delivery systems, and it also serves as a starting point for their own model. Along with other heat and mass transfer-based models in the literature (Clark & Barakat, 1965; Grayson, 1995; Greer, 1999; Holt, Majumdar, Steadman, & Hedayat, 2000; Majumdar & Steadman, 2001; Nein & Thompson, 1965), Zilliac and Karabeyoglu's model incorporates the effects of draining on the pressurization processes in the tank, unlike the equilibrium models. As can be expected, these early heat and mass transfer models required more computational power, which is not as much of an issue today as it was back in the 1960s. In earlier models, scaling was sometimes used to simplify equations in order to eliminate some computational complexity (Nein & Thompson, 1965; O'Loughlin, 1965). In more recent models, both in-house codes as well as commercially available software such as FLOW-3D and Fluent have been used for these computational analyses. One example of an in-house code is Holt, Majumdar, Steadman, and Hedayat (2000) which uses a computer program called GFSSP to not only model the self-pressurization processes in both fuel and oxidizer tanks during draining but also includes a complete model of the entire helium pressurization system during engine firing as well as during feedline and pump priming prior to testing. Panzarella and Kassemi (2003) and Barsi and Kassemi (2007) introduce a CFD model assuming a stratified liquid coupled with a lumped-thermodynamic-vapor to be compared with the equilibrium model in their work. Again, their general finding was that a "purely thermodynamic" model is not adequate to describe the self-pressurization behavior of a cryogenic propellant tank due to its inability to capture initial transients in the system.

  The basis for the current work is that of Zilliac and Karabeyoglu (2005). They provide a heat and mass transfer model for a hybrid rocket oxidizer tank using the

assumptions laid out by Morey & Traxler (Ring, Ed., 1964) as a basis. To fit the experimental data generated from nitrous oxide tank draining experiments, the model requires the use of a large empirical factor in conjunction with a heat transfer coefficient associated with the evaporation rate of the oxidizer. This empirical factor is not predictable from theoretical principles or other experimental studies. They postulate that the need for such a large empirical factor indicates that the modeled heat transfer coefficient was too low; thus, they propose that this issue requires future study. However, it is also possible that this parameter compensates for other inaccuracies in the model, lumping them into the parameter itself.

There are some additional references that were reviewed that are related to the current work. Zilliac and Karabeyoglu (2005) cited literature that modeled evaporation using Statistical Rate Theory (Kumar, Danov, Durst, 2003; Ward & Fang, 1999). However, since this involves the use of quantum mechanics, it was immediately deemed to be outside the scope of this work. Several references were also found that focus on modeling aspects of pressurant delivery such as calculating the pressurant mass inflow necessary to regulate the propellant tank pressure to within a certain range, or assessing mass transfer behavior when adding pressurant to a non-draining tank (Liebenberg & Edeskuty, 1965; O'Loughlin, 1965; O'Loughlin & Glenn, 1965; Pasley, 1970; Roudebush & Mandell, 1965; Smithson & Scott, 1965; Tyler, 1965; Van Dresar, 1997). There are also several references on developing non-ideal equations-of-state (Martin & Hou, 1955; Redlich & Kwong, 1948), including the original publication by Peng-Robinson used in this thesis (Peng & Robinson, 1976). There are a few references on how the thermodynamic properties of substances are formally found (Giordano & De Serio, 2002; Wisniak & Golden, 1998), both pure and mixture, and how different equations-of-state can then be fitted to the data (Cabaas, Menduia, Pando, & Renuncio, 1998; Lemmon & Span, 2006; Span & Wagner, 2003). These references are useful for illustrating how a non-ideal equation-of-state can be used to capture the thermodynamic properties of substances. It also demonstrates the process required to quantify the properties of a real mixture, as mixture properties can vary appreciably from those of pure-component properties (Sandler, 2006).

2-3   Perspective on Current Study

Interestingly, the applications and goals of both the equilibrium models and the heat and mass transfer models in the above-cited literature are very similar. Most of this literature is focused on a different application than self-pressurized propellant delivery; it is primarily concerned with applications where the oxidizer or fuel is cryogenic, and sometimes pure with no pressurant. The tank in many of these models is a closed system with no flow out of the tank. Oftentimes, the fluid dynamics of the liquid-vapor interface is also of interest and investigated alongside the self-pressurization models because the interfacial orientation can change the pressurization behavior in normal- and zero-gravity situations. For the closed tank models, the intended applications generally involve long term propellant storage, where small amounts are drained at one time and likely produce little effect on the instantaneous pressure. Liquid hydrogen has been of particular interest to NASA since the 1960s, and is almost always the model fluid of choice. In the 1960s, NASA's space exploration program used liquid hydrogen as a rocket fuel, chosen for its favorably high specific impulse (Abdalla, Frysinger, & Andracchio, 1965; Aydelott, 1967a,b). When there was resurgence in studying pressurized tank delivery in the 1990s, liquid hydrogen was still the model fluid of choice. However, applications for cryogenic fluids in general include not just chemical and nuclear propulsion but also life support and thermal control systems meant for long-duration missions. This is part of NASA's next-generation human/robotic space exploration program involving trips to Earth's orbit, the Moon, Mars, and other areas of interest in the solar system (Hasan, Lin, & Van Dresar, 1991; Panzarella & Kassemi, 2003; Barsi, Kassemi, Panzarella, & Alexander, 2005). The main focus for the space missions addressed in the literature is to understand what variables affect the tank pressure, and to keep the pressure at a fairly even and low level. Thus, keeping the temperature controlled is also an area of focus, which is where the importance of heat transfer into the tank is relevant. If heat continues to leak into a cryogenic tank, the tank will eventually need to be vented to relieve the pressure. This not only would result in considerable propellant mass loss over a long-duration mission, but could also, in space applications, result in liquid and vapor draining as well as prohibit manned extra-vehicular activity in close proximity to the storage tanks. Ultimately, safe and efficient cryogen storage and utility is vital for the financial feasibility of these missions.

Based on the above-cited literature, the need for a more complex heat and mass transfer model to accurately describe liquid hydrogen self-pressurization behavior appears to be justified, and may be justified in the general context of cryogenic systems that have been studied. Previous studies have focused predominantly on cryogenic applications, where liquid vapor pressures are extremely low. However, the literature does not necessarily indicate that such sophisticated models are required for accurate modeling of self-pressurized delivery of fuels or oxidizers at ambient temperatures, where liquid vapor pressures can be extremely high.

The application that this thesis examines is the complete liquid draining of a hybrid rocket oxidizer tank at ambient temperatures, where nitrous oxide is used as the oxidizer and helium as the pressurant. The fact that the oxidizer and pressurant are not cryogenic and are not in an extreme environment such as space may make them less sensitive to heat transfer through the tank walls. Furthermore, this application focuses on short-term tank draining since the tank is drained during launch in less than a half-minute; the short launch time will restrict the amount of heat transferring into the tank throughout rocket flight. For the purposes of this work, the effects of heat transfer into the tank have been neglected but can be added into the model if it is believed it would have a significant effect on the tank conditions during launch.

The focus of this work is to determine the effect of the self-pressurizing behavior of the oxidizer on its outflow from the tank. While there were more sophisticated heat and mass transfer models found in the literature that model cryogenic propellant outflow over a short period of time, a relatively simple equilibrium model that examines this hybrid propellant tank draining configuration has not been found. Thus, two equilibrium models of a draining propellant tank are introduced in Chapter 3. The assumptions of these equilibrium-based models need to be critically assessed against experiments before complications of heat and mass transfer are considered; this sophistication should only be added if the equilibrium models do not provide the desired predictive ability for the system.

CHAPTER 3

ANALYSIS

3-1   Physical/Mathematical Model

Consider a tank of total internal volume V, containing a self-pressurizing oxidizer and a non-condensable pressurant. The model pressurant used in this thesis is helium and is referred to in notation as component 1. The model oxidizer is nitrous oxide and is referred to in notation as component 2. There is initially n_{2T} moles of nitrous oxide in the tank as well as n_{1_o} moles of helium. The initial temperature T_O of the tank contents is known. The oxidizer tank liquid drains through a feedline to the combustion chamber, where flow is driven by the pressure difference between the oxidizer tank and the combustion chamber. The combustion chamber pressure history is also specified. The purpose of the analysis is to predict the time history of all key parameters throughout the liquid oxidizer draining period. The tank's contents as well as the tank itself are assumed to be in thermodynamic equilibrium prior to and throughout the draining process. The liquid phase is assumed to be pure nitrous oxide while the gas phase is a mixture of nitrous oxide vapor and helium gas. The amount of helium in the gas phase remains constant during the drain. The tank walls are assumed to be adiabatic.

To analyze this configuration, it is natural to consider the well-known conservation laws. Conservation of mass and energy are key laws that provide the essential backbone physics of the problem. In their unaltered form, they are valid for all physical circumstances, but assumptions are often made (as is done here) to simplify the mathematics and thus make the problem easier to solve. The basic approach adopted here is to start simple and to introduce complexity if the desired accuracy is not attained; this assessment is ultimately made by comparison of theory and experiment. Two models have been completed in this thesis: the first assumes ideal behavior while the second assumes non-ideal behavior.
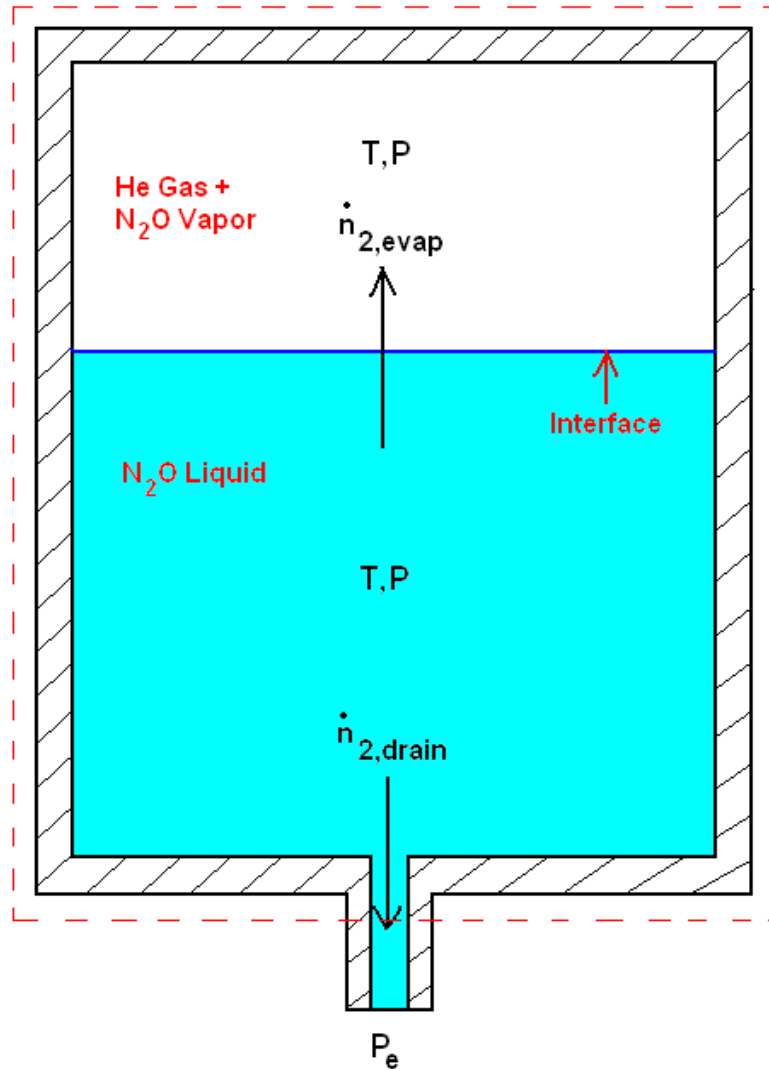
Figure 3.1: Draining Problem Schematic

Figure 3.1 shows the basic schematic for both the ideal and non-ideal models. T and P are the tank temperature and pressure, respectively, at any instant in time in the draining process. The exit pressure is denoted by P_e, which is a specified function of time. The nitrous oxide liquid draining rate and evaporation rate are denoted by $\dot{n}_{2,drain}$ and $\dot{n}_{2,evap}$, respectively.

Assumptions:

1. The tank drains such that the temperature, T, and the pressure, P, of the liquid and gas phases are uniform for all instants in time throughout the draining process; thus, the tank contents are always in phase equilibrium.

2. Neglect gravitational head in tank.

3. Tank walls are adiabatic to its surroundings.

4. Tank walls are in thermal equilibrium with the tank contents at all times.

5. Neglect potential and kinetic energy of liquid and gas phases.

6. A particular equation-of-state is used to supply P-V-T relationships (See Section 3-2)

    a. Ideal Gas Law

        i. No molecular interactions

        ii. Colligative law (particular material types do not matter)

        iii. Vapor-liquid equilibrium constraint is based on Raoult's Law, which utilizes pure-component vapor pressures to construct mixture vapor pressures.

    b. Non-Ideal Equation-of-State:

        i. Molecular interactions accounted for.

        ii. Dependent on substance characteristic properties, i.e. critical constants of nitrous oxide and helium, etc.

        iii. Liquid-vapor equilibrium dependent on substance characteristics, and more complex interactions between components than characterized by Raoult's Law.

7. Helium gas is non-condensable and resides totally in the gas phase.

8. Pressure drop between the oxidizer tank and the combustion chamber drives flow, and these effects are incorporated via a discharge coefficient. All other frictional losses are neglected in the tank and feedline.

9. The amount of helium in the gas phase is constant with no influx during draining.

10. Evaporation occurs at the interface between the liquid and gas phases. Due to the equilibrium nature of the models, no boiling occurs in the tank.

3-2   Ideal versus Non-Ideal Equations-of-State

The first model assumes ideal gas behavior, which has the following physical characteristics. The ideal gas law assumes that molecular interactions are negligible among the substances present together in the gas phase. It is a colligative law, meaning the relationship between pressure and temperature is only affected by the number of molecules in the gas phase, and not by their identity.

Raoult's law, used in the ideal model as the vapor-liquid equilibrium constraint, assumes ideal gas behavior. It states that the equilibrium state of the system is dependent only on the vapor pressure of the liquid (at low pressures), which in this case has been assumed to be pure nitrous oxide. Therefore, the amount of helium in the tank does not affect how the nitrous oxide distributes into the liquid and gas phases. To illustrate this point, suppose a tank of set volume is filled with a certain quantity of liquid nitrous oxide at a known temperature. The space above the liquid is initially assumed to be devoid of nitrous oxide, but has helium gas present. Vapor-liquid equilibrium applied to the tank will show that the liquid nitrous oxide will evaporate and distribute between the liquid and gas phases until equilibrium is satisfied (assuming that all of the liquid nitrous oxide does not evaporate so no liquid is present). The ideal gas assumption yields the interesting result that the amount of nitrous oxide in either the gas or liquid phases will not change whether the tank originally has helium in the gas phase or not. The ideal gas assumption therefore only makes physical sense at *low* gas pressures, where the gas molecules do not interact. In addition, the ideal gas law does not have the ability to predict phase behavior; in a model using the ideal gas law, the only way to solve for the molar distribution between the liquid and gas phases is to couple the ideal gas law with Raoult's Law, which pulls the nitrous oxide vapor pressure from experimental data. Furthermore, Raoult's law makes use of pure-component vapor pressures to determine the phase behavior in mixtures. This experimental data is often correlated with high accuracy in handbooks. Recall the constraint that a gas can typically be considered ideal if the molar volume, $\hat{V}_g$, for non-diatomic gases and gas mixtures is greater than 20 L/mol (Felder & Rousseau, 1978).

The second model assumes that the pressure-volume-temperature (P-V-T) relationship can be described accurately by a non-ideal, cubic equation-of-state: Peng-Robinson. Non-ideal equations-of-state account for molecular interactions in the gas phase. They are also valid for higher pressure systems for which the ideal gas law is not valid. While there are multiple choices for non-ideal equations-of-state (an appropriate equation-of-state is determined via experimental measurement), the Peng-Robinson equation-of-state was chosen for this thesis work due to its use in Zilliac and Karabeyoglu (2005). The Peng-Robinson equation-of-state and the non-ideal equilibrium constraint are dependent on the substances' physical characteristics (in this case, nitrous oxide and helium), such as critical

constants, and the material-specific molecular interaction accounted for by using a specified mixing rule. In this non-ideal model, *both* the liquid and gas phases have an equation-of-state because they have different compositions of helium and nitrous oxide. Also, both equations-of-state are needed in order to calculate the equilibrium constraint, which states that the partial fugacities of nitrous oxide in both phases must be equal at equilibrium. The fugacity calculations require the calculation of both the liquid and gas nitrous oxide compressibilities extracted from their respective equations-of-state. Completing the equilibrium constraint calculation inherently extracts the vapor pressure of nitrous oxide at the given temperature. So in this model, the vapor pressure is not taken from correlation but is instead a predicted result of the equilibrium calculation. Therefore, any discrepancies between the correlated vapor pressure and the vapor pressure calculated from the equation-of-state at a given temperature would indicate a divergence in Peng-Robinson's ability to accurately extract the vapor pressure.

3-3   Solution Structure

The equations which constrain the tank draining problem at hand are the same for both the ideal and non-ideal models, except for the equation-of-state and the equilibrium constraint. The important thing to remember is that changing the equation of state will also require a corresponding change in the form of the equilibrium constraint.

Table 3.1 provides the six equations used in solving this problem. The molar conservation equation states that the rate of change of total gas and liquid moles in the tank, denoted as n_g and n_{2l} respectively, must be equal to the liquid nitrous oxide flow rate out of the tank, $\dot{n}_{2,drain}$. Note that the total moles of gas, n_g, is equal to the sum of the nitrous oxide vapor, n_{2v}, and the helium gas, n_{1_o}. The energy conservation equation states that the rate of change of the total internal energy in the system (including the tank specific internal energy, $\overline{U}_T$, the liquid molar internal energy, $\hat{U}_{2l}$, and the gas molar internal energy, $\hat{U}_g$) is equal to the rate of change of liquid enthalpy exiting the tank. The flow relation relates the nitrous oxide liquid flow rate, $\dot{n}_{2,drain}$, to the discharge coefficient, C_D, the area of the injector into the combustion chamber, $A_{injector}$, the molecular weight of nitrous oxide, $(MW)_2$, the

pressure in the tank, P, the combustion chamber pressure, P_e, and the molar volume of the nitrous oxide liquid, $\hat{V}_{2l}$. The volume constraint simply states that the total internal volume of the tank, V, is equal to the sum of the liquid phase volume, V_l, and the gas phase volume, V_g. The ideal gas law relates the pressure in the tank, P, to the total gas molar volume, $\hat{V}_g$, and the temperature T with a compressibility equal to unity. The Peng-Robinson equation-of-state, however, incorporates a gas mixture compressibility, Z_g, into the gas equation-of-state and a pure liquid compressibility, Z_{2l}, into the liquid equation of state. Refer to Appendix C for further detail on the Peng-Robinson equation-of-state. The ideal vapor-liquid equilibrium constraint is Raoult's Law, which relates the partial pressure of nitrous oxide (which is equal to the mole fraction of nitrous oxide in the gas phase, y_2, times the total tank pressure P) to the pure-component vapor pressure of nitrous oxide. The non-ideal vapor-liquid equilibrium constraint states that the partial fugacities of nitrous oxide must be equal in both phases, which can also be written in terms of the partial fugacity coefficients for the liquid and gas phases, denoted as ϕ_{2l} and ϕ_{2v}, respectively. Refer to Appendix D for further detail on the enthalpies and fugacity coefficients corresponding to the Peng-Robinson equation-of-state.

Constraint	Ideal Model	Non-Ideal Model
Molar Conservation	$\dfrac{d}{dt}\left(n_g + n_{2l}\right) = \dfrac{d}{dt}\left(n_{2v} + n_{2l}\right) = -\dot{n}_{2,drain}$	
Energy Conservation	$\dfrac{d}{dt}\left(m_T \bar{U}_T + n_{2l}\hat{U}_{2l} + n_g \hat{U}_g\right) = -\dot{n}_{2,drain}\hat{H}_{2l}$	
Flow Relation	$\dot{n}_{2,drain} = \dfrac{C_D A_{injector}}{(MW)_2}\sqrt{\dfrac{2(MW)_2(P-P_e)}{\hat{V}_{2l}}}$	
Volume Constraint	$V = V_g + V_l = V_g + n_{2l}\hat{V}_{2l}$	
Equation of State	Ideal Gas Law $$P\hat{V}_g = RT$$	Peng-Robinson Liquid (Pure 2): $P\hat{V}_{2l} = Z_{2l}RT$ $Z_{2l} = Z_{2l}(T,P)$ Gas (Mixture of 1 & 2 vapor): $P\hat{V}_g = Z_g RT$ $Z_g = Z_g(T,P,y_2)$
Vapor-Liquid Equilibrium	Raoult's Law $$y_2 P = P_2^*(T)$$	$\phi_{2l} = y_2 \phi_{2v}$ $\phi_{2l} = \phi_{2l}(T,P,Z_{2l})$ $\phi_{2v} = \phi_{2v}(T,P,Z_g,y_2)$

Table 3.1: Solution Structure

These six constraints produce the solution for both the ideal and non-ideal models. The solution is reduced to three equations with three unknowns for the ideal model: T, n_{2l}, and n_{2v} as functions of time; the solution is reduced to four equations with four unknowns for the non-ideal model: T, P, n_{2l}, and n_{2v} as functions of time. The ideal model does not have pressure as an unknown because it is inherent in an ideal system that thermodynamic quantities such as internal energy and enthalpy are only functions of temperature, not pressure. However, in a non-ideal equation of state, these quantities are indeed pressure dependent and can be significantly altered at high pressures. Note that all non-ideal

equations-of-state limit to the ideal gas law at low enough pressures. While internal energy, enthalpy, fugacity, etc. are important quantities that describe the system, it should be noted that each of these is a function of the measurable quantities of temperature, pressure, mass, volume, and time. Thus, the solutions track the measurable attributes of the system.

Model 1:

$$
\begin{bmatrix}
\dfrac{dT}{dt} \\[2ex]
\dfrac{dn_{2l}}{dt} \\[2ex]
\dfrac{dn_{2v}}{dt}
\end{bmatrix}
=
\begin{bmatrix}
f_1\left(T, n_{2l}, n_{2v}\right) \\[1ex]
f_2\left(T, n_{2l}, n_{2v}\right) \\[1ex]
f_3\left(T, n_{2l}, n_{2v}\right)
\end{bmatrix}
\tag{3.1}
$$

Model 2:

$$
\begin{bmatrix}
\dfrac{dT}{dt} \\[2ex]
\dfrac{dP}{dt} \\[2ex]
\dfrac{dn_{2l}}{dt} \\[2ex]
\dfrac{dn_{2v}}{dt}
\end{bmatrix}
=
\begin{bmatrix}
f_1\left(T, P, n_{2l}, n_{2v}\right) \\[1ex]
f_2\left(T, P, n_{2l}, n_{2v}\right) \\[1ex]
f_3\left(T, P, n_{2l}, n_{2v}\right) \\[1ex]
f_4\left(T, P, n_{2l}, n_{2v}\right)
\end{bmatrix}
\tag{3.2}
$$

The right-hand-side of Equations 3.1 and 3.2, as quantified by the functions f_i (i = 1,2,3,4), are large algebraic expressions. Details of the derivation of the above equations as well as the precise form of these functions are provided in appendices. Appendices A and B provide details for the ideal and non-ideal (Peng-Robinson) solutions, respectively.

Initial conditions are necessary in order to make the system of Equations 3.1 and 3.2 well posed. The equations used to calculate the initial condition are some of the same equations used in calculating the time histories, including the equations-of-state, the vapor-liquid equilibrium constraint, and the volume constraint. However, the numerical algorithm

18

used to solve for these initial conditions is different. The details of the initial condition calculation are included in each model's appendix: Appendix A for the ideal model and Appendix B for the non-ideal model.

CHAPTER 4

EXPERIMENTAL DATA COMPARISON

4-1   Experiments

In the following chapter, both the ideal and non-ideal draining tank models are compared with experimental data published by Zilliac and Karabeyoglu (2005). Zilliac provides data for four separate experimental runs. Note that for these four tests, the following parameters are held fixed to within experimental error and are used as inputs into the models. All tests were performed for a pure nitrous oxide system; no helium was added to the oxidizer tank. The tank is 6061-T6 Aluminum with a mass of 6.4882 kg and an internal volume of 0.0354 m^3. The total injector area is 0.0001219352 m^2. Since the Peng-Robinson binary interaction parameter, k_{12}, for a nitrous oxide/helium mixture is unknown, it was assumed to be zero. A study provided in Section 5-3-4 of Chapter 5 as well as Section F-2 of Appendix F shows insensitivity to this parameter value; therefore, this assumption is not restrictive. The nitrous oxide and helium critical constants used for the models were that found in Sandler's (2006) CD accompanying the textbook. Note that the constants in *Perry's Chemical Engineers' Handbook* (1997) were slightly different from those of Sandler. A sensitivity study of the draining histories to these two sets of critical constants is also provided in Section 5-3-4 of Chapter 5 as well as Section F-3 of Appendix F.

Each of the four tests had different inputs: initial temperature, T_i, initial nitrous oxide mass loaded, m_{loaded}, discharge coefficient, C_D, and exit pressure history, P_e. Note that the exit pressure used in both models was a polynomial fit of the experimental combustion chamber pressure as a function of time, t, excluding initial transients.

Test Number	T_i (K)	m_{loaded} (kg)	C_D	P_e (Pa)
1	286.5	19.32933	0.425	$-2924.42t^6 + 46778.07t^5 - 285170.63t^4 + 813545.02t^3 - 1050701.53t^2 + 400465.85t + 1175466.2$
2	278.5	16.23298	0.365	$95.92t^6 - 2346.64t^5 + 21128.78t^4 - 87282.73t^3 + 186675.17t^2 - 335818.91t + 3029190.03$
3	271.5	14.10076	0.365	$58.06t^6 - 1201.90t^5 + 8432.11t^4 - 22175.67t^3 + 21774.66t^2 - 99922.82t + 2491369.68$
4	291.3	23.62427	0.09	$-4963.73t + 910676.22$

Table 4.1: Initial conditions for each of four tests published by Zilliac and Karabeyoglu (2005)

It should be noted that the initial nitrous oxide mass reported in the test matrix of Zilliac and Karabeyoglu (2005) are approximate values, but the values stated in Table 4.1 reflect the actual initial mass loaded for each experiment. In addition, Zilliac and Karabeyoglu state that the initial temperature of the nitrous oxide prior to draining was assumed to be equal to the ambient temperature at the time of the test; the temperature was not measured inside the tank. The tank contents were not given a significant amount of time between tank filling and draining in order to ensure that the tank contents had come to equilibrium with its surroundings (Zilliac, personal communication, 2009). Furthermore, Zilliac and Karabeyoglu (2005) state that the discharge coefficient was determined empirically based on each feed system configuration.

4-2   Experimental Data/Model Comparison Plots

The results for each test are presented in a set of four plots in the following order: total tank pressure versus time, total nitrous oxide in the tank versus time, nitrous oxide distribution into liquid and gas phases versus time, and tank temperature versus time. The first two plots for each test provide comparisons of the ideal and non-ideal theories to the experimental data. However, experimental data is not available for comparison with theory in the latter two plots. Conditions for all plots are as described in Section 4-1 and Table 4.1 for each test.
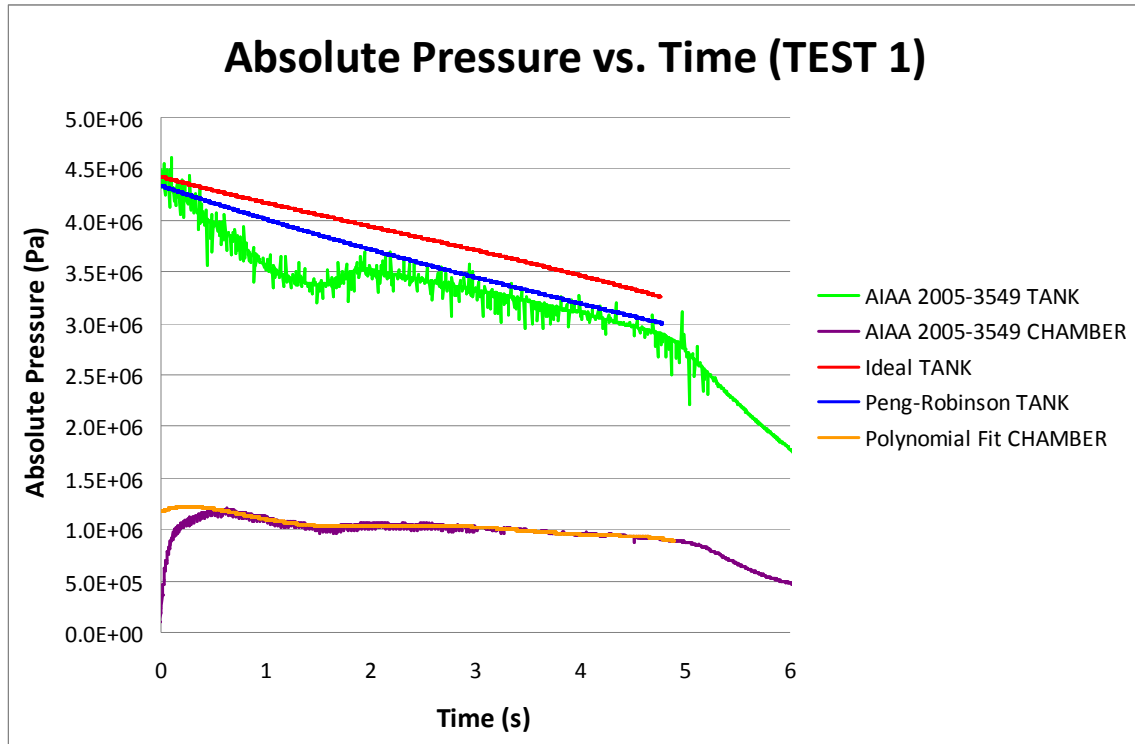
Figure 4.2.1a: Experimental data (Zilliac & Karabeyoglu, 2005: labeled "AIAA 2005-3549" in legend) and theoretical (ideal, non-ideal) predictions for the absolute pressure in the draining tank as a function of time, for parameter values as set in Section 4-1 for Test 1.
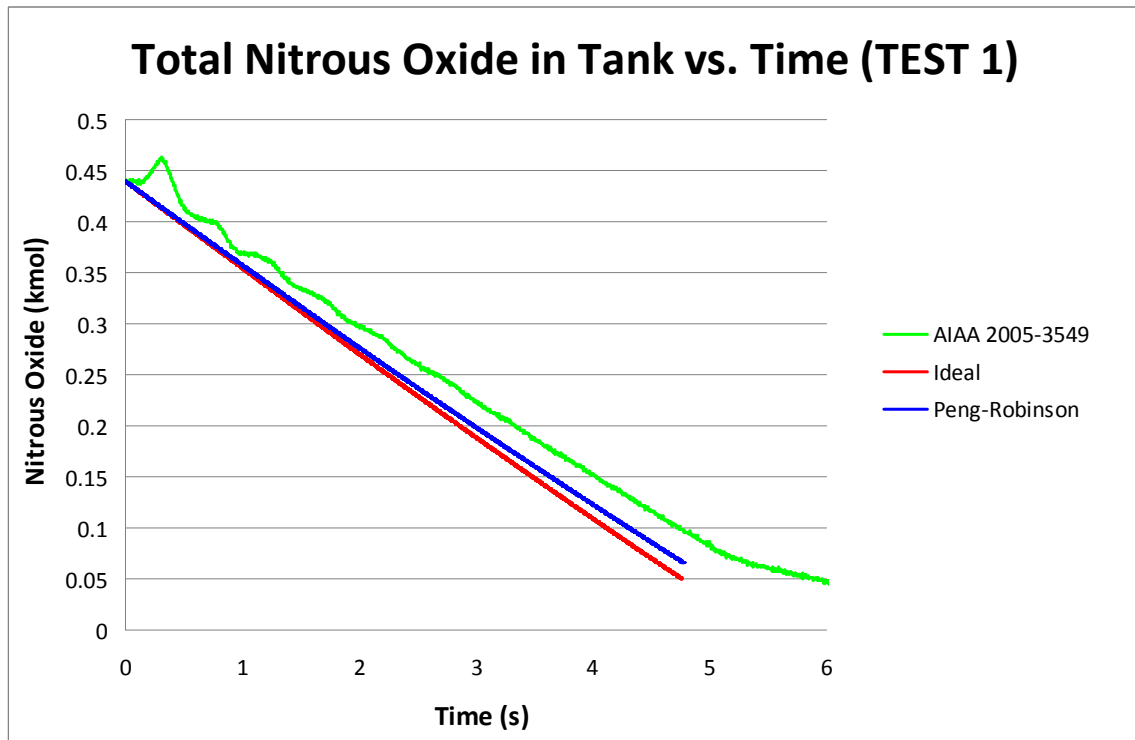
Figure 4.2.1b: Experimental data (Zilliac & Karabeyoglu, 2005: labeled "AIAA 2005-3549" in legend) and theoretical (ideal, non-ideal) predictions for the total moles of nitrous oxide in the draining tank as a function of time, for parameter values as set in Section 4-1 for Test 1.
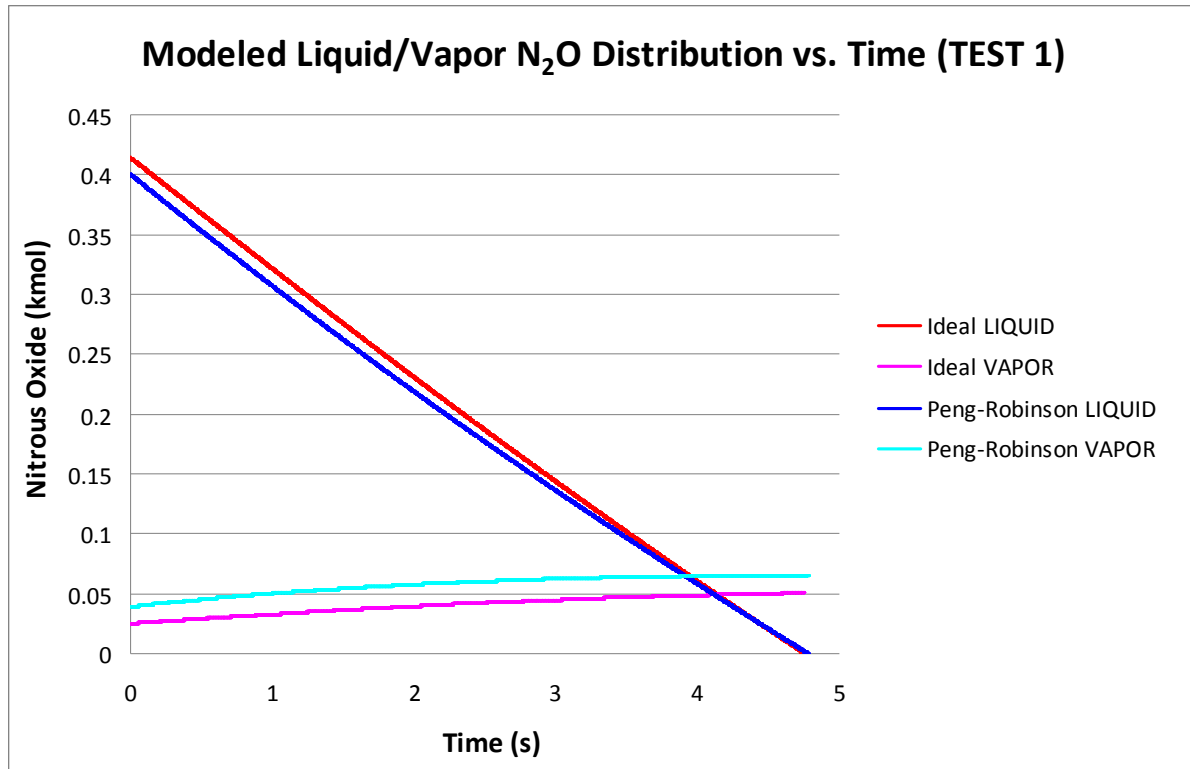
Figure 4.2.1c: Theoretical (ideal, non-ideal) predictions for the moles of nitrous oxide liquid and vapor in the draining tank as a function of time, for parameter values as set in Section 4-1 for Test 1.
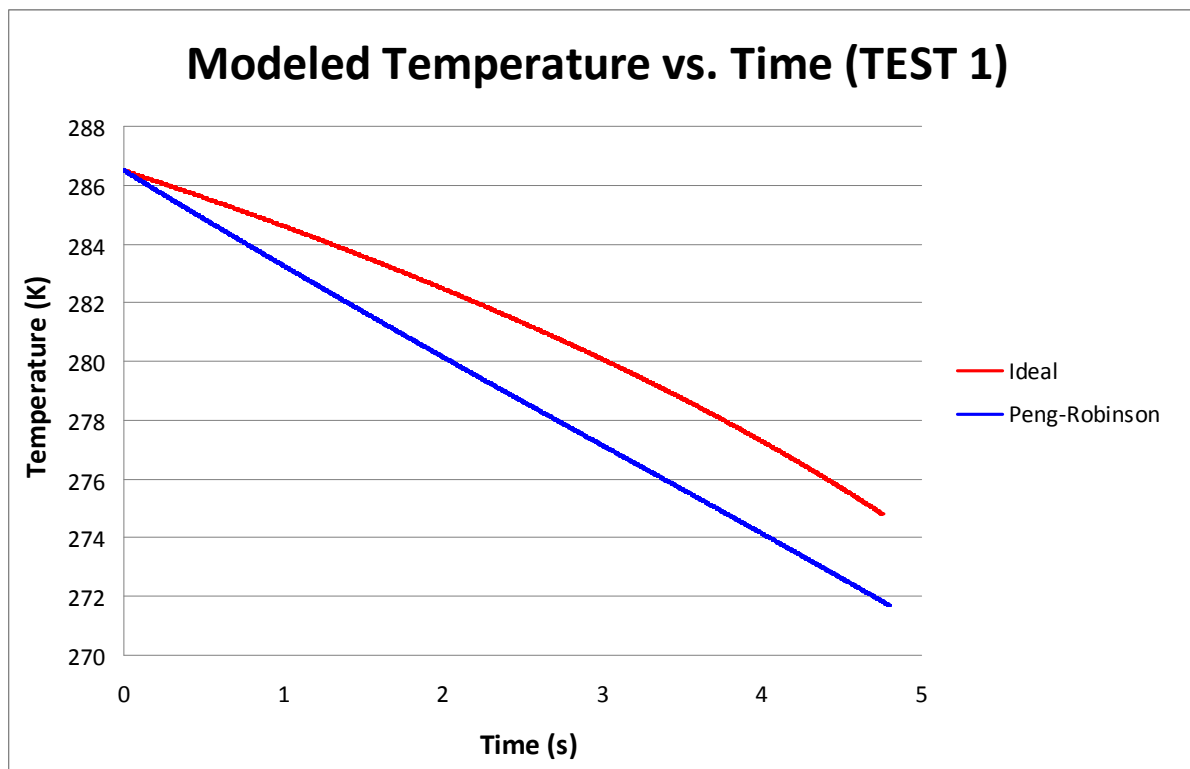
Figure 4.2.1d: Theoretical (ideal, non-ideal) predictions for the temperature in the draining tank as a function of time, for parameter values as set in Section 4-1 for Test 1.

23

The pressure data in Figure 4.2.1a shows an initial dip in pressure that is not captured by either the ideal or non-ideal models. While this phenomenon has been seen by Zilliac elsewhere in the literature (Zilliac, personal communication, 2009), it is unknown why this behavior is exhibited under these test conditions. Additionally, as experiment repeats were not available, it is not clear if these results would be repeatable in another test under the same conditions. For these two reasons, the models' ability to predict this feature of the pressure history of this tank draining test is inconclusive, while it is plainly seen that neither model would predict this outcome. It is also observed that the non-ideal model is closer to the experimental pressure history than the ideal model. Observation of the pressure history (Figure 4.2.1a) at approximately five seconds reveals that the experimental pressure variation transitions to a steeper slope. This slope change indicates that all the liquid has drained out of the tank; the remaining vapor continues to leave the tank, however, at a different rate. This latter behavior is not modeled in this thesis; combustion is predominantly maintained with the liquid oxidizer flow. In this particular test, both the ideal and non-ideal models predict draining times very close to the measured draining time (Figure 4.2.1b). Another interesting observation is that the experimental amount of nitrous oxide in the tank initially increases before decreasing (Figure 4.2.1b). Since mass is always leaving the tank, this measurement is not assumed to be accurate. The source of error in this measurement might be due to some influence in the test on the load cell, but its origin is not known.
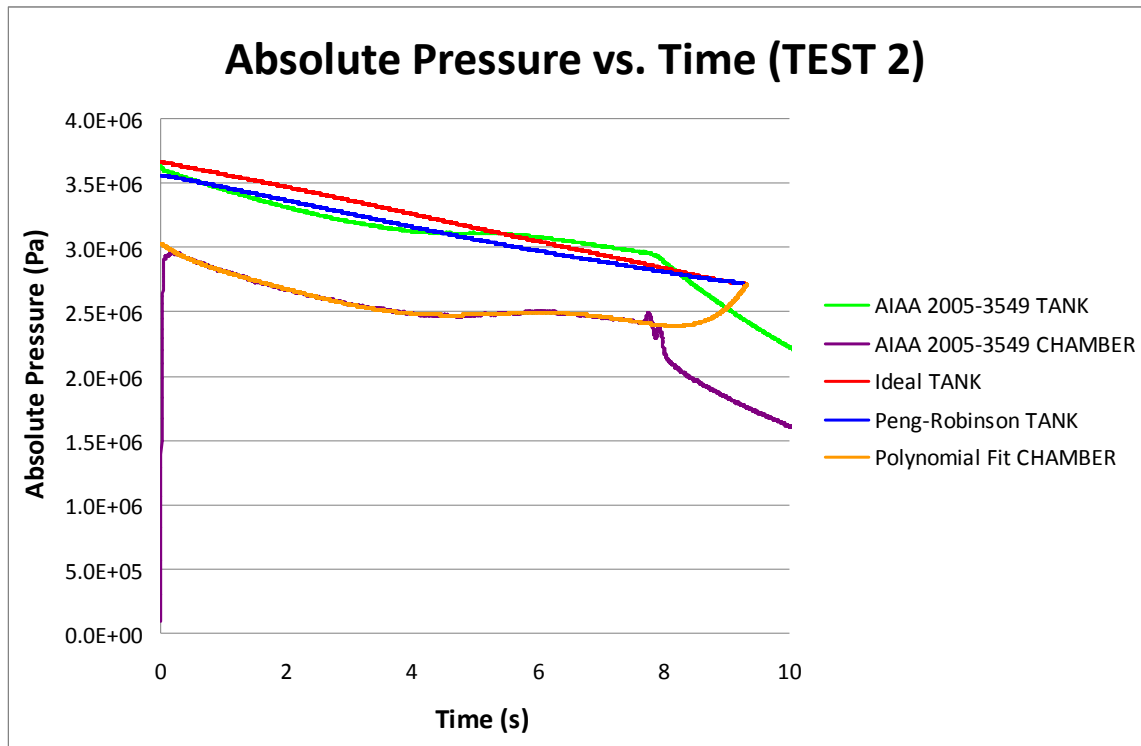
Figure 4.2.2a: Experimental data (Zilliac & Karabeyoglu, 2005: labeled "AIAA 2005-3549" in legend) and theoretical (ideal, non-ideal) predictions for the absolute pressure in the draining tank as a function of time, for parameter values as set in Section 4-1 for Test 2.
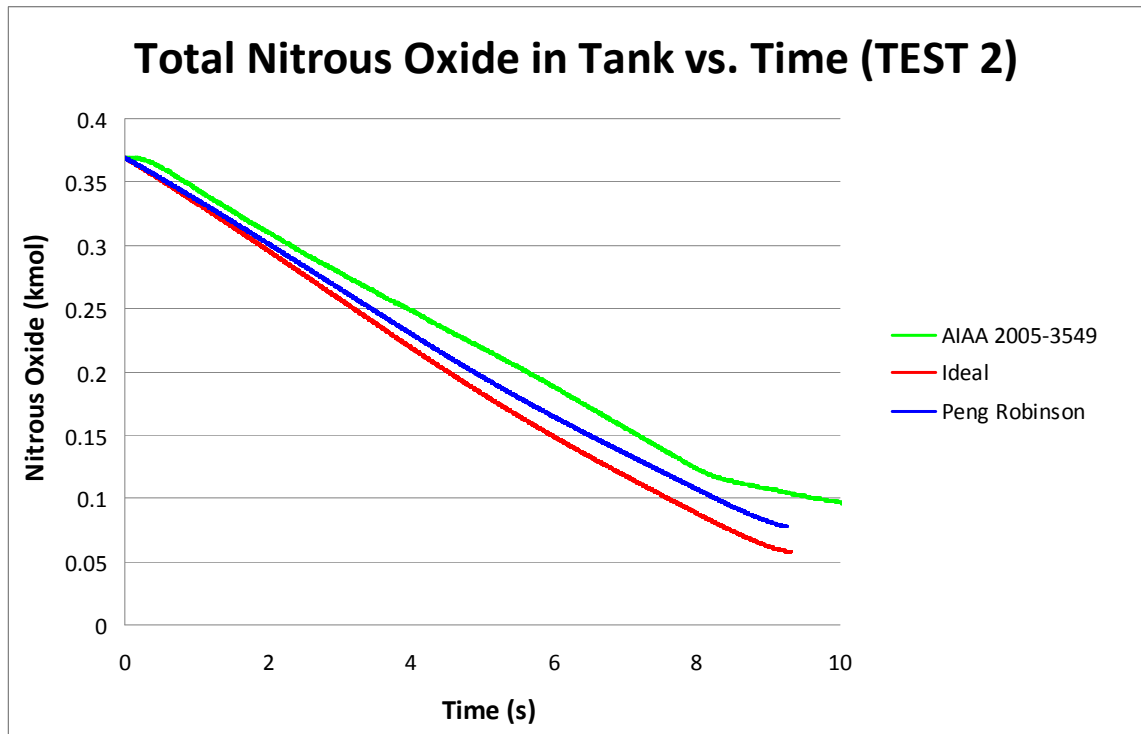
Figure 4.2.2b: Experimental data (Zilliac & Karabeyoglu, 2005: labeled "AIAA 2005-3549" in legend) and theoretical (ideal, non-ideal) predictions for the total moles of nitrous oxide in the draining tank as a function of time, for parameter values as set in Section 4-1 for Test 2.
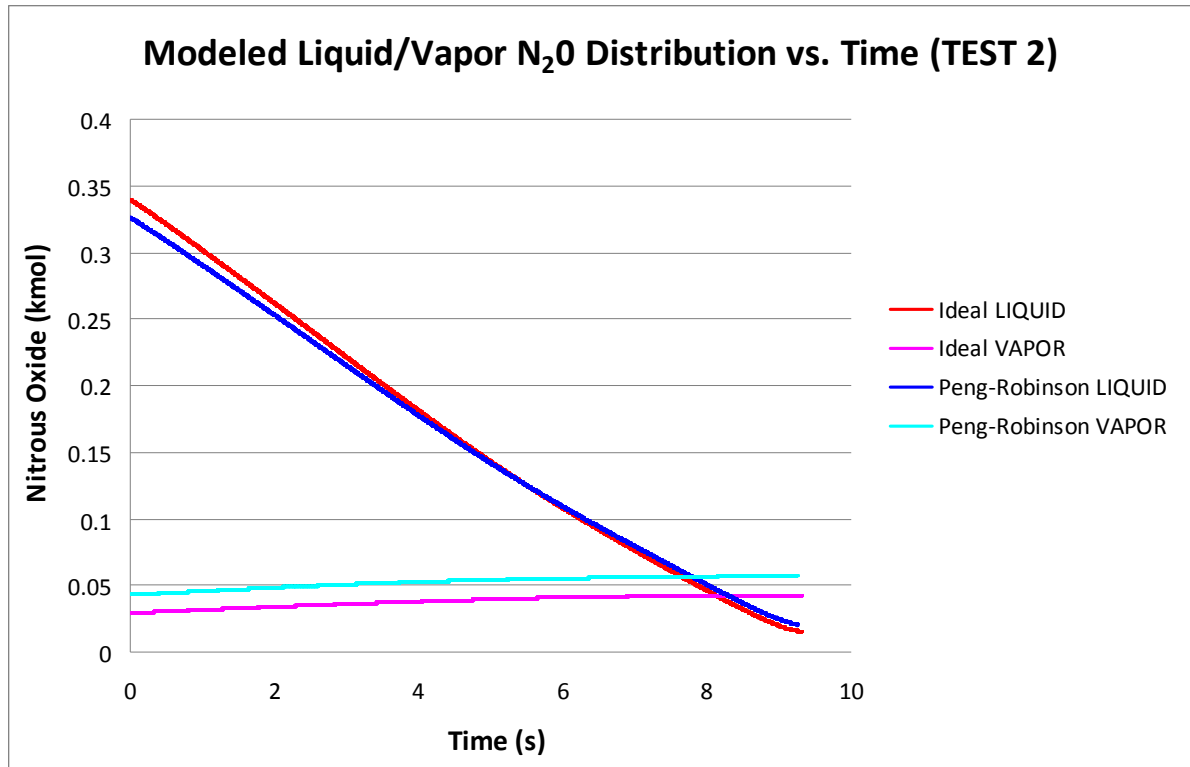
Figure 4.2.2c: Theoretical (ideal, non-ideal) predictions for the moles of nitrous oxide liquid and vapor in the draining tank as a function of time, for parameter values as set in Section 4-1 for Test 2.
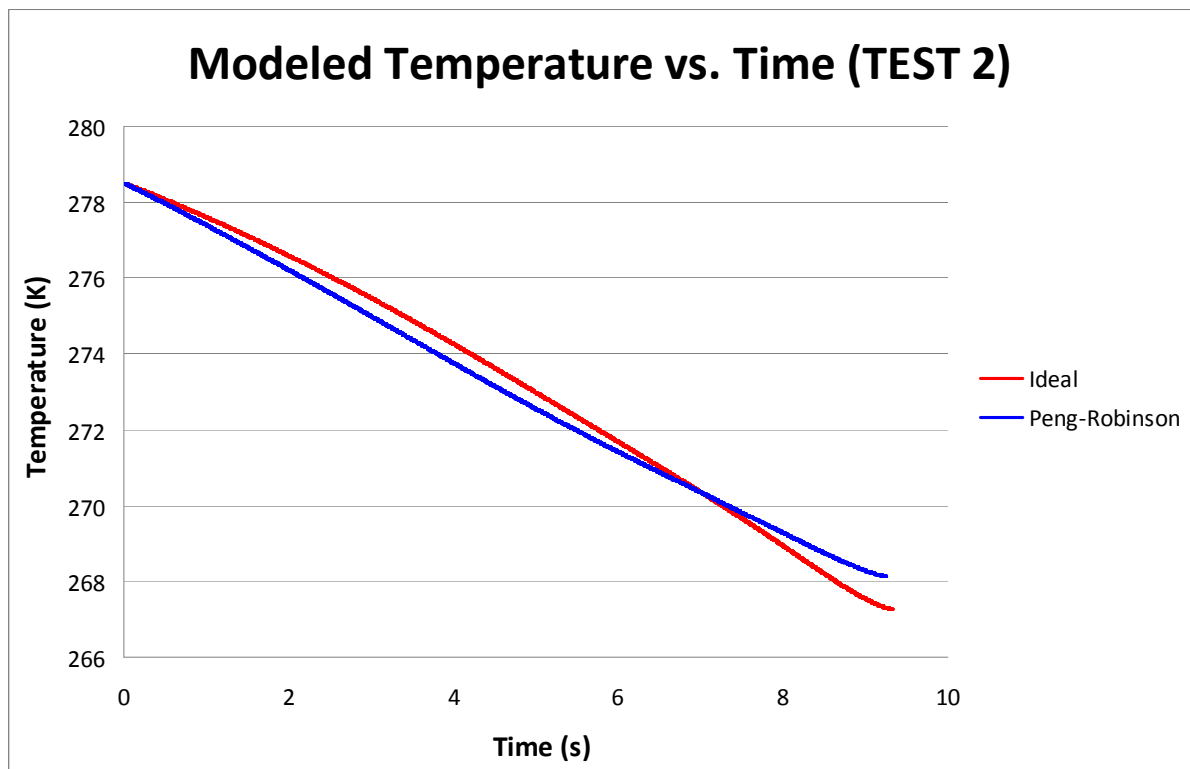
Figure 4.2.2d: Theoretical (ideal, non-ideal) predictions for the temperature in the draining tank as a function of time, for parameter values as set in Section 4-1 for Test 2.

For this test, it can be seen from both the pressure and total nitrous oxide histories (Figures 4.2.2a and 4.2.2b, respectively) that the drain time predicted by both models is over one second longer than what was measured in the experimental data. However, there are two unusual observations in the experimental data. First, note that the oxidizer tank pressure mirrors the trend of the combustion chamber pressure (Figure 4.2.2a). This is unexpected because the oxidizer tank pressure is a function of temperature in the tank itself through the vapor pressure of the liquid. The flow rate depends on the difference in pressure between the oxidizer tank and the combustion chamber, not on the chamber pressure alone. Therefore, even if the chamber pressure experiences some oscillations, the oxidizer pressure should not experience the same oscillations; only the flow rate of the draining nitrous oxide should be affected. Therefore, it is postulated that the observed coupling of the oxidizer pressure and chamber pressure was due to cavitation in the feedline during the experiment. Cavitation is very likely to happen in a pure component system when no pressurant is present since the vapor pressure of nitrous oxide can easily exceed that of the surrounding liquid as pressure is dissipated through flow (the nitrous oxide system is already saturated in the tank, so any pressure losses can lead to cavitation). The net result of this would be an inaccurate discharge coefficient, which was correlated with a liquid nitrous oxide molar volume (see flow relation in Table 3.1 of Chapter 3). Another significant observation is that the total nitrous oxide history has a small flat-line at the beginning of the drain (Figure 4.2.2b). The pressure history (Figure 4.2.2a) indicates a loss in pressure at the same time, so it is believed that this initial flat-line is not physical. Notice, however, that the flow rate after this initial flat-line (i.e., the slope of the curve) is quite close to that predicted by the non-ideal model.

Absolute Pressure vs. Time (TEST 3)
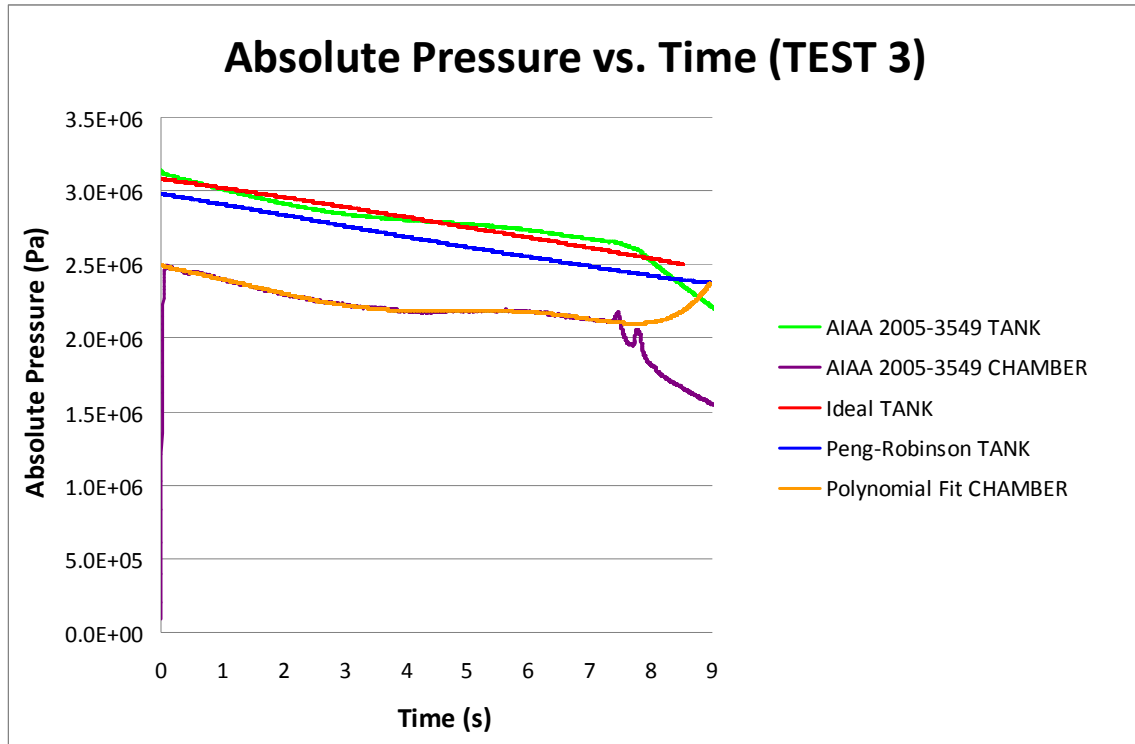
Figure 4.2.3a: Experimental data (Zilliac & Karabeyoglu, 2005: labeled "AIAA 2005-3549" in legend) and theoretical (ideal, non-ideal) predictions for the absolute pressure in the draining tank as a function of time, for parameter values as set in Section 4-1 for Test 3.

Total Nitrous Oxide in Tank vs. Time (TEST 3)
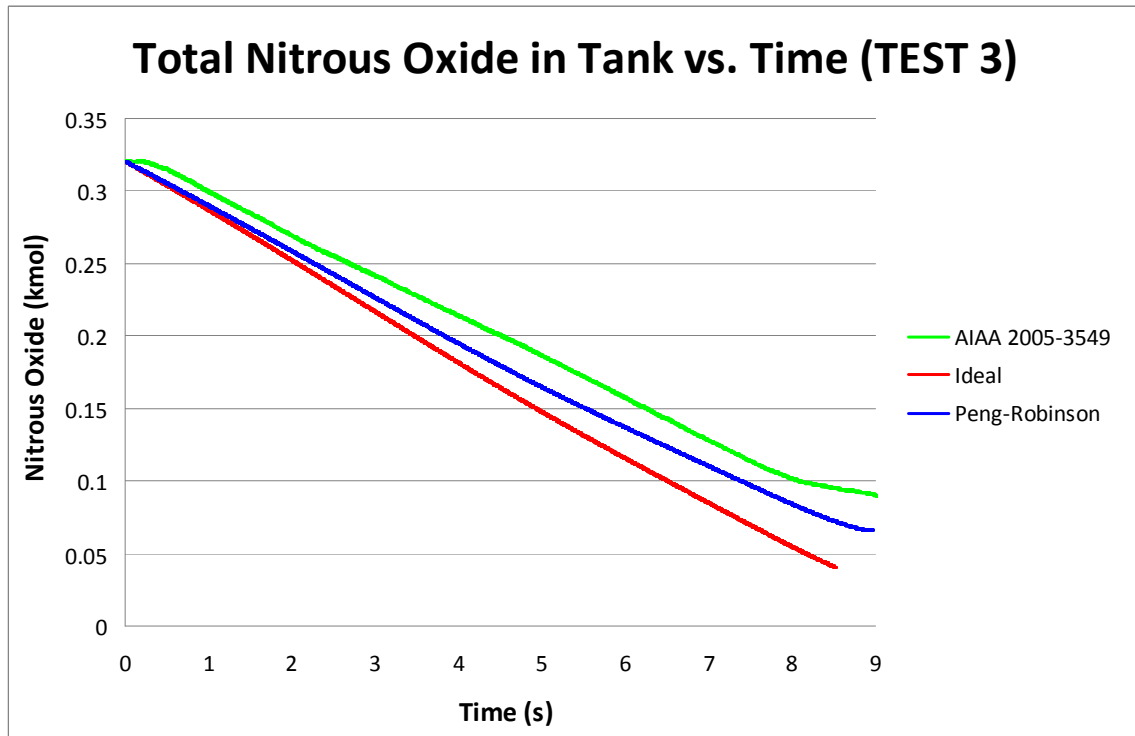
Figure 4.2.3b: Experimental data (Zilliac & Karabeyoglu, 2005: labeled "AIAA 2005-3549" in legend) and theoretical (ideal, non-ideal) predictions for the total moles of nitrous oxide in the draining tank as a function of time, for parameter values as set in Section 4-1 for Test 3.
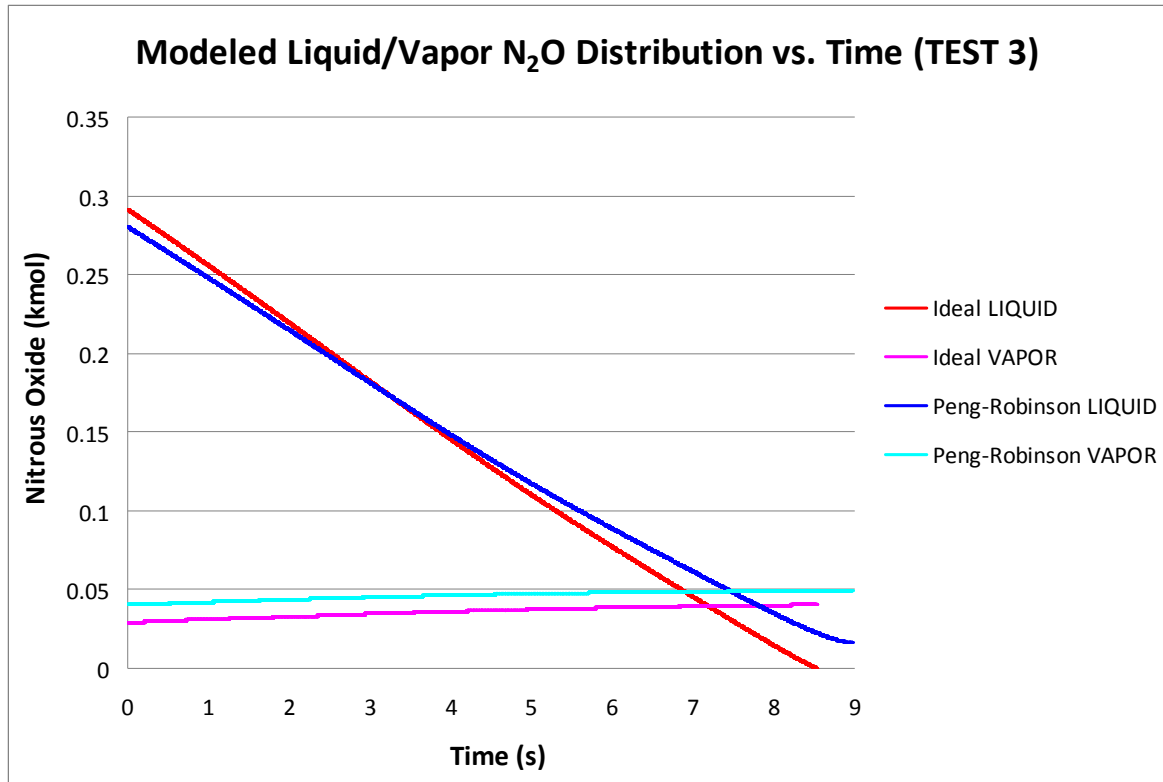
Figure 4.2.3c: Theoretical (ideal, non-ideal) predictions for the moles of nitrous oxide liquid and vapor in the draining tank as a function of time, for parameter values as set in Section 4-1 for Test 3.
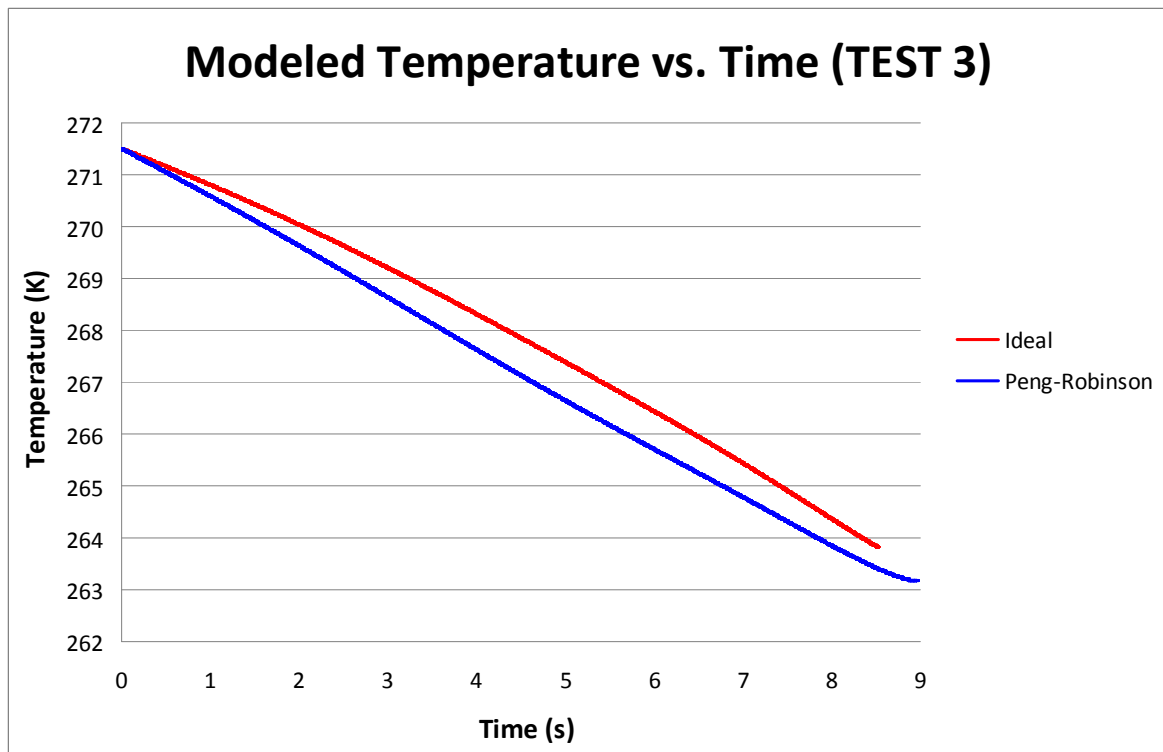
Figure 4.2.3d: Theoretical (ideal, non-ideal) predictions for the temperature in the draining tank as a function of time, for parameter values as set in Section 4-1 for Test 3.

The characteristics of this test are very similar to that for Test 2. This test exhibits the same coupling between the oxidizer tank pressure and the chamber pressure trends (Figure 4.2.3a). There is also the same initial flat-line in the total nitrous oxide history (Figure 4.2.3b). The drain time predicted by both models was, again, longer than the observed liquid drain time (Figure 4.2.3b).

4-2-4   Test 4 Model Comparison
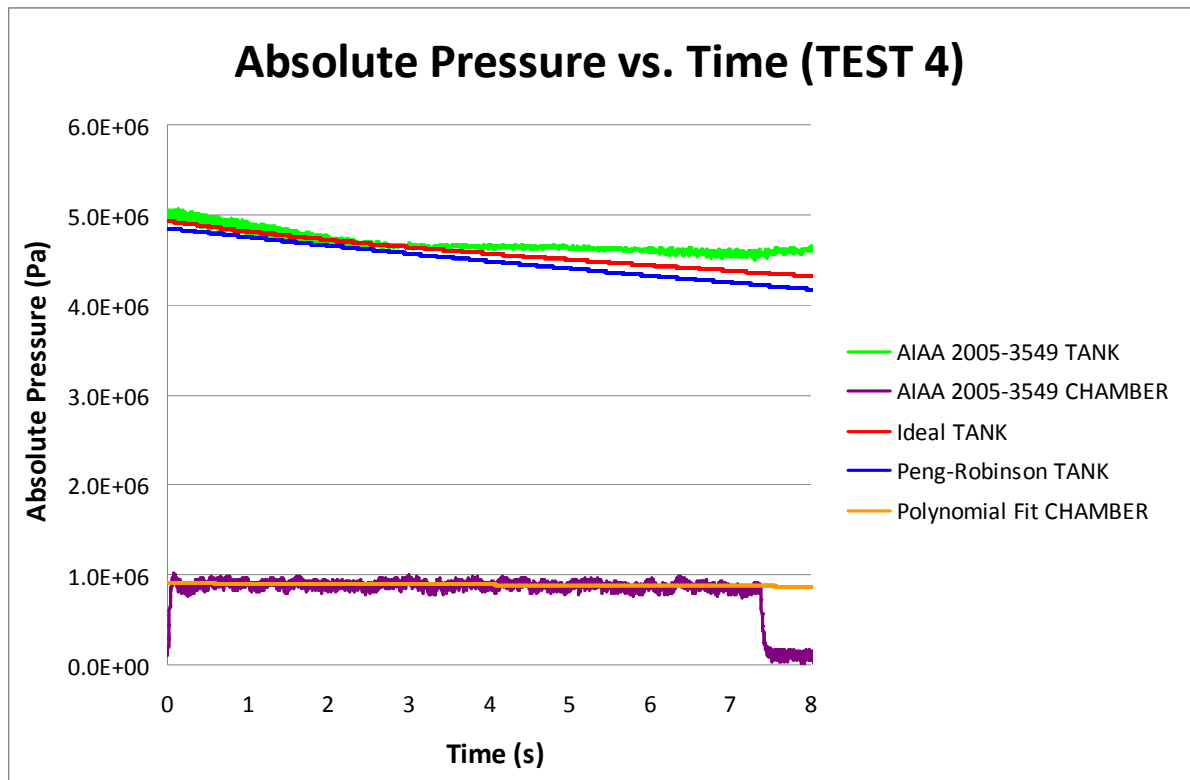
Figure 4.2.4a: Experimental data (Zilliac & Karabeyoglu, 2005: labeled "AIAA 2005-3549" in legend) and theoretical (ideal, non-ideal) predictions for the absolute pressure in the draining tank as a function of time, for parameter values as set in Section 4-1 for Test 4.

Figure 4.2.4b: Experimental data (Zilliac & Karabeyoglu, 2005: labeled "AIAA 2005-3549" in legend) and theoretical (ideal, non-ideal) predictions for the total moles of nitrous oxide in the draining tank as a function of time, for parameter values as set in Section 4-1 for Test 4.

Figure 4.2.4c: Theoretical (ideal, non-ideal) predictions for the moles of nitrous oxide liquid and vapor in the draining tank as a function of time, for parameter values as set in Section 4-1 for Test 4.

31

Figure 4.2.4d: Theoretical (ideal, non-ideal) predictions for the temperature in the draining tank as a function of time, for parameter values as set in Section 4-1 for Test 4.

Unlike the other tests, the tank was not drained to completion in this experiment (Figure 4.2.4b,c). Note that there is a longer initial flat-line in the total nitrous oxide history (Figure 4.2.4b). With the exception of this initial flat-line, the flow rate predicted by both models is very close to the measured flow rate (Figure 4.2.4b). However, the pressure history begins to level out around three seconds and afterward (Figure 4.2.4a). Since the nitrous oxide history shows a steady drain through this portion of the test as evidenced by the constant slope of the nitrous oxide versus time curve (Figure 4.2.4b), this measured pressure is presumed to be in error; further experiments would be required to verify this conclusively.

4-3   Discussion of Experimental and Theoretical Results

While the agreement between the models and the experimental data varies in each test, the overall closeness of the results is very encouraging. However, a firm assessment of the agreement between theory and experiment cannot be made as the experimental variability has not been provided by Zilliac and Karabeyoglu (2005). The theoretical predictions use only published material properties and no empirically determined parameters, and the models

are definitely close enough to the experimental data to evoke interest in further experiments to assess the validity of the models.

It is observed that in all cases, the initial pressure predicted by the ideal and non-ideal models are slightly different for the same given initial temperature and nitrous oxide loaded mass, even for a pure component system. Recall that the adherence of nitrous oxide's thermodynamic properties to the Peng-Robinson equation-of-state is an assumption. Also recall that the ideal model determines the vapor pressure of nitrous oxide at a given temperature from a handbook correlation (Perry & Green, Eds., 1997), given that the ideal gas law cannot extract vapor-liquid equilibrium behavior. On the other hand, the Peng-Robinson equation-of-state *predicts* the vapor pressure of the system. Therefore, at a given temperature, the ideal model will provide the correct vapor pressure (experimentally correlated) for a pure nitrous oxide system. So any deviation between the initial vapor pressure predicted by the ideal model and the Peng-Robinson model would indicate that the Peng-Robinson equation-of-state is deviating from the correlated, and thus accepted, nitrous oxide vapor pressure.

Note that the total flow rates are very similar for the ideal and non-ideal models, but in general are closer for the Peng-Robinson model. As the drain progresses, the flow results predicted by the ideal model begin to deviate more from the experimental data at lower fill levels. This interesting behavior has been observed in other data sets, and an explanation is provided in Chapter 6.

Overall, the agreement between the models and the experiments is favorable. However, there are a few issues with the experimental data which needs refinement so that validation of the theoretical models can be completed:

1) The experiments were not repeated. Thus, there are no error bars for the data, and the experimental error cannot be established. Therefore, the goal of predicting the drain histories to within ± 5% cannot be assessed.

2) There is evidence of downstream pressure feedback from the combustion chamber in two of the four tests, which is an unexpected result both intuitively and based on the theoretical results. This finding may indicate that there was cavitation in the feedline

during the experiment. Close experimental observation of the downstream flow should be made to assure that cavitation is not occurring in the system.

3) The tank temperature was not measured inside the draining tank. The initial temperature was assumed to be equal to ambient temperature, which may or may not be accurate given the possibility that thermodynamic filling effects (e.g. cooling through a valve) may have an effect on the temperature; furthermore, there was not a significant amount of time between tank filling and tank draining to allow the tank contents to come to equilibrium with its surroundings. This initial condition, therefore, is not well characterized. The sensitivity studies in Chapter 5 show that the initial temperature has a significant effect on the draining history, and thus, better characterization of the initial temperature is required for validation.

In light of these observations, there is not enough evidence to verify or disprove that the models in this thesis are sufficient to describe the draining tank history to within the desired accuracy. The purpose of these four tests cited above for the Peregrine Project was primarily to study the processes in the combustion chamber, not the pressurization processes of the oxidizer. Testing of the oxidizer delivery system must be more controlled and repeatable, with more measurements of key properties of interest throughout the drain, in order to further determine the legitimacy of the models provided in this thesis. Please refer to Appendix G for a proposal for future experimental testing that targets key parameters of tank draining.

4-4   Other Available Peregrine Project Data

Currently, the pressurization system to be used in the final Peregrine sounding rocket to be launched from NASA Wallops has not been chosen. Zilliac proposed the use of what he calls a "helium-augmented" pressurization system (Zilliac, personal communication, 2009), which is what has been modeled in this thesis. Shown in Figure 1.1 in Chapter 1, this pressurization system is used to avoid cavitation in the oxidizer flow draining from the tank. This is a simple option because the pressurant is added to the oxidizer tank prior to launch and, due to its non-condensable nature, remains present only in the gas phase throughout the entire oxidizer liquid drain.

Another possible pressurization system option includes a separate pressurant (helium) tank that feeds pressurant into the oxidizer tank during draining. This pressurization method has also been used in both small- and large-scale Peregrine ground tests. All of the tests completed to date that have incorporated the use of pressurant have utilized this pressurization method. This data, however, is inadequate to verify the helium-augmented pressurization behavior assumed in the models. The inflow of pressurant to the oxidizer tank during draining will further convolute the physics of the system by forcing more assumptions to be made. For these nitrous oxide/helium tests, the helium tank pressure is monitored, but the temperature is not. The amount of helium being added to the oxidizer tank is not being tracked, and a regulator is present in the helium feedline. However, the regulator is unable to maintain a constant pressure in the oxidizer tank, so the pressure history still decreases in these tests. Thus, the discharge coefficient for the helium feedline into the tank is unknown.

Additionally, the inability to use the data including pressurant prohibits verification of the Peng-Robinson equation-of-state for a nitrous oxide/helium mixture in the Peregrine system. Thus, it is not possible to verify the predicted initial equilibrium state, and this can have a large effect on the subsequent draining of the tank (see sensitivity study in Chapter 5). Therefore, a procedure has been introduced in Appendix G that could guide future experiments required to fully verify the models provided in this study.

CHAPTER 5

SENSITIVITY STUDY

5-1   Introduction

This chapter contains the results of two sensitivity studies. The first is called the "big picture" study. Here, key parameters including temperature, fill-level, and amount of pressurant (helium in this case) were varied over a wide range in order to extract the key behaviors of both the ideal and non-ideal models when pushed to physical extremes. The second is called the "error" sensitivity study. Since the experimental error was not stated for the four tests published in Zilliac and Karabeyoglu (2005), this study assesses how small input deviations affect the model predictions and can give insight into the dominant sources of error likely to be seen in the experiments (of course, assuming that the models accurately capture the behavior of the tank draining process). Another purpose of the error study is to help in the design of future experiments by focusing on measurements that are the most sensitive when assessing the model validity. Note that the big picture study was completed for both the ideal and non-ideal models while the error study was only completed for the non-ideal model.

For each of these studies, only one parameter was varied while keeping the others fixed in order to isolate the effects of that one parameter. This approach was sensible due to the highly nonlinear nature of the governing system of equations; complex interactions between parameters are not only possible but likely. The constant parameters are taken from Test 1 of Zilliac and Karabeyoglu (2005) and are specified in Chapter 4.

5-2   Big Picture Study

The inputs for the "big picture" sensitivity study are as follows. The volume of the tank, V, is 0.0354 m^3. The tank is made of 6061-T6 Aluminum (although pure aluminum properties are used in the models) with a mass, m_T, of 6.4882 kg. The discharge coefficient, C_D, is 0.425, and the total injector area, $A_{injector}$ is 0.0001219352 m^2. The binary interaction parameter, k_{12}, is assumed to be equal to zero (this assumption is examined both in Section 5-3-4 and in Appendix F), and the exit pressure, P_e (labeled as "chamber" pressure in

figures), is a constant $1 \cdot 10^6$ Pa, which was taken as a representative value based on Zilliac and Karabeyoglu (2005). Table 5.1 below shows the sensitivity parameters and corresponding ranges of values investigated. Note that, in the plot legends, "P-R" stands for the Peng-Robinson non-ideal model data.

Sensitivity Parameter	Parameter Range
Initial Fill Level	25%, 50%, 85%
Initial Temperature, T_i	250 K, 270 K, 295 K
Helium moles, nHe	0 kmol, 0.005 kmol, 0.01 kmol

Table 5.1: Parameters varied in "big picture" sensitivity study

Each study consists of five to seven plots showing both the ideal and non-ideal drain histories as a function of time in the following order: temperature, pressure, total nitrous oxide in tank, nitrous oxide liquid in tank, and nitrous oxide vapor in tank. In some cases, the temperature and/or pressure histories were split into separate ideal and non-ideal plots for the sake of clarity. As stated in Section 5-1, all parameters other than the one isolated for study can be found in Section 4-1 of Chapter 4 for Test 1.

Figure 5.2.1a: Theoretical (non-ideal) predictions for the temperature in the draining tank as a function of time, for parameter values as set in Section 5-2 for the initial fill-level "big picture" sensitivity study.
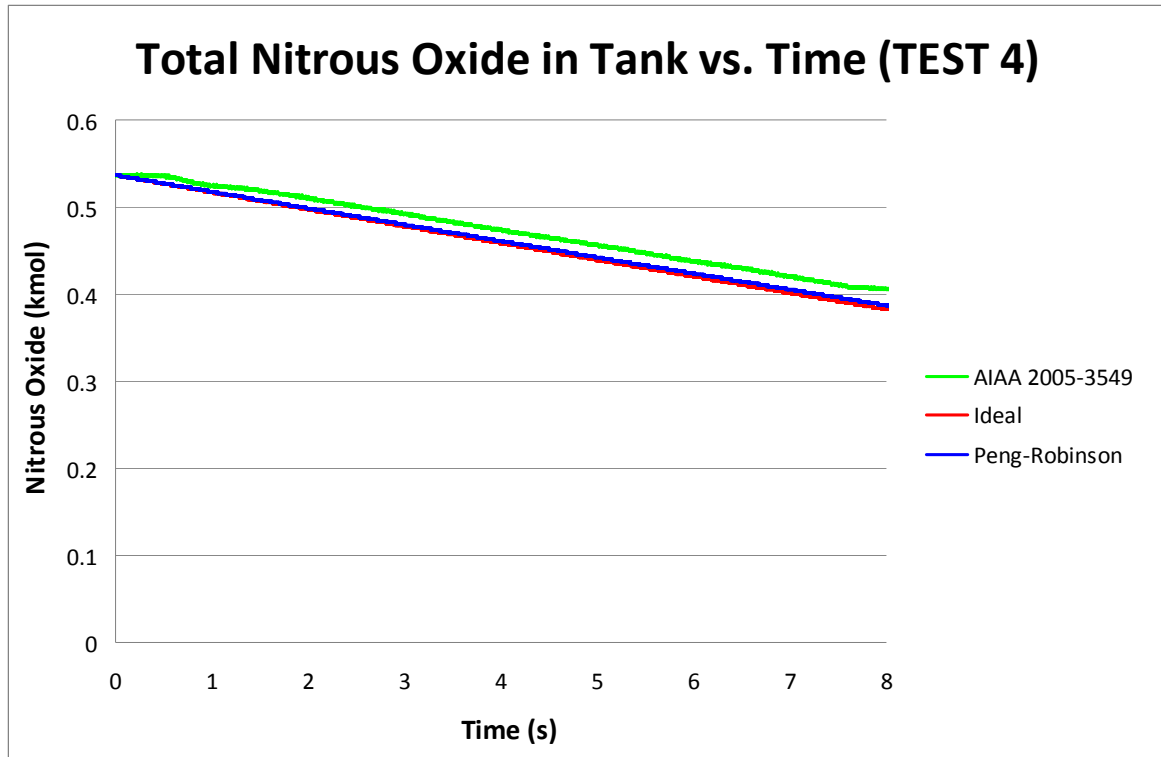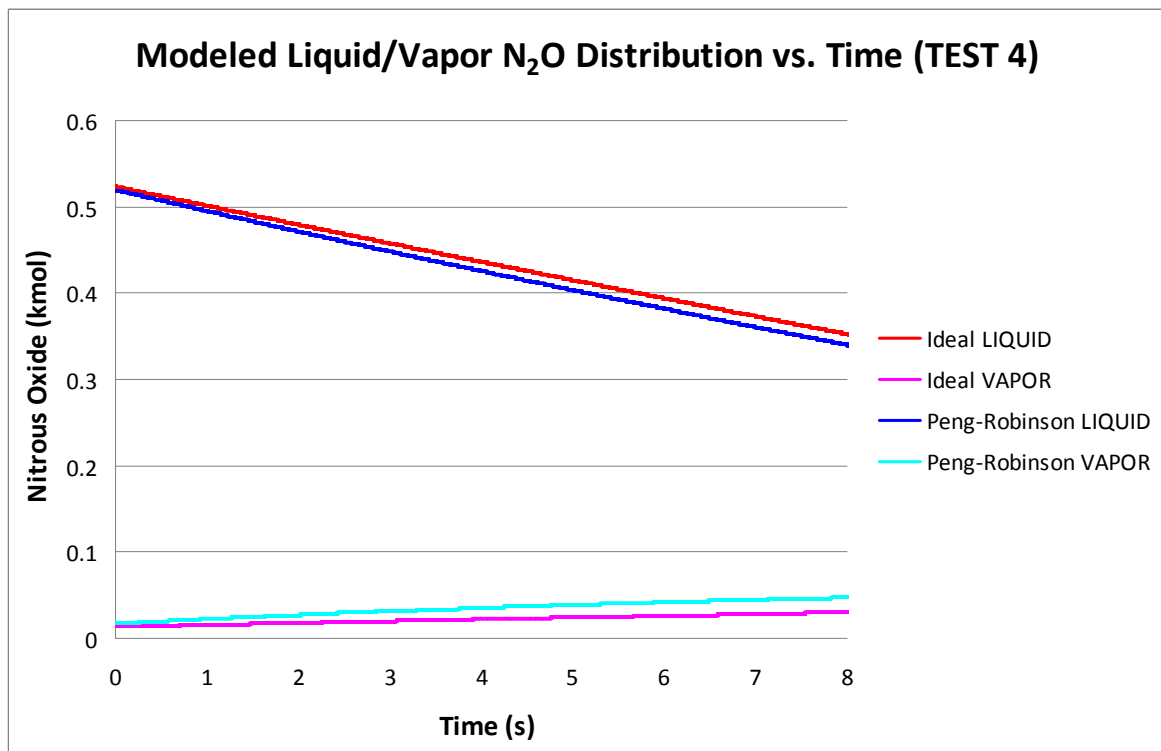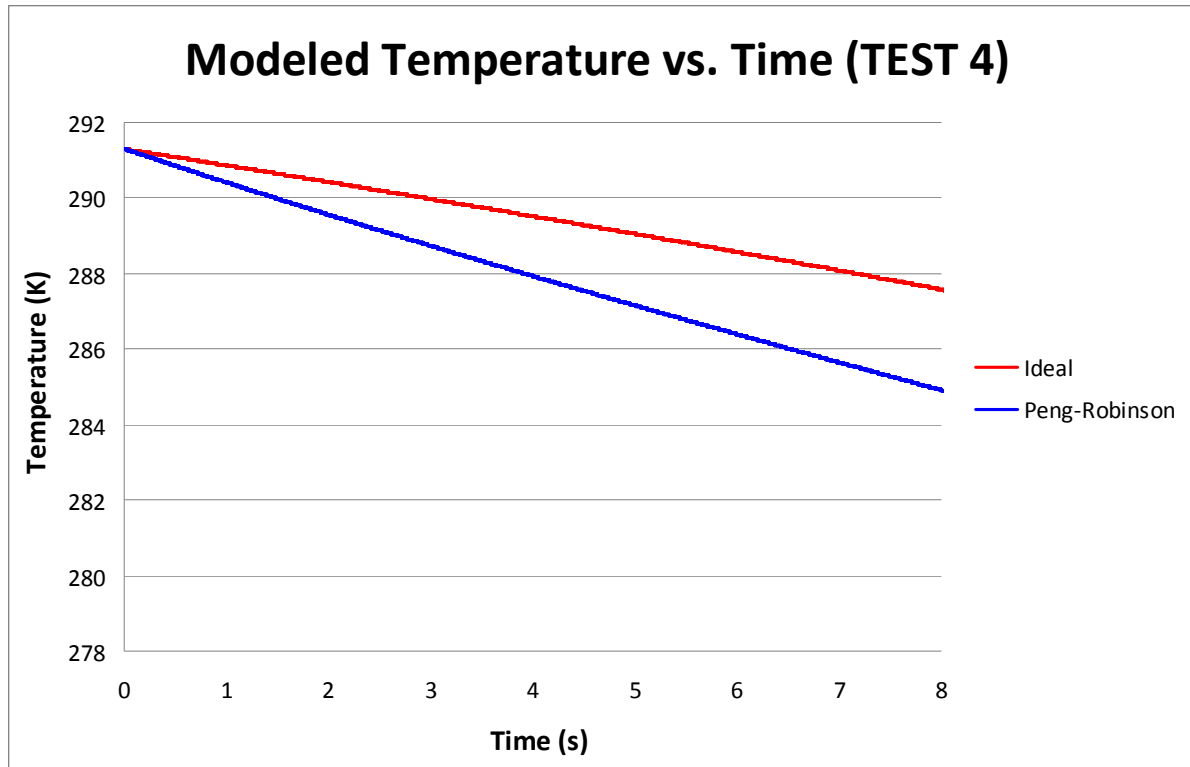

Figure 5.2.1b: Theoretical (ideal) predictions for the temperature in the draining tank as a function of time, for parameter values as set in Section 5-2 for the initial fill-level "big picture" sensitivity study.

Figure 5.2.1c: Theoretical (non-ideal) predictions for the absolute pressure in the draining tank as a function of time, for parameter values as set in Section 5-2 for the initial fill-level "big picture" sensitivity study.

Figure 5.2.1d: Theoretical (ideal) predictions for the absolute pressure in the draining tank as a function of time, for parameter values as set in Section 5-2 for the initial fill-level "big picture" sensitivity study.

Figure 5.2.1e: Theoretical (ideal, non-ideal) predictions for the total moles of nitrous oxide in the draining tank as a function of time, for parameter values as set in Section 5-2 for the initial fill-level "big picture" sensitivity study.

Figure 5.2.1f: Theoretical (ideal, non-ideal) predictions for the moles of nitrous oxide liquid in the draining tank as a function of time, for parameter values as set in Section 5-2 for the initial fill-level "big picture" sensitivity study.

Figure 5.2.1g: Theoretical (ideal, non-ideal) predictions for the moles of nitrous oxide vapor in the draining tank as a function of time, for parameter values as set in Section 5-2 for the initial fill-level "big picture" sensitivity study.

In this study, the number of moles necessary to fill the tank completely with nitrous oxide liquid was determined; no helium is present in the tank. The percent-fill is the corresponding percent of that maximum amount of liquid moles, not the liquid fill level after evaporation and equilibrium is achieved for the given initial temperature in the tank. The percent liquid fill-level, however, will be close but slightly more than the fill level used here due to this evaporation of liquid to saturate the gas phase.

Note the initial pressure in both models is not dependent on fill-level since the initial temperature is the same, and the saturated pressure in the tank is only dependent on temperature. However, as stated in Chapter 4, the initial pressure for the ideal model is slightly different than the non-ideal model for a pure component system, indicating that the Peng-Robinson equation-of-state is not extracting the exact vapor pressure of nitrous oxide at the given initial temperature (for pure-component systems, the vapor pressure extracted from the Peng-Robinson equation-of-state should agree with the empirically measured vapor pressure used in the ideal model). Note that the temperature and pressure histories for the non-ideal model are reasonably linear (Figures 5.2.1a,c) while the histories for the ideal

41

model are more curved (Figure 5.2.1b,d). As the slopes of the lines in Figure 5.2.1e are essentially parallel, the total and liquid molar flow rates are nearly identical for all fill-levels. Furthermore, the slopes do not seem to be affected by the ideal versus non-ideal model. However, the distribution between liquid and vapor deviates more at lower fill-levels when comparing the ideal to the non-ideal models. This indicates that the non-ideality (and thus the equation-of-state) affects the gas phase more than the liquid phase because the liquid is not as compressible; consequently, when the gas phase is a larger percent of the whole system at low fill levels and at longer drain times, it has a larger effect on the draining history. It is very interesting that this difference in gas/liquid phase distribution between the two models is mostly evident in the total flow history (Figure 5.2.1e) in the drain time and *not* in the flow rate itself (i.e., the slopes of the ideal and non-ideal curves are very similar).

5-2-2   Initial Temperature Study

Figure 5.2.2a: Theoretical (ideal, non-ideal) predictions for the temperature in the draining tank as a function of time, for parameter values as set in Section 5-2 for the initial temperature "big picture" sensitivity study.

Figure 5.2.2b: Theoretical (ideal, non-ideal) predictions for the absolute pressure in the draining tank as a function of time, for parameter values as set in Section 5-2 for the initial temperature "big picture" sensitivity study.

Figure 5.2.2c: Theoretical (ideal, non-ideal) predictions for the total moles of nitrous oxide in the draining tank as a function of time, for parameter values as set in Section 5-2 for the initial temperature "big picture" sensitivity study.

43

Figure 5.2.2d: Theoretical (ideal, non-ideal) predictions for the moles of nitrous oxide liquid in the draining tank as a function of time, for parameter values as set in Section 5-2 for the initial temperature "big picture" sensitivity study.

Figure 5.2.2e: Theoretical (ideal, non-ideal) predictions for the moles of nitrous oxide vapor in the draining tank as a function of time, for parameter values as set in Section 5-2 for the initial temperature "big picture" sensitivity study.

44

This study was performed with pure nitrous oxide; no helium is in the tank. Note that temperature and pressure histories (Figures 5.2.2a,b) are very close at low initial temperatures and differ a little more at higher temperatures. The total and liquid nitrous oxide histories (flow rates and drain times) in Figures 5.2.2c,d appear to be closer at higher initial temperatures than at lower temperatures. Also note that there is more divergence between the ideal and non-ideal nitrous oxide vapor histories at higher initial temperatures (Figure 5.2.2e). The temperature, pressure and nitrous oxide drain histories (Figures 5.2.2a,b,e) indicate, as expected, that the ideal model will diverge from the Peng-Robinson model at high pressures, and thus at high temperatures close to the critical point. However, the total and liquid nitrous oxide drain histories (Figures 5.2.2c,d) indicate unexpectedly that the ideal and non-ideal models diverge at lower initial temperatures.

5-2-3   Helium Study
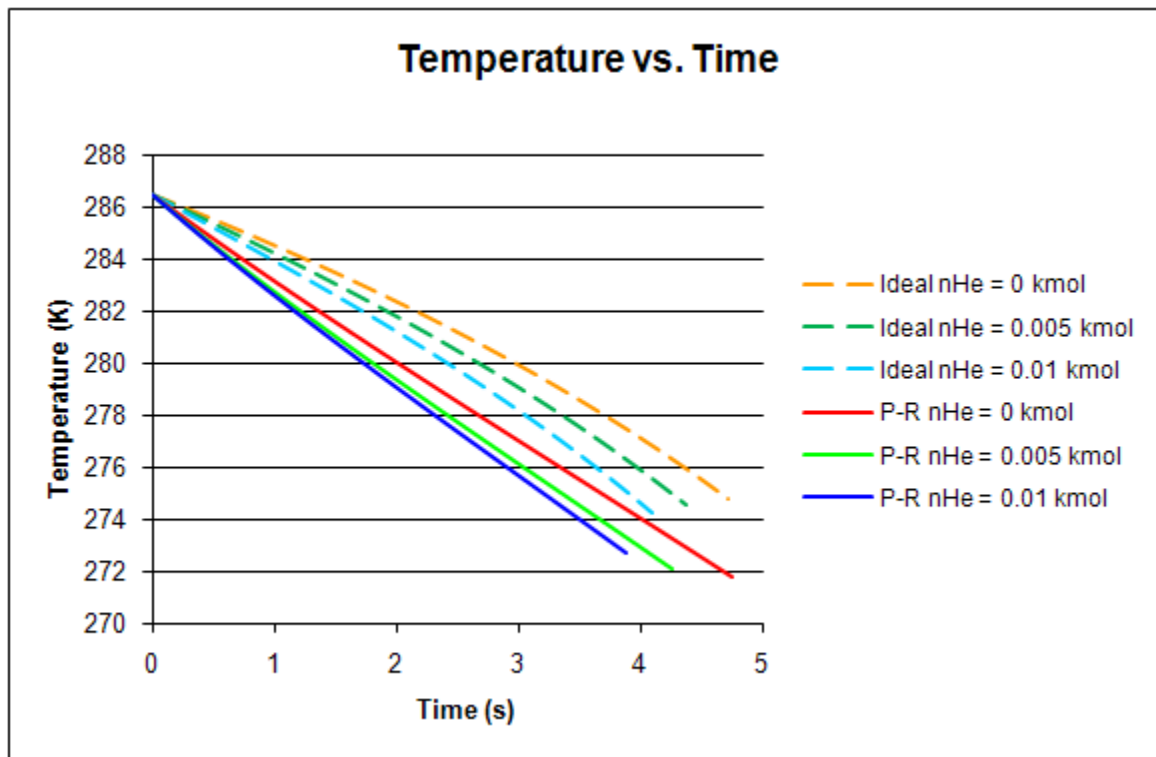
Figure 5.2.3a: Theoretical (ideal, non-ideal) predictions for the temperature in the draining tank as a function of time, for parameter values as set in Section 5-2 for the helium "big picture" sensitivity study.
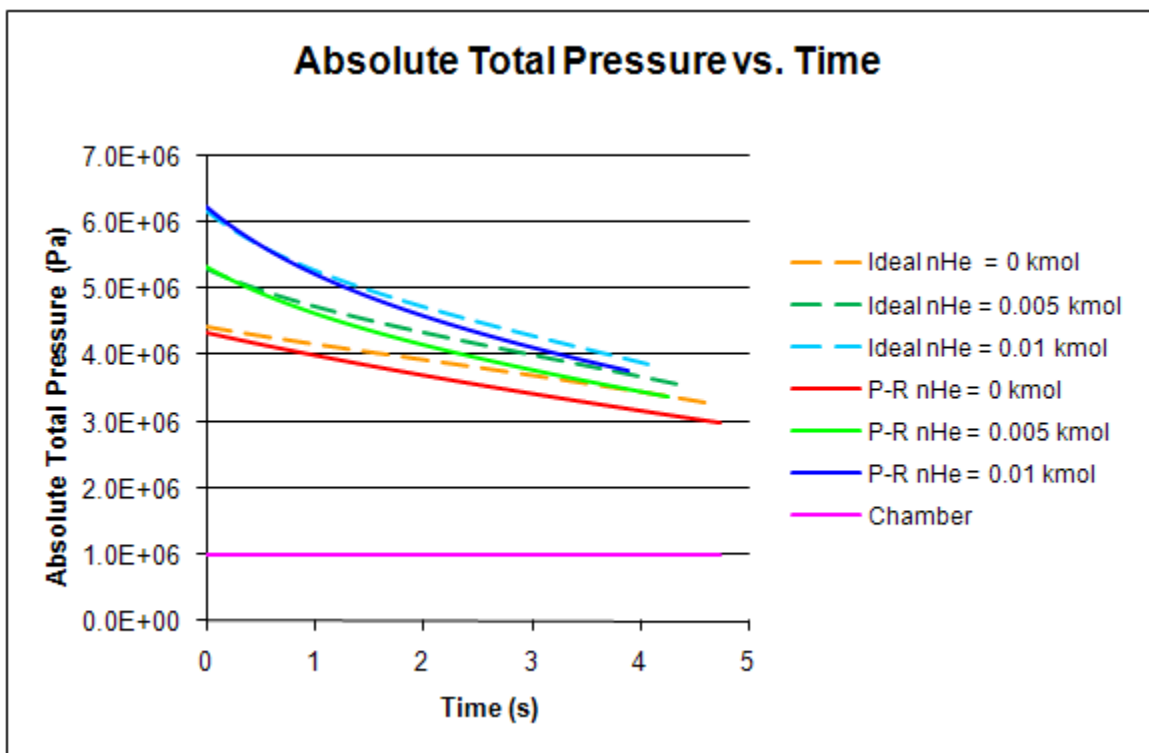
Figure 5.2.3b: Theoretical (ideal, non-ideal) predictions for the absolute total pressure in the draining tank as a function of time, for parameter values as set in Section 5-2 for the helium "big picture" sensitivity study.
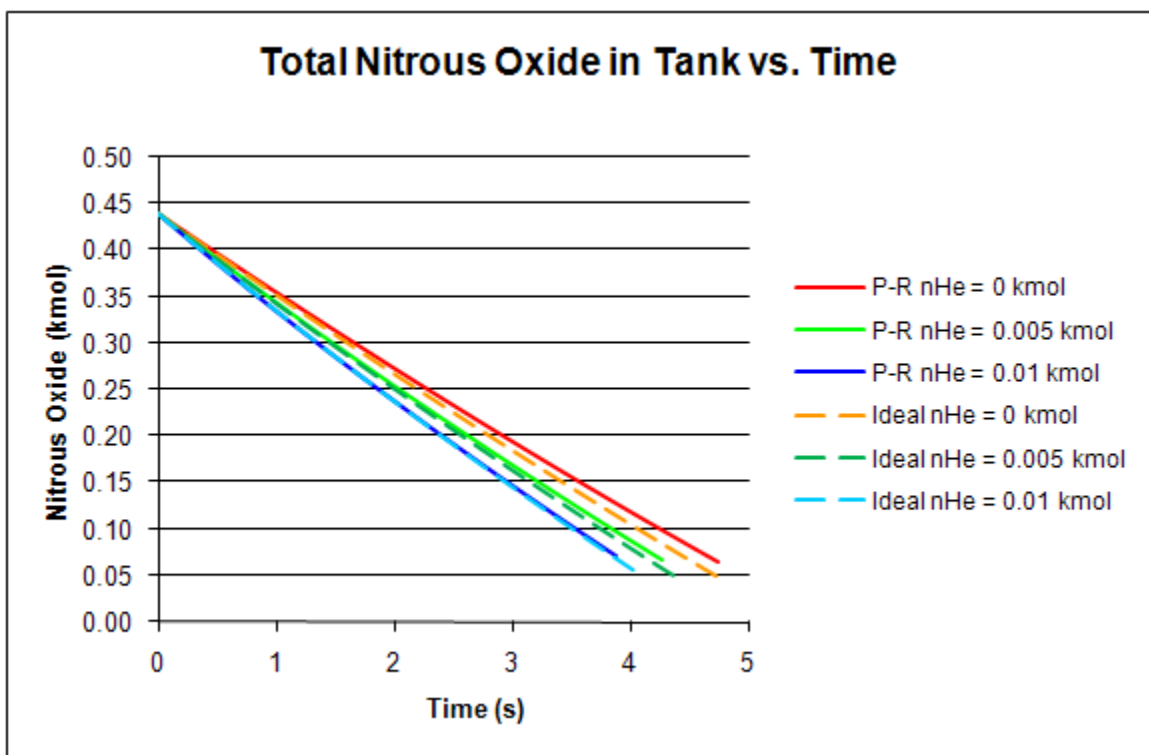
Figure 5.2.3c: Theoretical (ideal, non-ideal) predictions for the total moles of nitrous oxide in the draining tank as a function of time, for parameter values as set in Section 5-2 for the helium "big picture" sensitivity study.

Figure 5.2.3d: Theoretical (ideal, non-ideal) predictions for the moles of nitrous oxide liquid in the draining tank as a function of time, for parameter values as set in Section 5-2 for the helium "big picture" sensitivity study.

Figure 5.2.3e: Theoretical (ideal, non-ideal) predictions for the moles of nitrous oxide vapor in the draining tank as a function of time, for parameter values as set in Section 5-2 for the helium "big picture" sensitivity study.

47

As seen in the previous two studies, the temperature and pressure histories (Figures 5.2.3a,b) of the Peng-Robinson model are quite linear, while the ideal model is more curved. The previous two parameter studies were for pure nitrous oxide in the tank; the effect of helium addition is now introduced in this study. Note that the drain times diverge more between ideal and non-ideal at higher helium amounts (Figure 5.2.3d), but the total nitrous oxide history is close for both models. Also note how the ideal model predicts the same distribution of nitrous oxide into the liquid and gas phases, regardless of how much helium is added to the tank (Figures 5.2.3d,e). This is a result of the ideal equilibrium constraint, Raoult's Law, where the partial pressure of nitrous oxide is defined to be equal to the pure-component vapor pressure of nitrous oxide. Therefore, the amount of helium present in the tank has no bearing on the nitrous oxide distribution.

An interesting result observed in this data trend is that, for the Peng-Robinson model, more helium added leads to *more* nitrous oxide in the gas phase (Figure 5.2.3e). If this trend is taken to its limit, it predicts that for a given amount of nitrous oxide in liquid-vapor equilibrium at a given temperature, if enough helium is added to the tank, all the nitrous oxide will be vaporized, and liquid-vapor equilibrium will no longer exist in the tank. The same trend does not occur in the ideal gas model. It should be noted that the opposite extreme is impossible: that is, there must always be some nitrous oxide in the gas phase. It would appear from this finding that adding helium to a closed tank of nitrous oxide in vapor-liquid equilibrium at a specified temperature has an effect similar to adding heat to that same tank of pure nitrous oxide. In both cases, eventually all the liquid will vaporize. Indeed, adding helium to the tank does add internal energy to the tank, and it is possible that the non-ideal interactions do impart energy to the nitrous oxide to induce further vaporization. All this is coupled through nonlinearities in the Peng-Robinson gas phase through mixing rules, which are empirically based. While it is clear that this is the physical limit that the Peng-Robinson model is achieving for increasing amounts of helium added to the tank, experiments are required to verify this predicted trend, and existing data is not available at this time.

5-3   Error Study

The inputs for the "error" sensitivity study are as follows. Each study is a pure-component nitrous oxide system with no helium added. The volume of the tank is 0.0354 m^3. The tank is made of 6061-T6 Aluminum (although pure aluminum properties are used in the models) with a mass of 6.4882 kg. The total injector area is 0.0001219352 m^2, and the exit pressure (labeled as "chamber" pressure in figures) is a constant $1 \cdot 10^6$ Pa, which was taken as a representative value based on Zilliac and Karabeyoglu (2005). Table 5.2 below shows the sensitivity parameters (initial temperature, T_i, initial nitrous oxide mass loaded, m_{loaded}, discharge coefficient, C_D, binary interaction parameter, k_{12}, and the nitrous oxide and helium critical constants found in two different sources) and corresponding ranges of values investigated.

Sensitivity parameter	Parameter Range
T_i	286.5 K ± 3 K
m_{loaded}	19.32933 kg ± 3.5%
C_D	0.425 ± 5%
k_{12}	0, -0.02, 0.136
Critical Constants	Sandler (2006), Perry's Handbook (1997)

Table 5.2: Parameters used in error sensitivity study

Each study consists of five plots showing the non-ideal drain histories as a function of time in the following order: temperature, pressure, total nitrous oxide in tank, nitrous oxide liquid in tank, and nitrous oxide vapor in tank. As stated in Section 5-1, all parameters other than the one isolated for study can be found in Section 4-1 of Chapter 4 for Test 1.

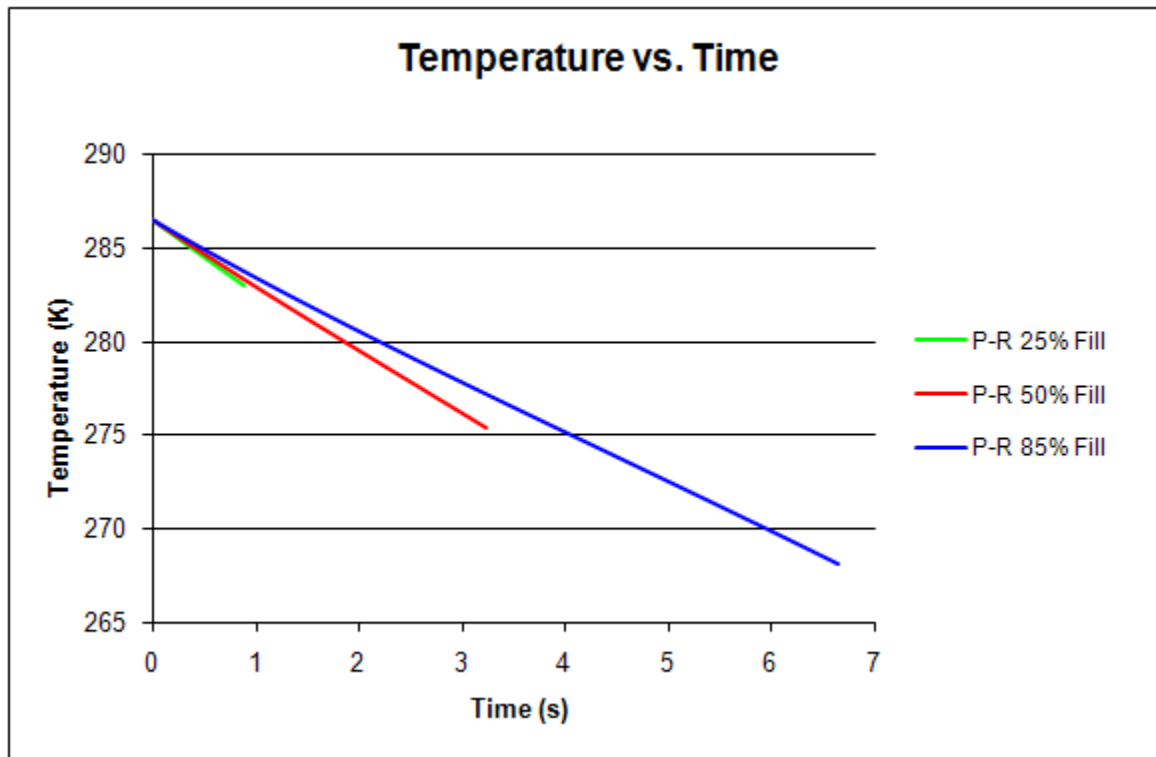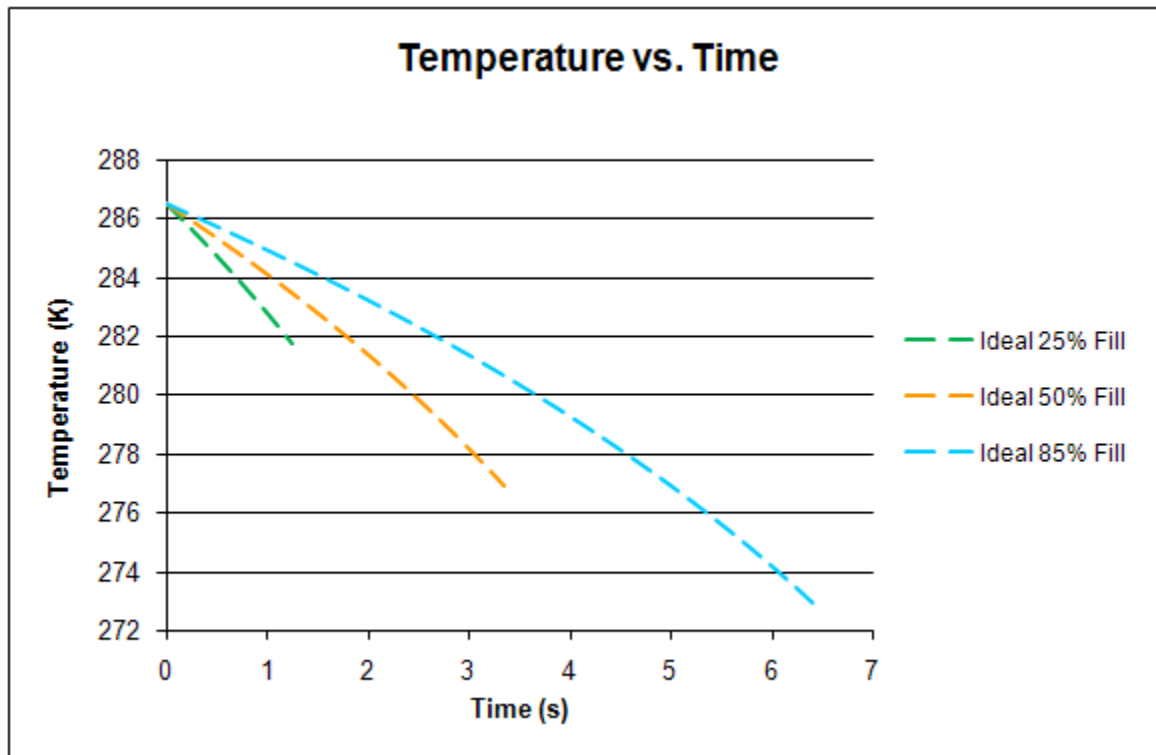## 5-3-1 Initial Nitrous Oxide Mass Loaded Study

Figure 5.3.1a: Theoretical (non-ideal) predictions for the temperature in the draining tank as a function of time, for parameter values as set in Section 5-3 for the initial N_2O mass loaded "error" sensitivity study.
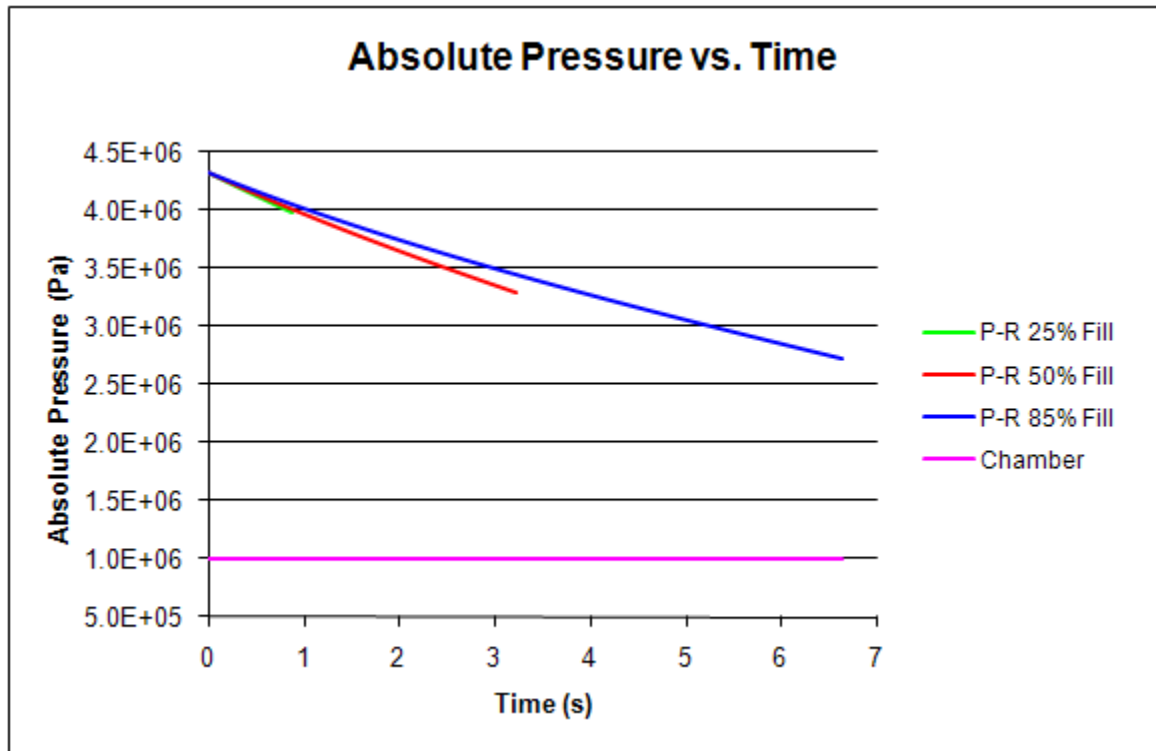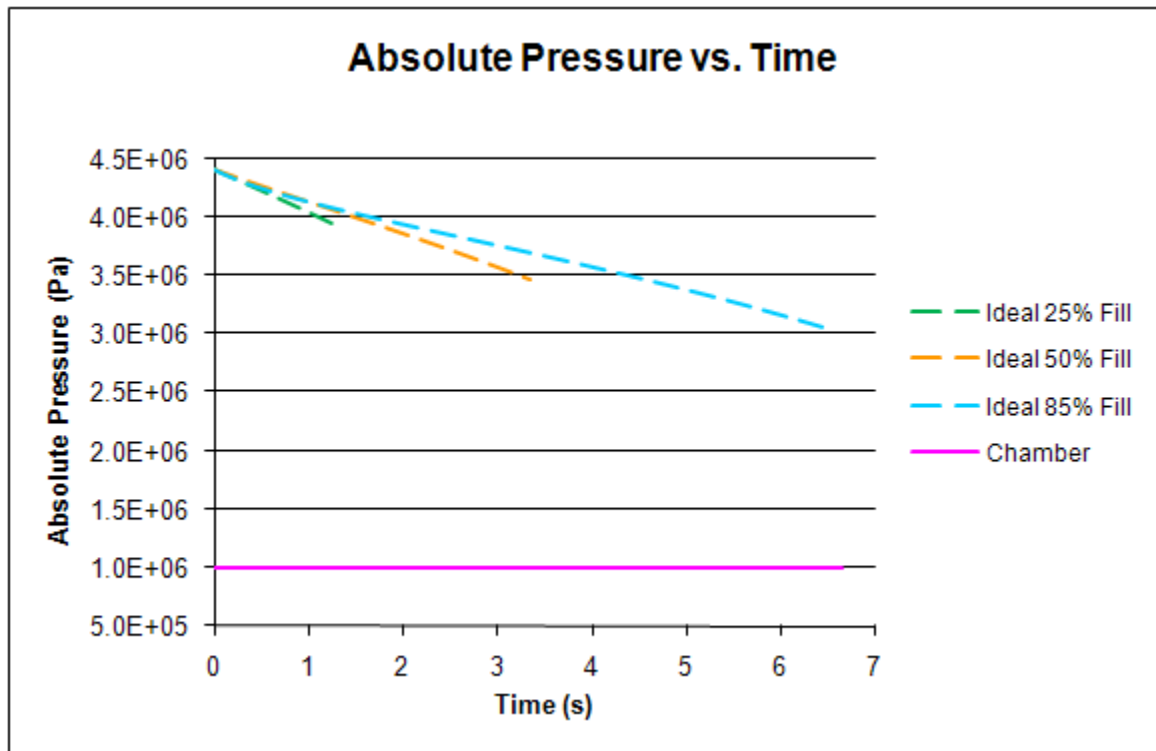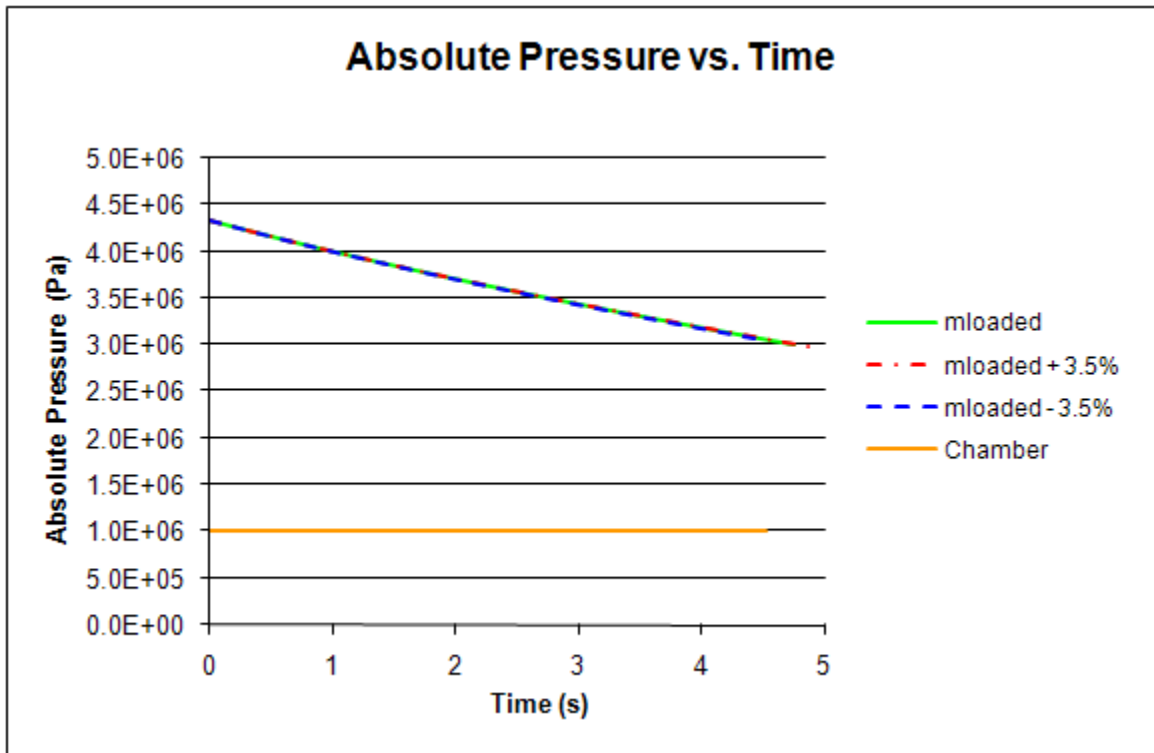

Figure 5.3.1b: Theoretical (non-ideal) predictions for the absolute pressure in the draining tank as a function of time, for parameter values as set in Section 5-3 for the initial N_2O mass loaded "error" sensitivity study.
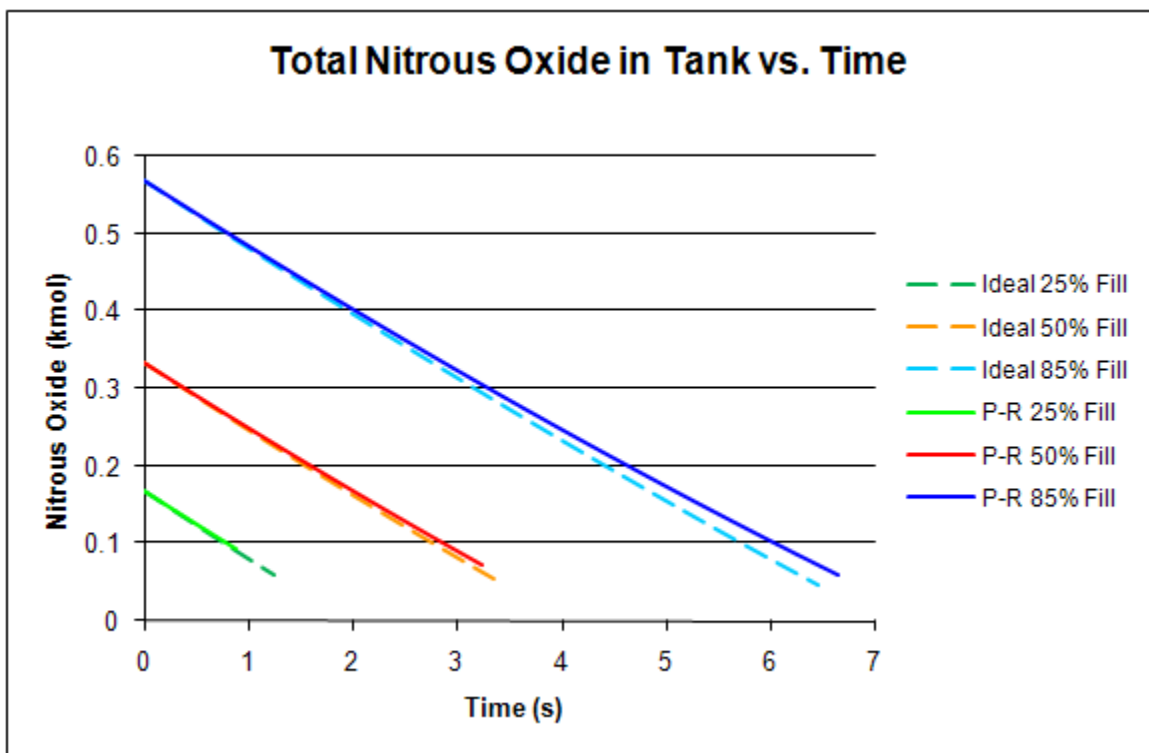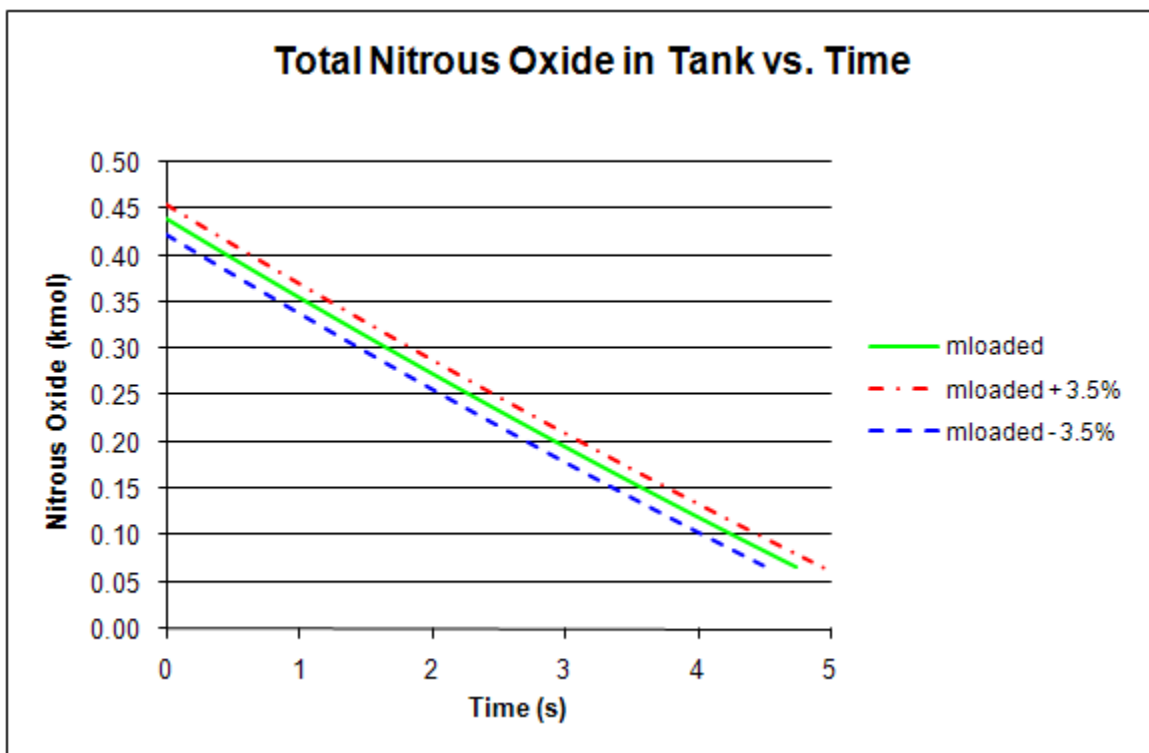
Figure 5.3.1c: Theoretical (non-ideal) predictions for the total moles of nitrous oxide in the draining tank as a function of time, for parameter values as set in Section 5-3 for the initial N_2O mass loaded "error" sensitivity study.
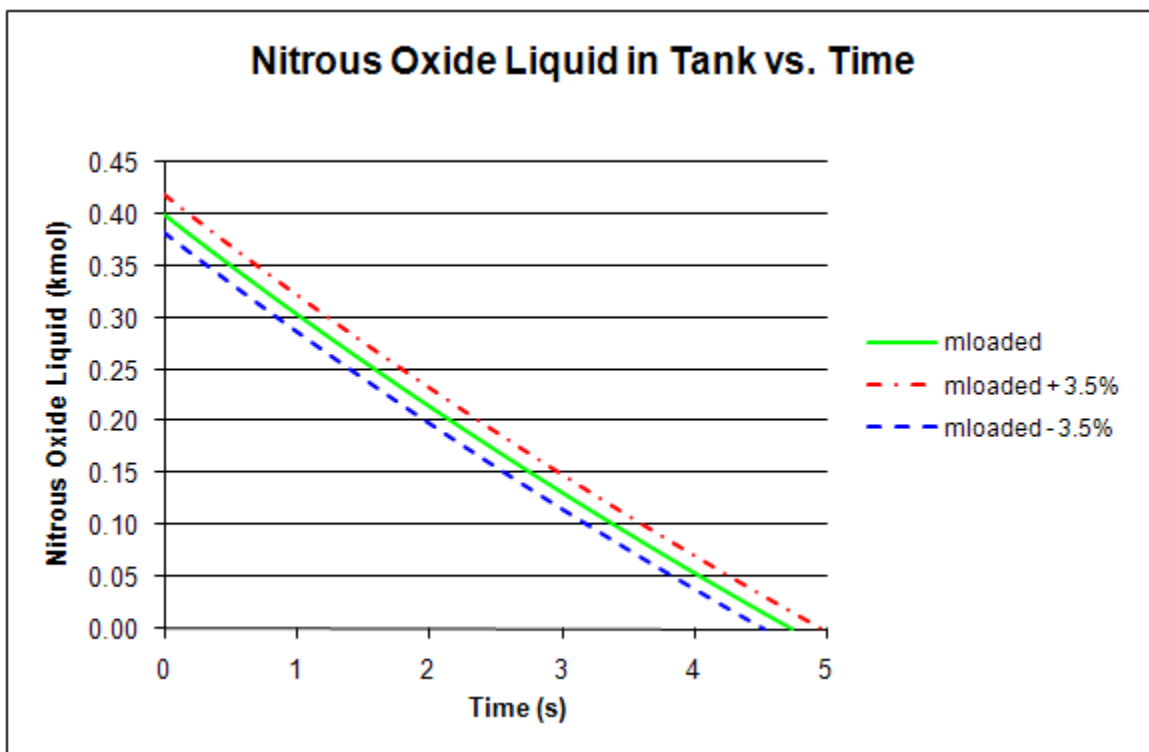
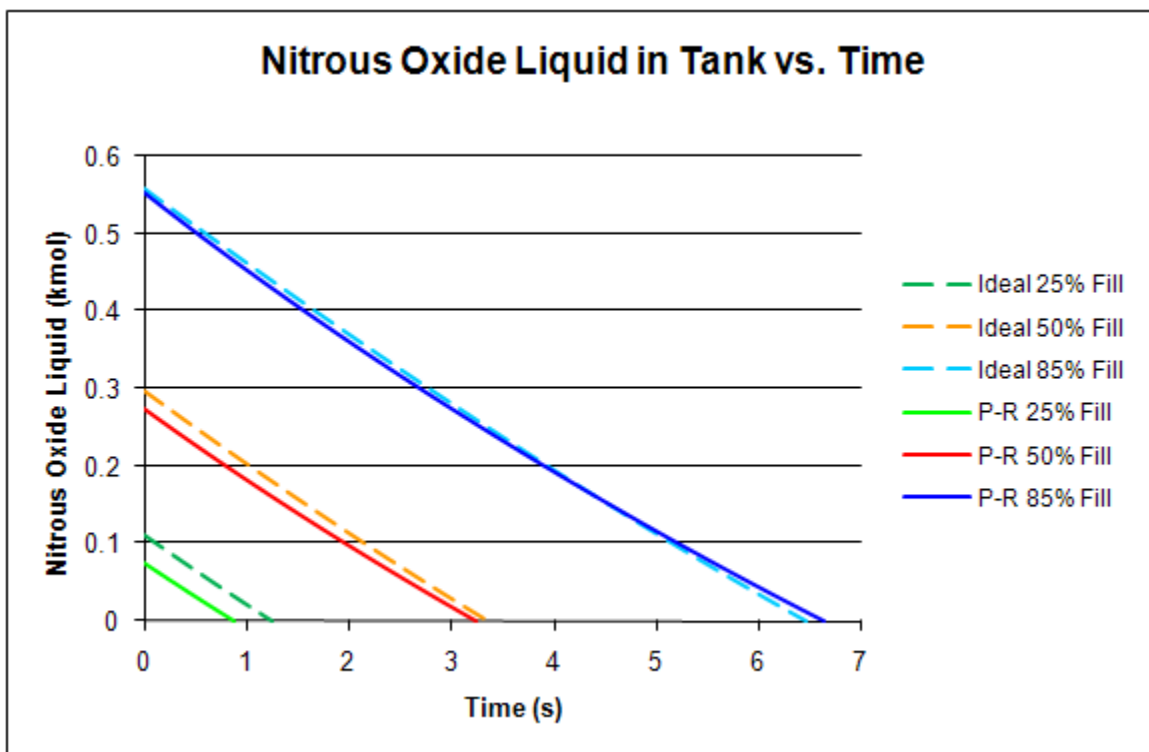

Figure 5.3.1d: Theoretical (non-ideal) predictions for the moles of nitrous oxide liquid in the draining tank as a function of time, for parameter values as set in Section 5-3 for the initial N_2O mass loaded "error" sensitivity study.
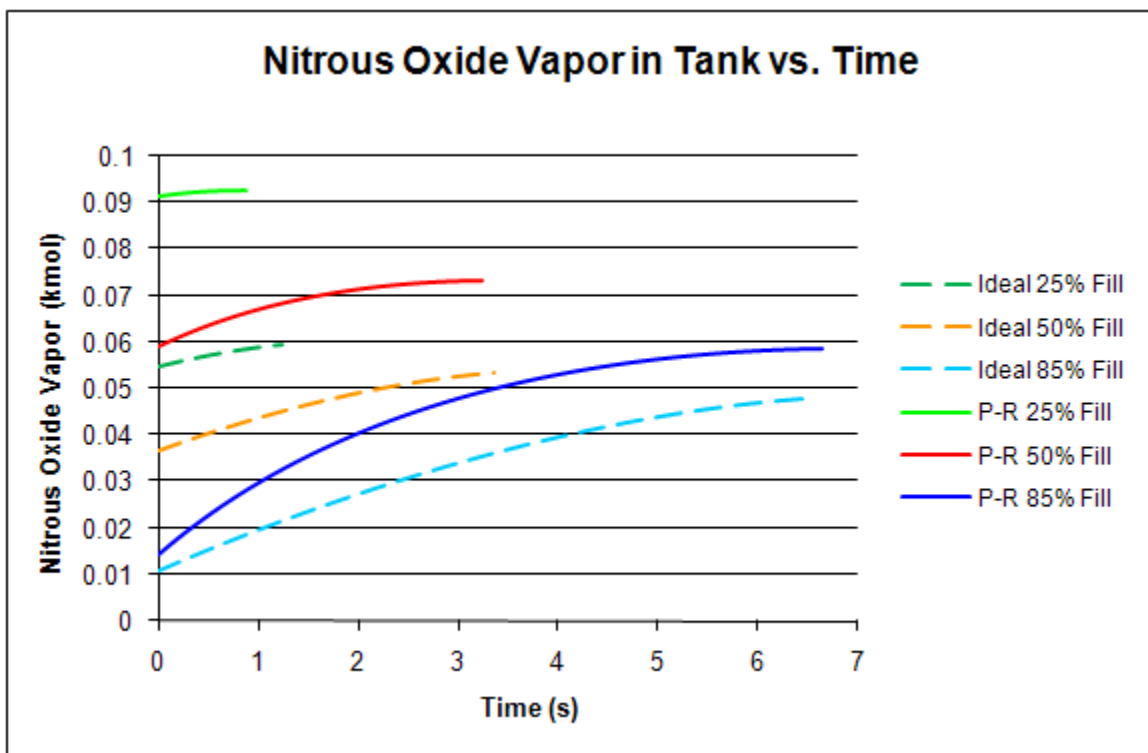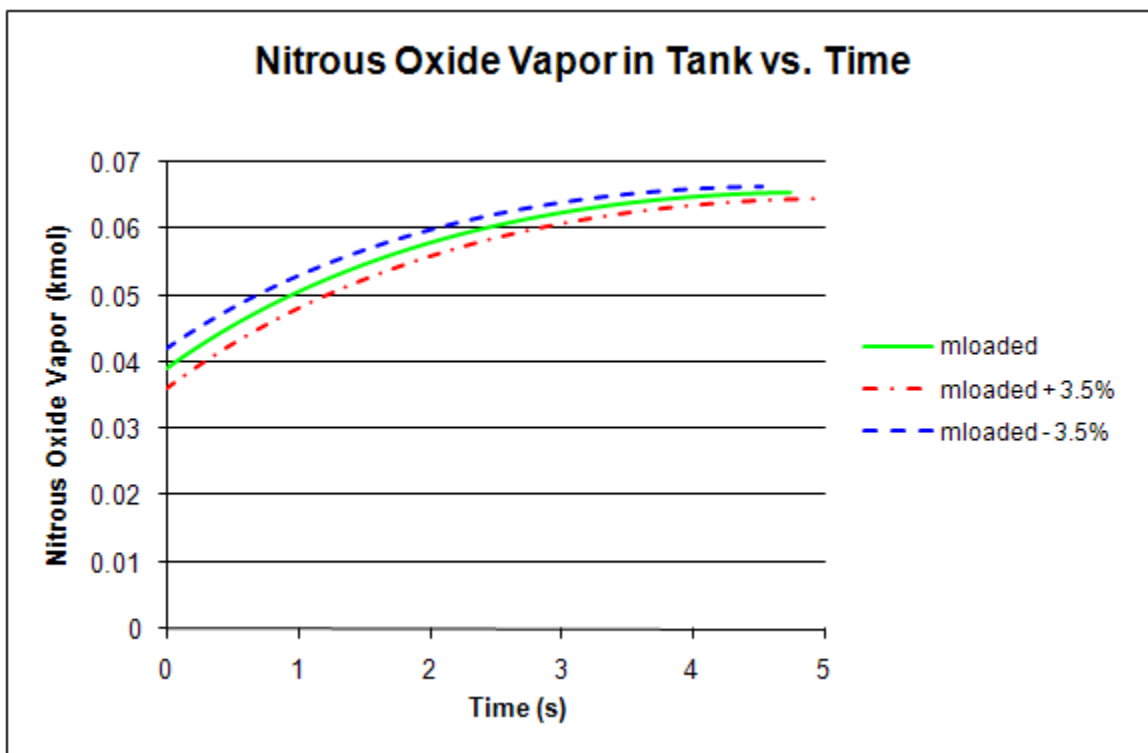
Figure 5.3.1e: Theoretical (non-ideal) predictions for the moles of nitrous oxide vapor in the draining tank as a function of time, for parameter values as set in Section 5-3 for the initial N_2O mass loaded "error" sensitivity study.

This study revealed some interesting results. Mainly, a 3.5% difference in loaded nitrous oxide mass made a difference in liquid drain time of approximately 0.224 seconds while hardly affecting the temperature or pressure histories. This is an approximate 4.7% error in drain time. This suggests that a small error in measured mass loaded would not show up in the temperature or pressure histories, nor in the nitrous oxide flow rate, but would be evident in the nitrous oxide drain time. This suggests that experimental measurements should be focused on liquid level in the tank if an accurate drain time is desired. Considering that the goal for model accuracy was supposed to be within 5% of experiment, a 3.5% error in mass would expend almost the entire available error budget.
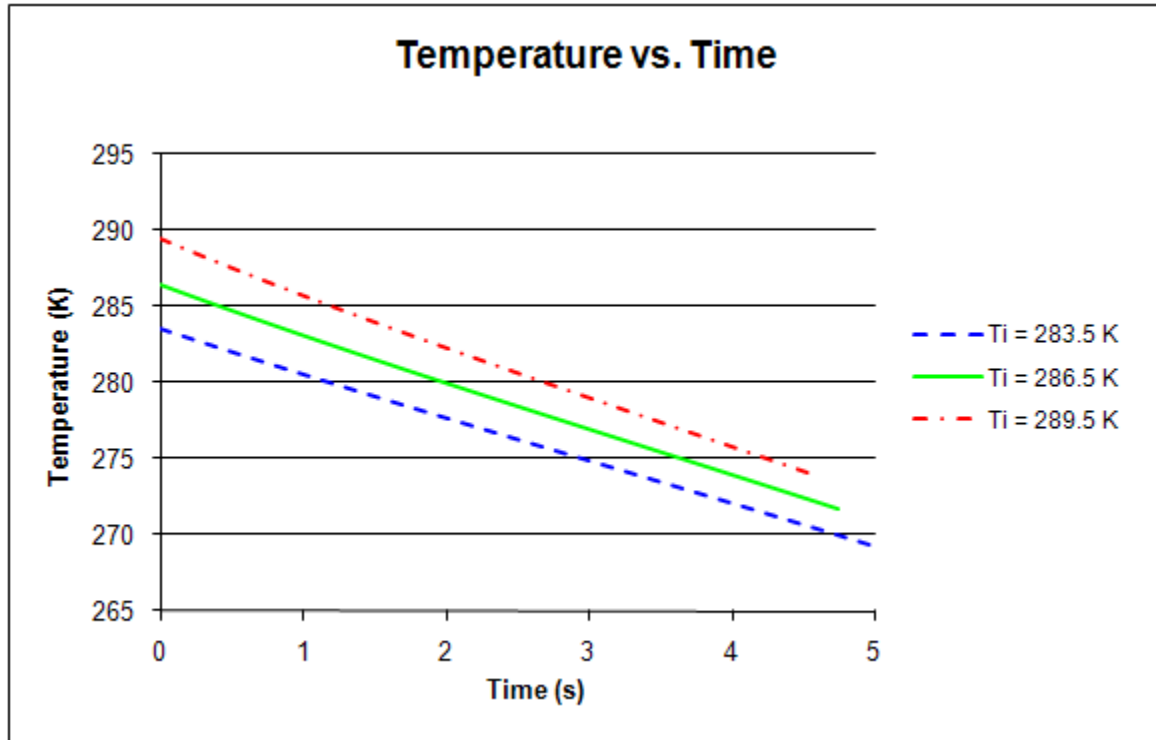
Figure 5.3.2a: Theoretical (non-ideal) predictions for the temperature in the draining tank as a function of time, for parameter values as set in Section 5-3 for the initial temperature "error" sensitivity study.
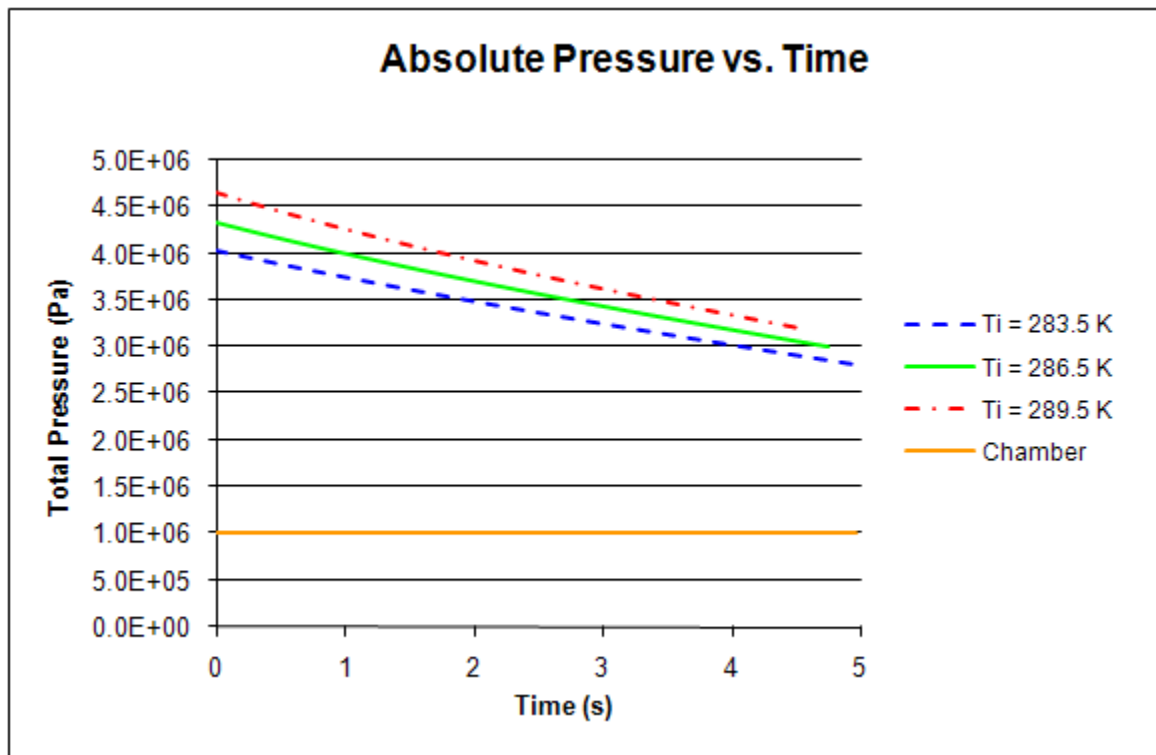
Figure 5.3.2b: Theoretical (non-ideal) predictions for the absolute pressure in the draining tank as a function of time, for parameter values as set in Section 5-3 for the initial temperature "error" sensitivity study.
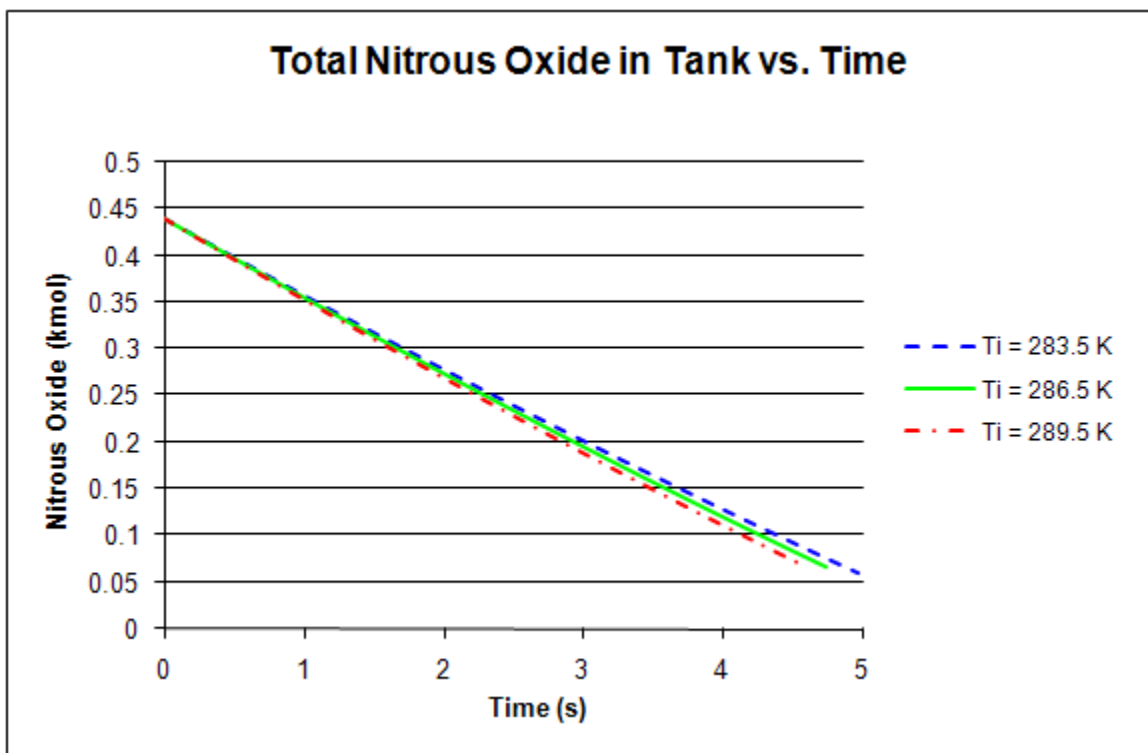
Figure 5.3.2c: Theoretical (non-ideal) predictions for the total moles of nitrous oxide in the draining tank as a function of time, for parameter values as set in Section 5-3 for the initial temperature "error" sensitivity study.
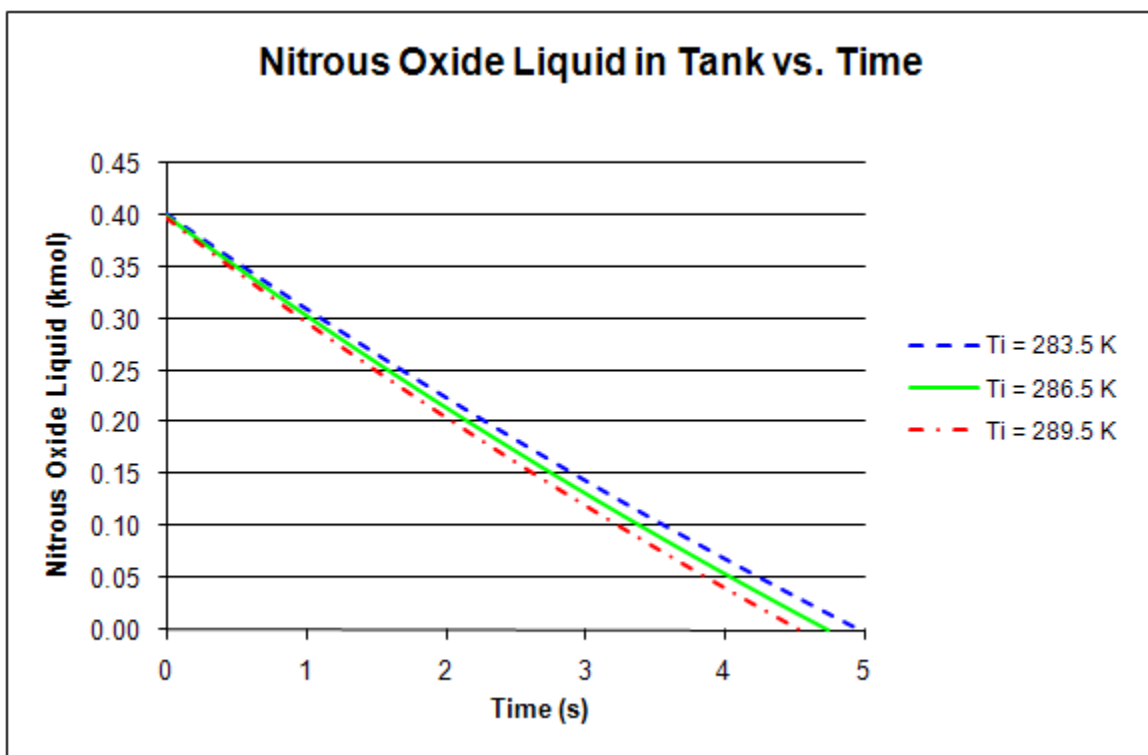
Figure 5.3.2d: Theoretical (non-ideal) predictions for the moles of nitrous oxide liquid in the draining tank as a function of time, for parameter values as set in Section 5-3 for the initial temperature "error" sensitivity study.
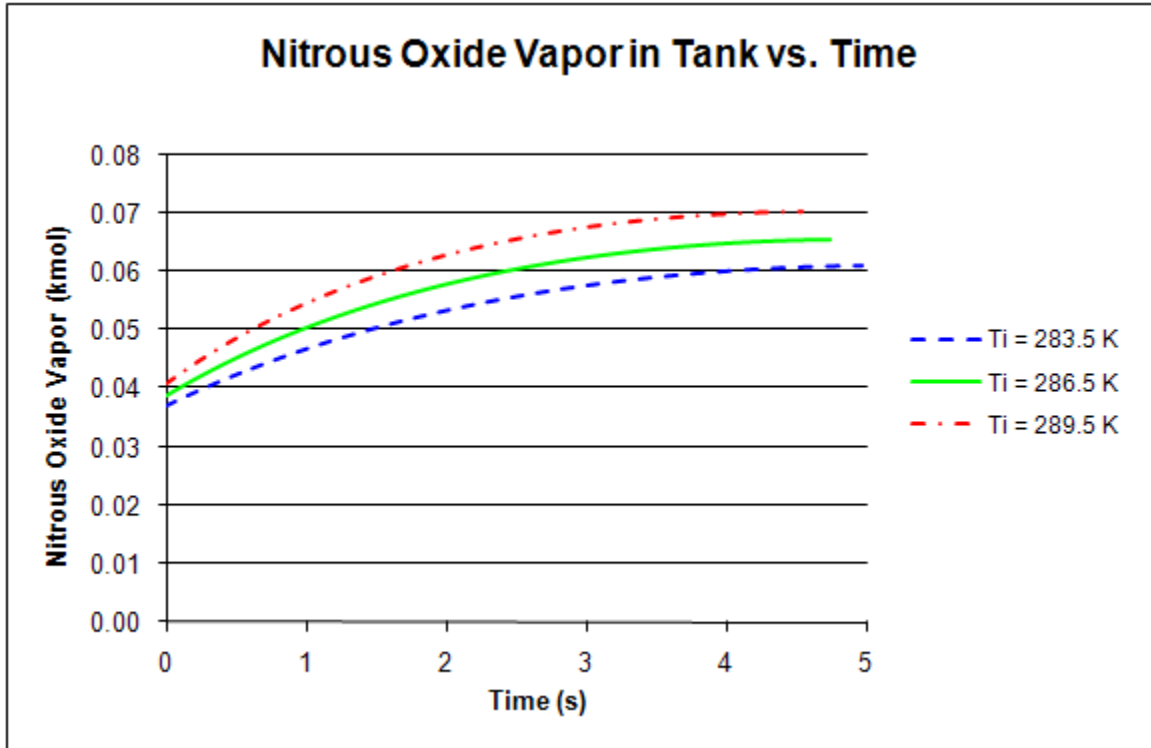
Figure 5.3.2e: Theoretical (non-ideal) predictions for the moles of nitrous oxide vapor in the draining tank as a function of time, for parameter values as set in Section 5-3 for the initial temperature "error" sensitivity study.

Note that a 3 K difference in T_i makes an approximately 317,000 Pa difference in initial pressure, which is an approximate 7.3% error. It also makes a difference in draining time of approximately 0.226 seconds, which is an approximate 4.8% error. These results indicate that the initial temperature must be measured quite accurately to minimize the variations in the model predictions to below 5%, the total error budget specified at the beginning of this work.

5-3-3   Discharge Coefficient Study
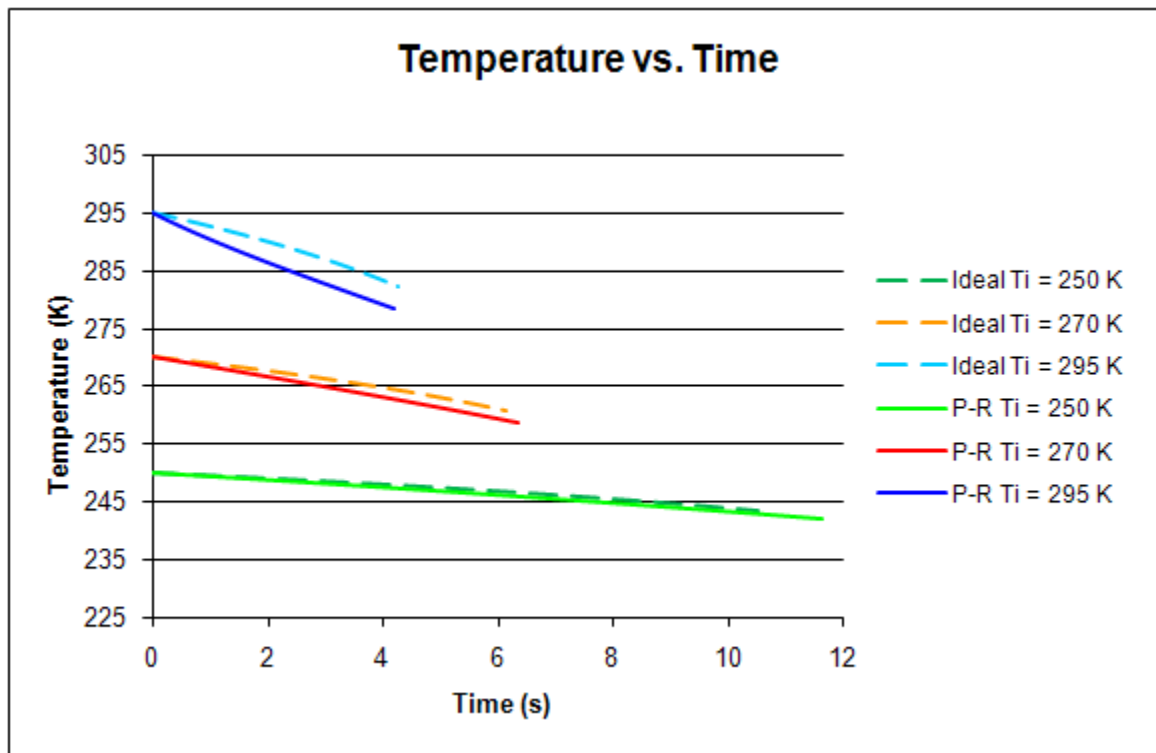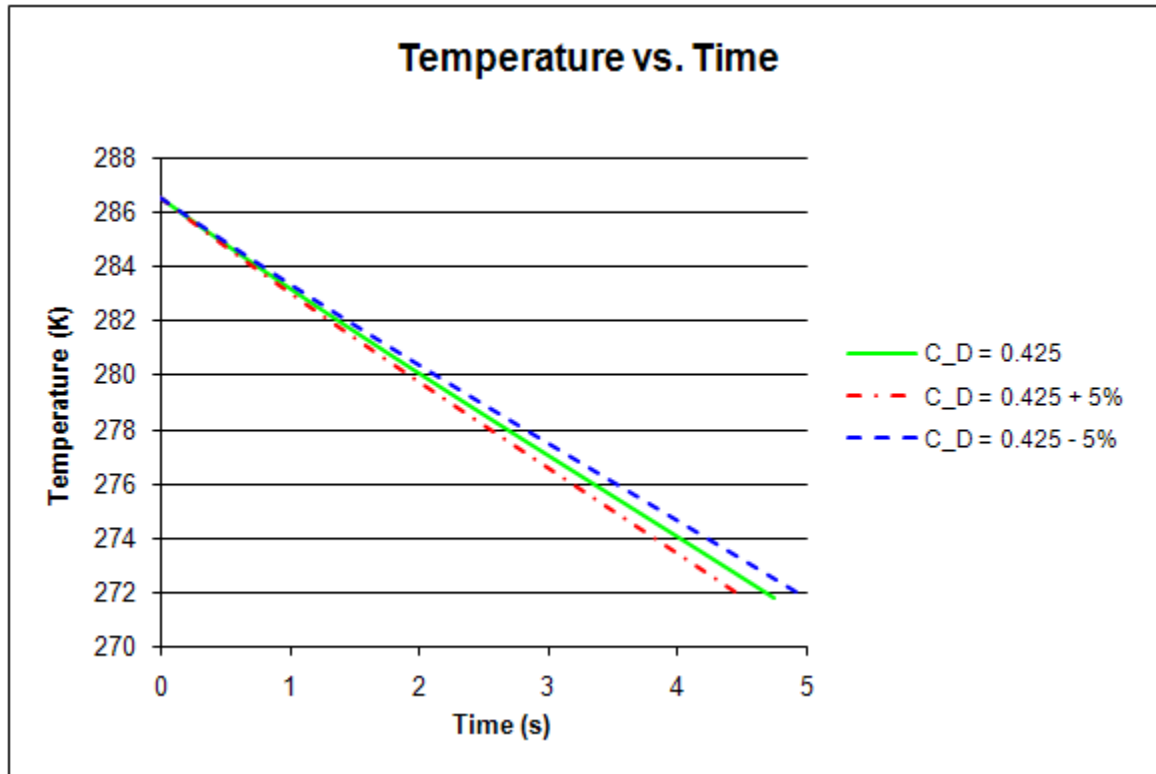

Figure 5.3.3a: Theoretical (non-ideal) predictions for the temperature in the draining tank as a function of time, for parameter values as set in Section 5-3 for the discharge coefficient "error" sensitivity study.
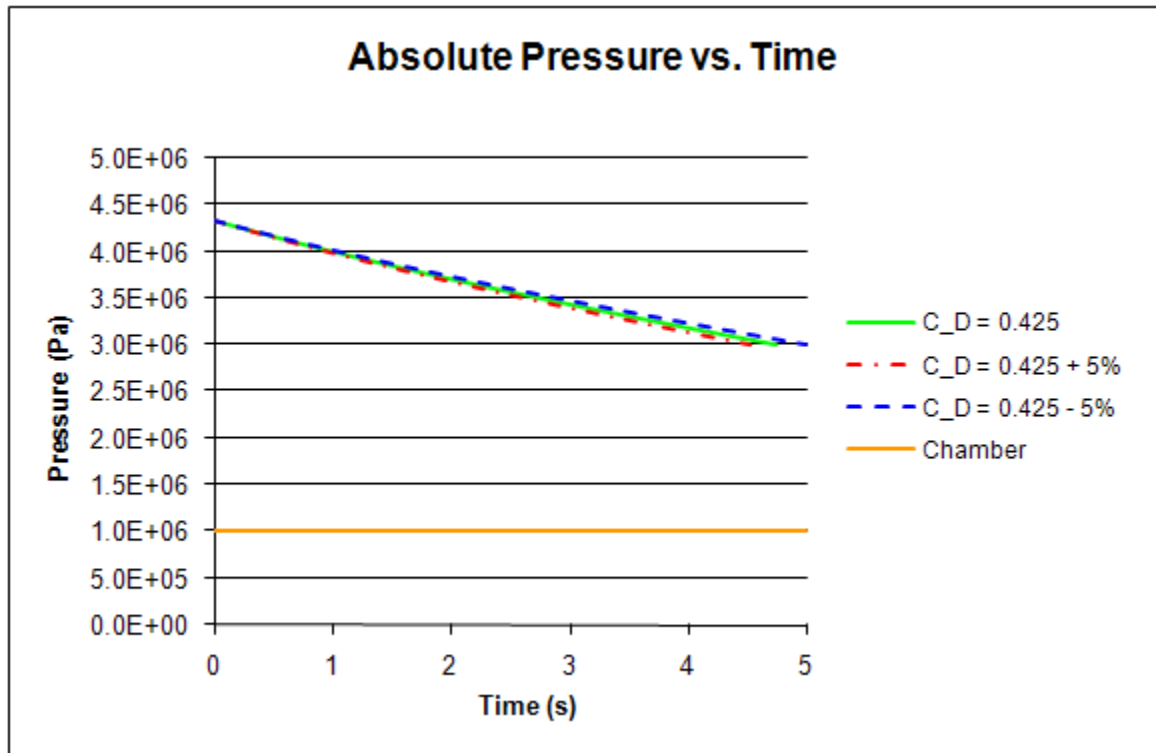
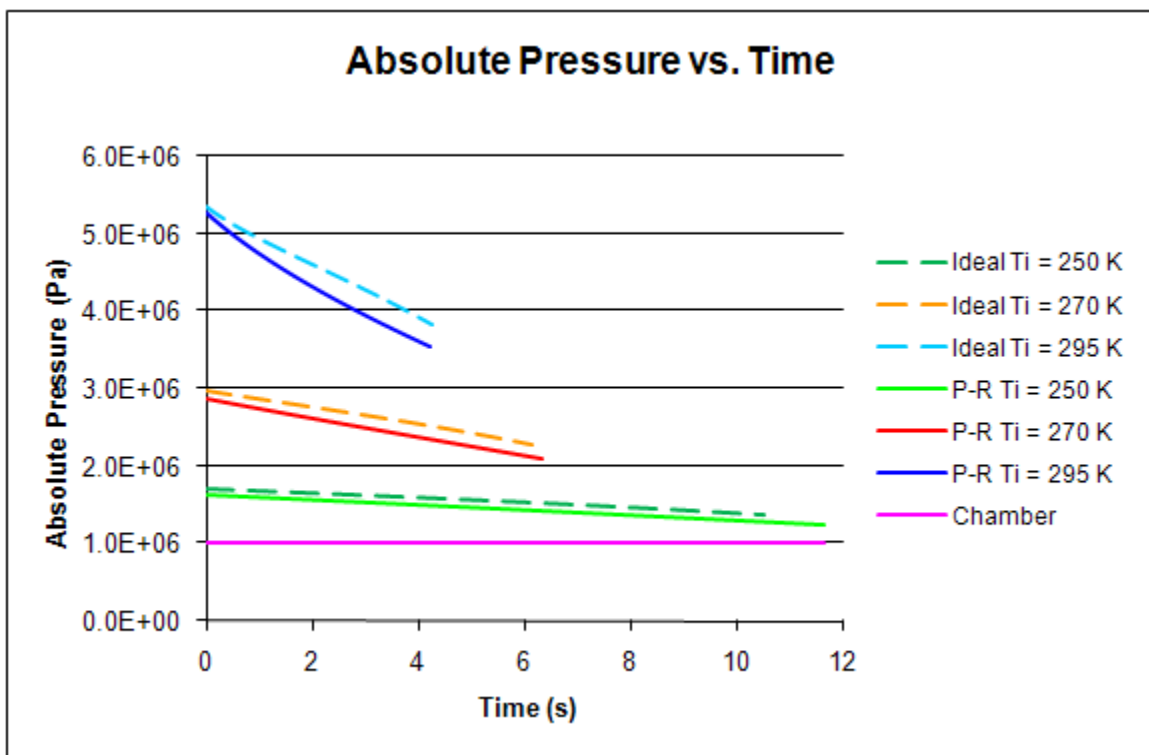Figure 5.3.3b: Theoretical (non-ideal) predictions for the absolute pressure in the draining tank as a function of time, for parameter values as set in Section 5-3 for the discharge coefficient "error" sensitivity study.
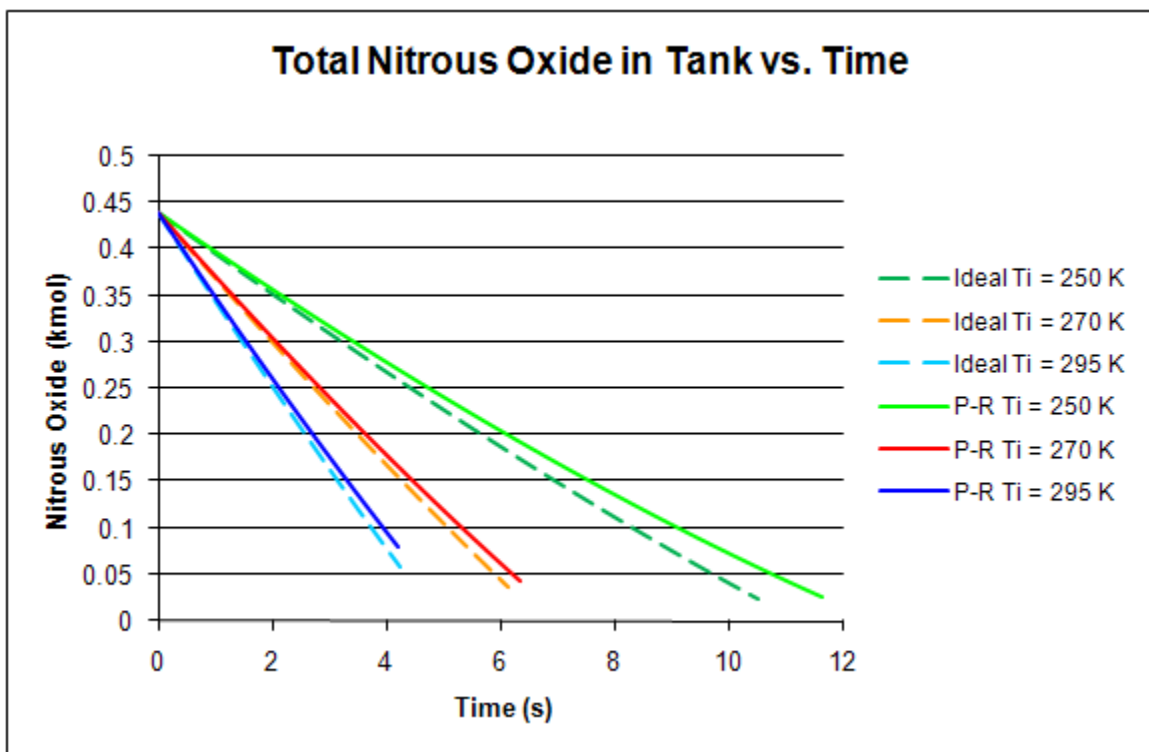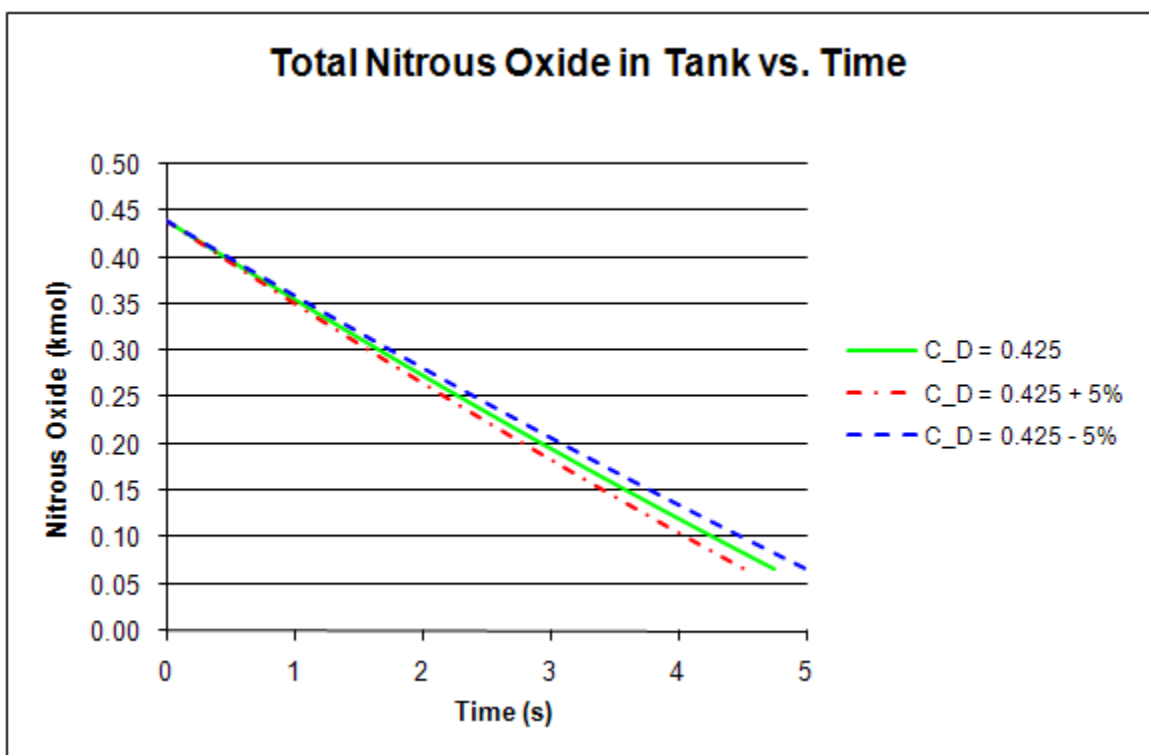
Figure 5.3.3c: Theoretical (non-ideal) predictions for the total moles of nitrous oxide in the draining tank as a function of time, for parameter values as set in Section 5-3 for the discharge coefficient "error" sensitivity study.
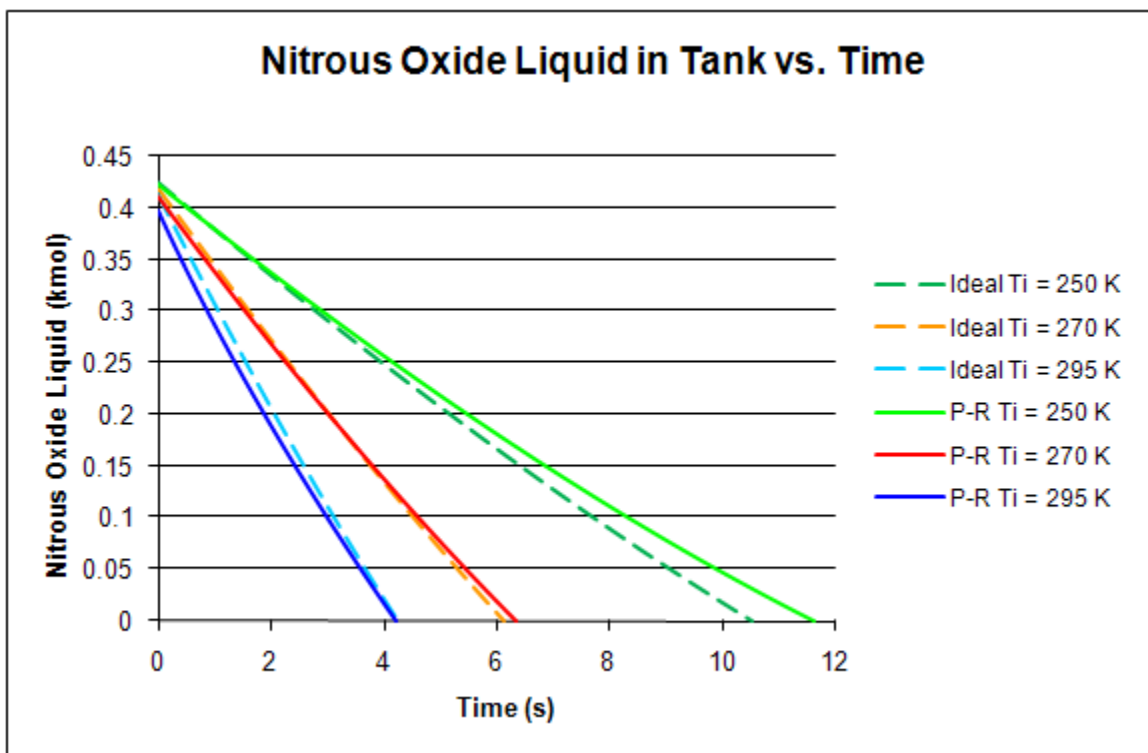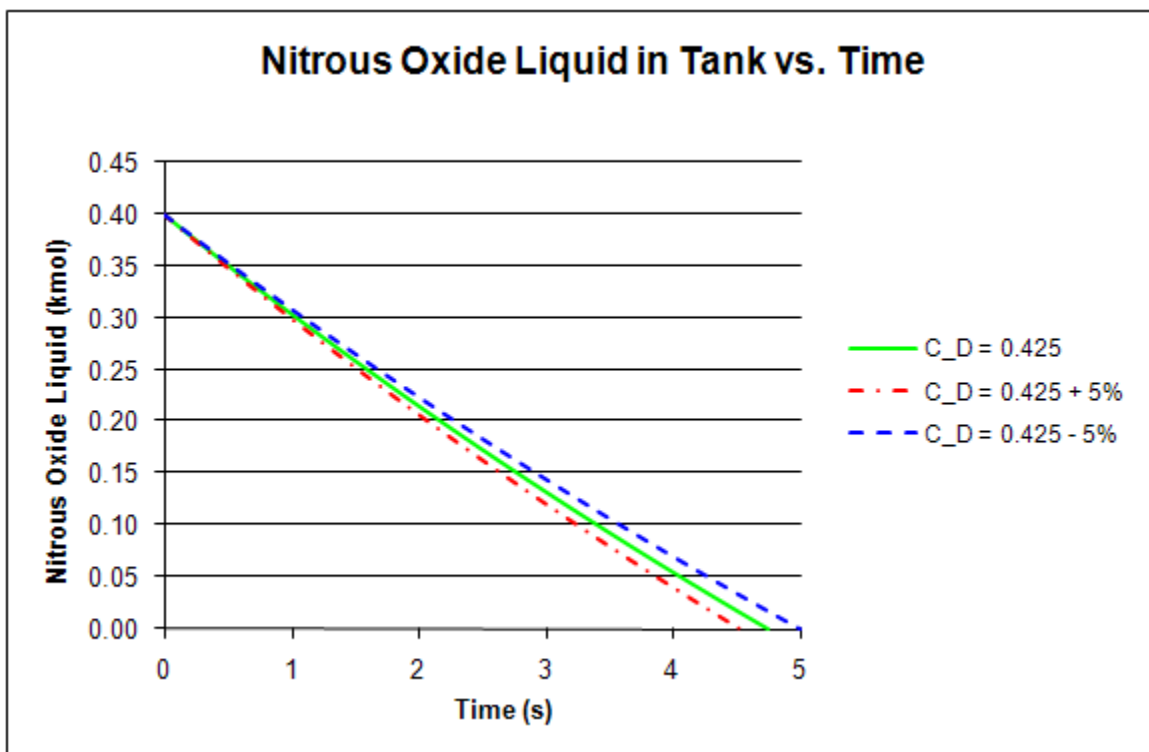

Figure 5.3.3d: Theoretical (non-ideal) predictions for the moles of nitrous oxide liquid in the draining tank as a function of time, for parameter values as set in Section 5-3 for the discharge coefficient "error" sensitivity study.
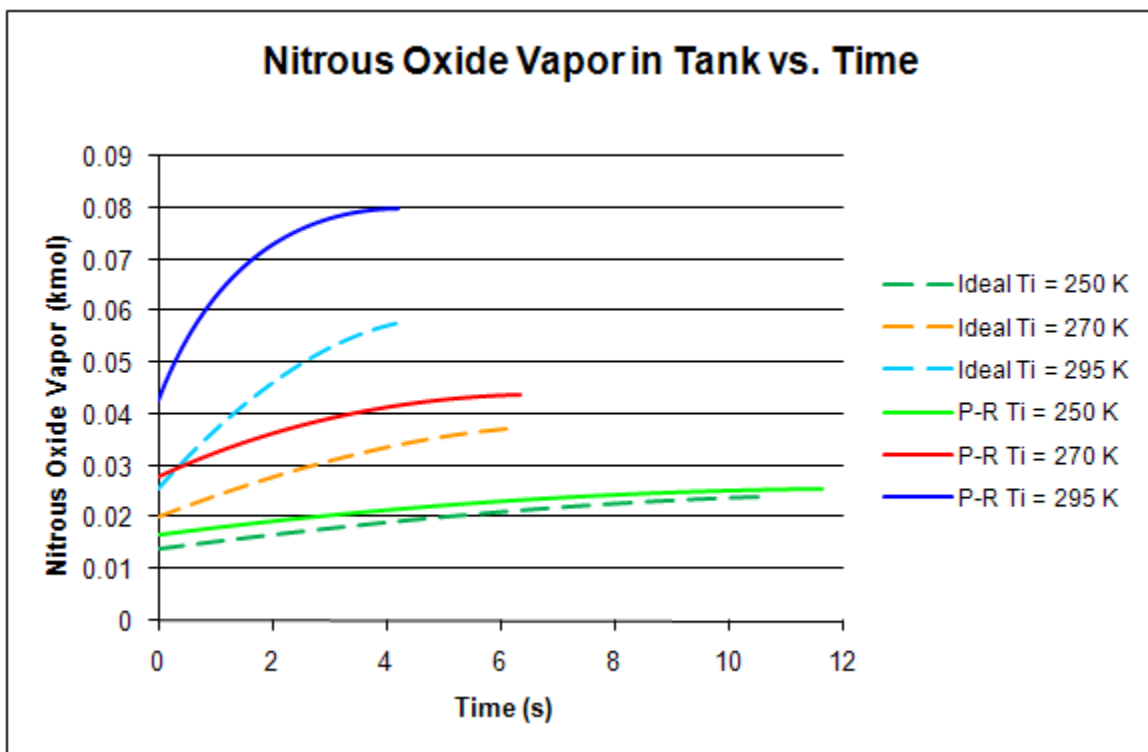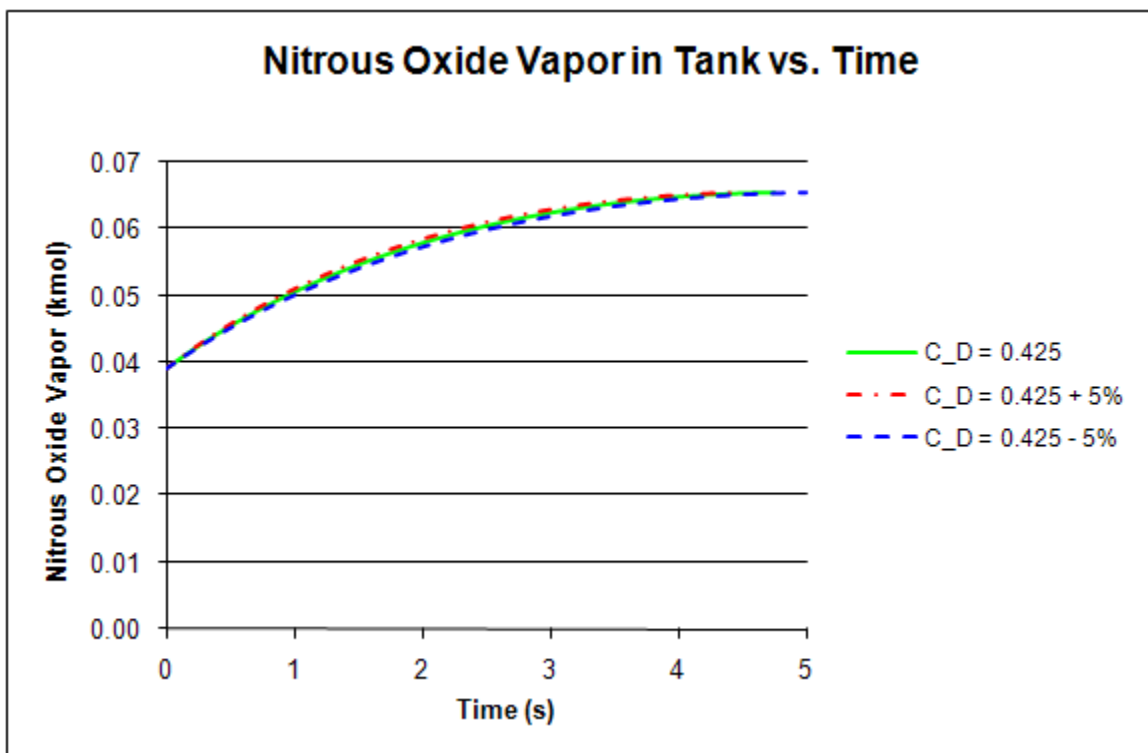
Figure 5.3.3e: Theoretical (non-ideal) predictions for the moles of nitrous oxide vapor in the draining tank as a function of time, for parameter values as set in Section 5-3 for the discharge coefficient "error" sensitivity study.

Note that a 5% difference in the discharge coefficient, C_D, makes an approximately 0.25 second difference in drain time, which is an error of approximately 5.3%. Also note that the divergence in drain time is due almost entirely to differences in the liquid drain history; the vapor drain histories are quite similar.

5-3-4   Binary Interaction Parameter Study and Critical Constant Study

Variations in the binary interaction parameter and the critical constants, which affect the Peng-Robinson equation-of-state predictions, lead to very small variations in draining history compared with the studies of Sections 5-3-1 through 5-3-3. Thus, variations in these parameters do not lead to significant variations in model predictions. Plots of these studies' results can be found in Appendix F for reference.

5-4   General Observations

The results of the "big picture" and "error" sensitivity studies call attention to the characteristics of both models. The big picture study demonstrates the deviation between the ideal and non-ideal models at low fill levels, high temperatures, and increasing amounts of helium to pressurize the tank above the nitrous oxide vapor pressure. The only divergence from these results is seen in the temperature sensitivity study where the total and liquid nitrous oxide drain histories (Figures 5.2.2c,d) indicate that the models actually diverged more at low temperatures. The cause of this result is unknown (refer to Section 5-2-2).

The error study demonstrates that small deviations in the initial conditions show up mostly as deviations in the drain time, which is a very important result because, if accuracy to within 5% is the goal of the theoretical model, then care must be taken in accurately measuring the initial conditions and discharge coefficient. Small deviations in the three error sensitivity studies discussed above show drain time errors of approximately 5%, which eats up the error budget set out at the onset of this study. Also note that small deviations have a significant effect on total molar (or mass) flow rate in the initial temperature and discharge coefficient studies. Since the total nitrous oxide flow rate is the most important aspect from a propulsion standpoint (Zilliac, personal communication, 2009), this result also supports the need to accurately measure these parameters.

CHAPTER 6

THEORETICAL LAUNCH SCENARIO

6-1   Introduction

As part of ongoing research of hybrid technology through cooperation between NASA Ames and Stanford University, a large-scale hybrid sounding rocket is currently being developed for a future launch from NASA Wallops. This chapter presents model predictions for the draining history that is expected for the Peregrine launch vehicle. This scenario utilizes the "helium-augmented" pressurization system proposed by Zilliac (personal communication, 2009) where a constant amount of pressurant is present in the oxidizer tank through the duration of the drain. Model predictions for the same system without added pressurant are also provided. For both pure and helium-augmented cases, ideal and non-ideal model predictions are included. These additional calculations provide physical insight into the draining process as will be discussed in Section 6-3.

The inputs to the calculation are as follows. The nitrous oxide initially loaded into the tank is 435 kg. The initial temperature of the tank contents is 297.1 K. The internal volume of the oxidizer tank is 0.624347 m^3 (38100 in^3). The discharge coefficient is 0.796. The total injector area is 0.00080064356 m^2 (1.241 in^2). The tank mass is 110 kg made from 2219-T6 Aluminum (note, however, that pure aluminum material properties are used in both models). Enough helium is added to the oxidizer tank in order to bring the total pressure up to 5.86055·10^6 Pa (850 psia); amounts are stated in Section 6-3. In addition, the drain history for the same system without added pressurant is also provided in the plots below for reference. The combustion chamber pressure is assumed to start at 700 psia and decreases linearly to approximately 400 psia at 21 seconds into the burn, which is an anticipated chamber history and liquid drain time.

6-2   Launch History Plots

Figures 6.2a-d show how the temperature, pressure, total nitrous oxide moles, and liquid and vapor molar distributions vary with time as the tank drains for input parameters specified in Section 6-1. Both ideal and non-ideal (labeled "P-R" for Peng-Robinson in figures) model predictions are provided for pure and helium-augmented oxidizer delivery.
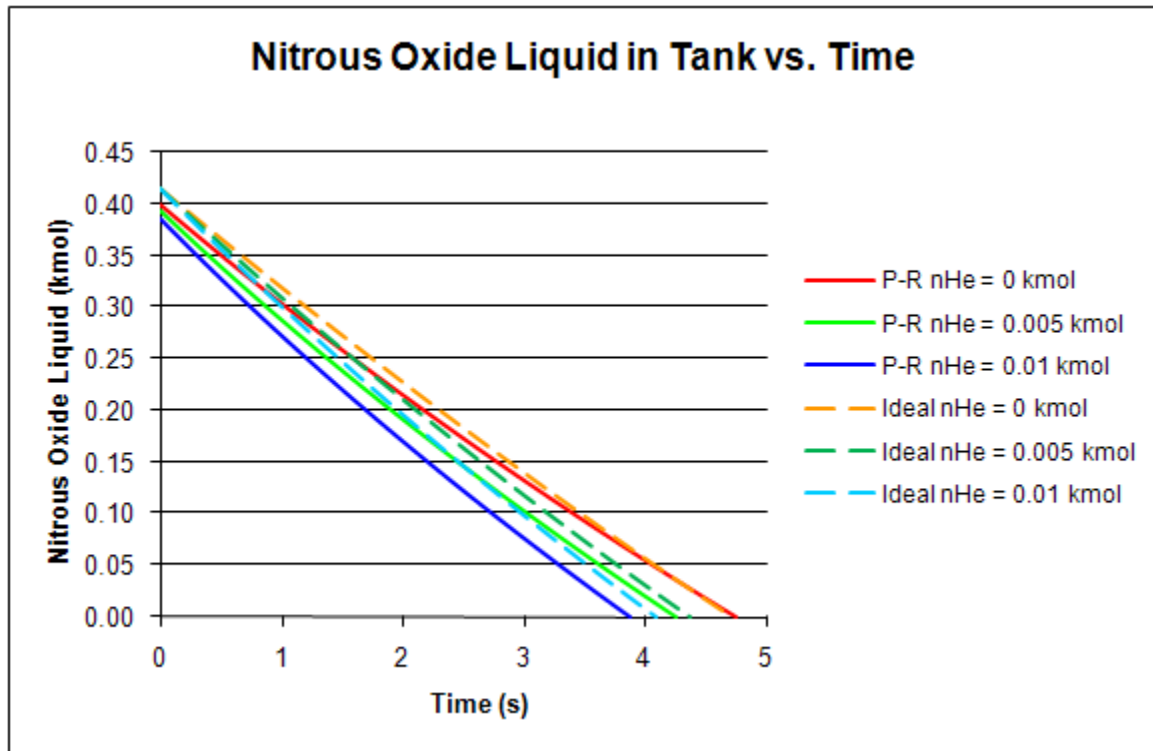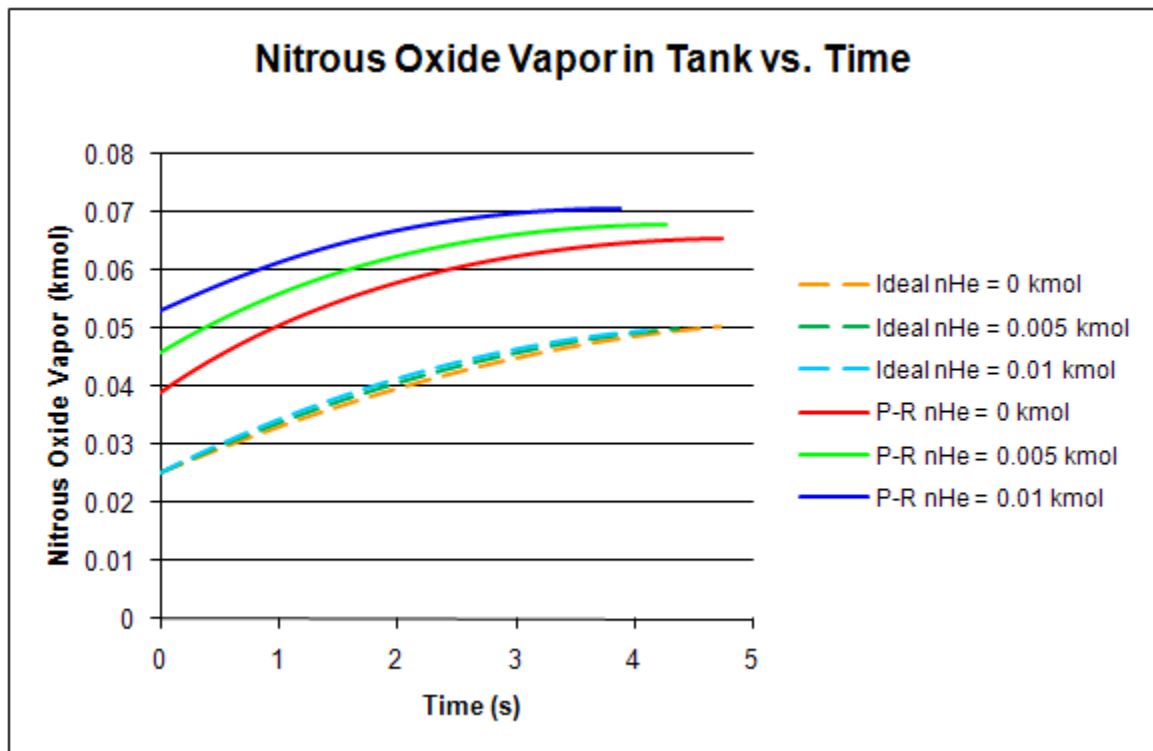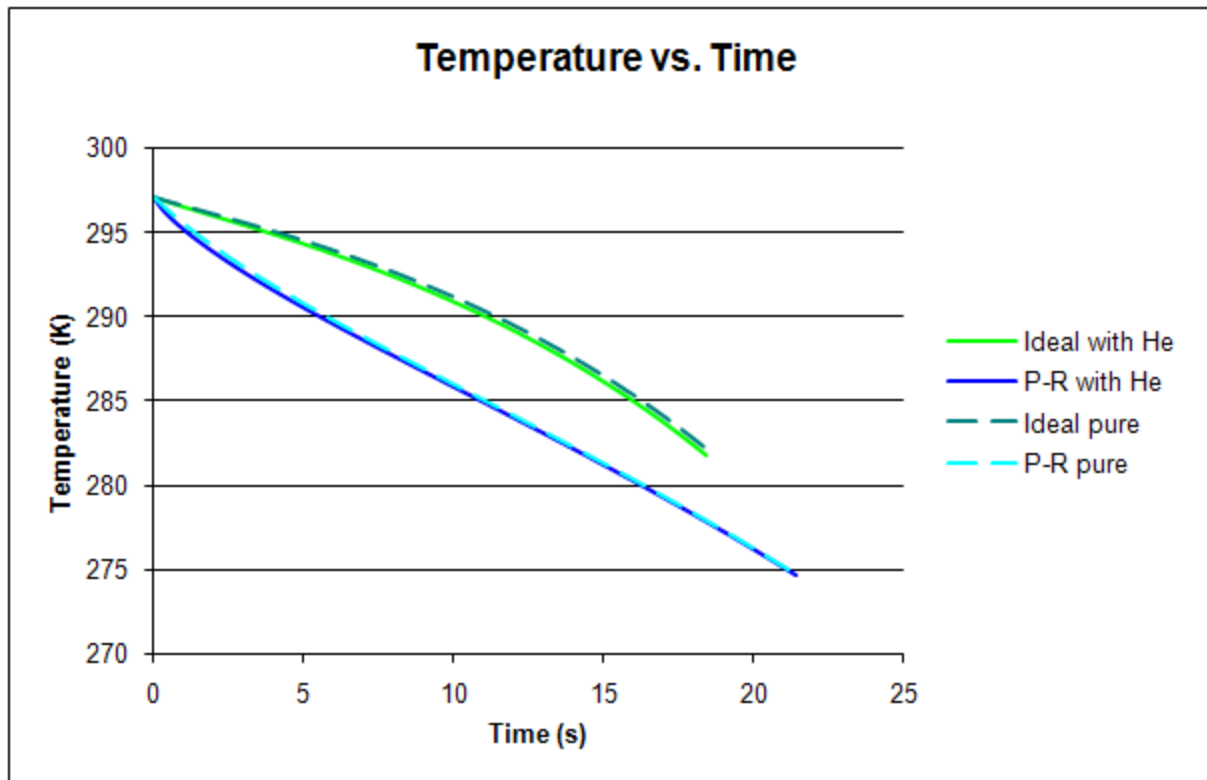
Figure 6.2a: Theoretical (ideal, non-ideal) predictions for the temperature in the draining tank as a function of time, for parameter values as set in Section 6-1 for the launch scenario.
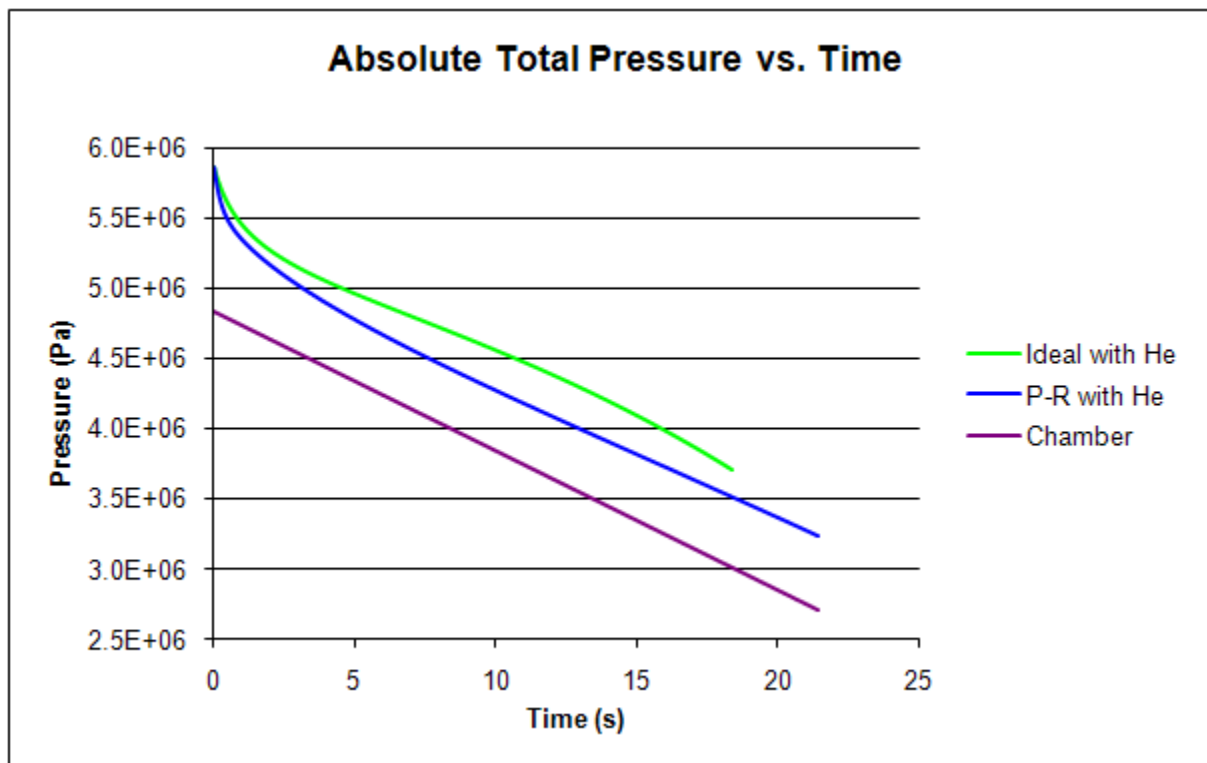
Figure 6.2b: Theoretical (ideal, non-ideal) predictions for the absolute total pressure in the draining tank as a function of time, for parameter values as set in Section 6-1 for the helium-augmented launch scenario.

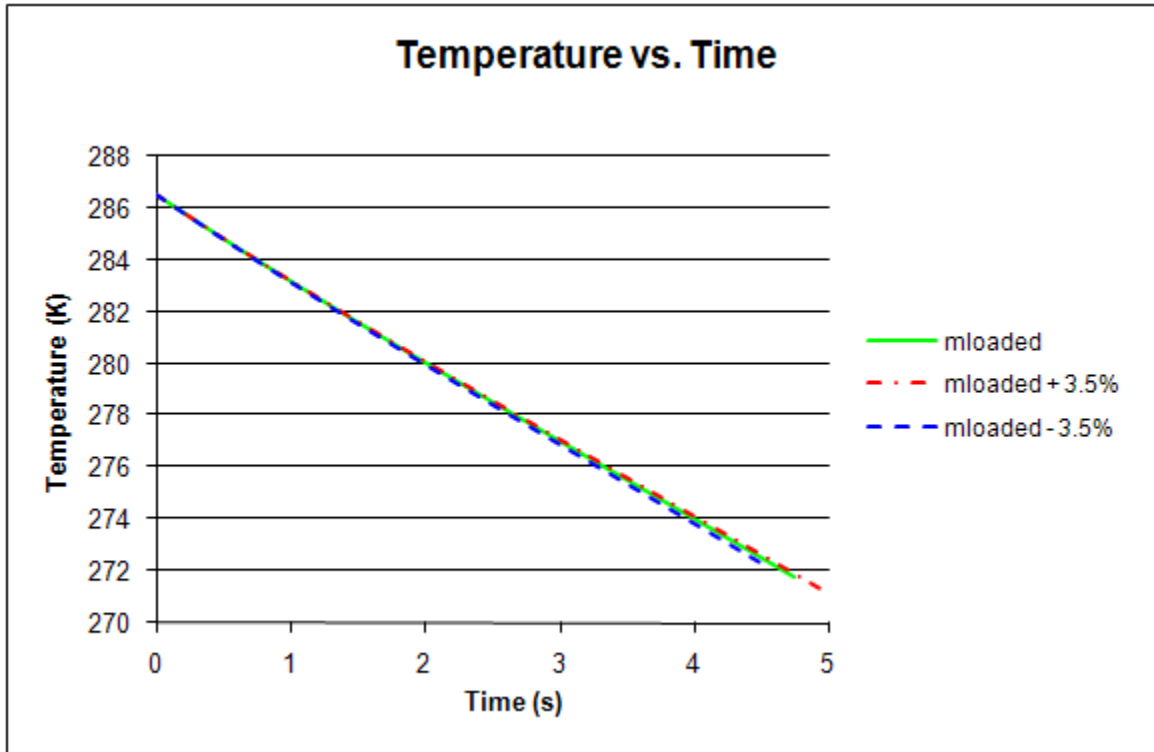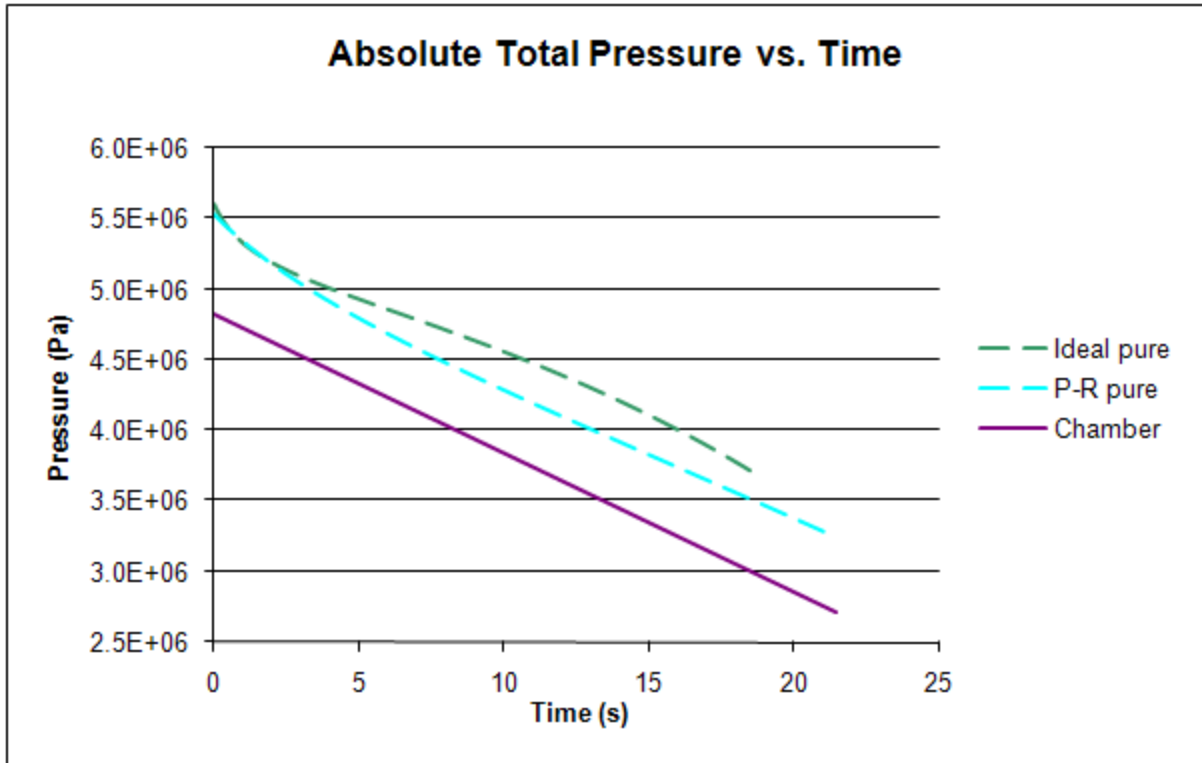Figure 6.2c: Theoretical (ideal, non-ideal) predictions for the temperature in the draining tank as a function of time, for parameter values as set in Section 6-1 for the pure nitrous oxide launch scenario.
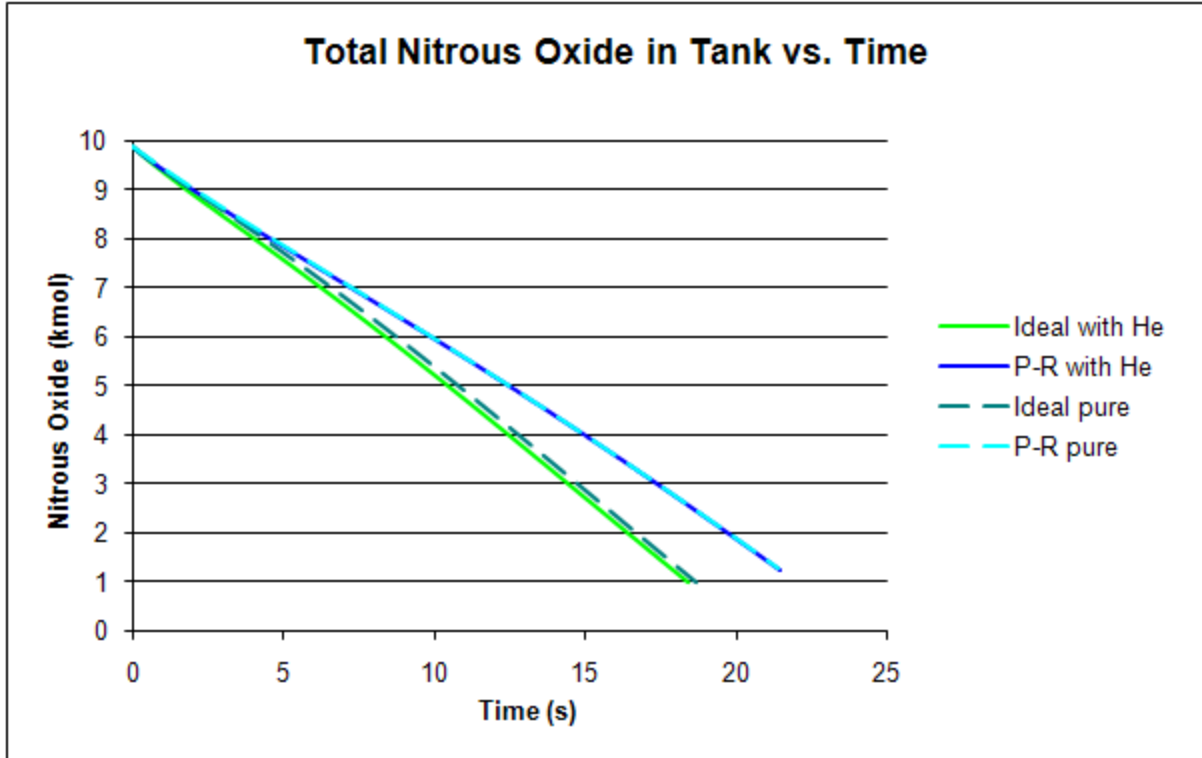
Figure 6.2d: Theoretical (ideal, non-ideal) predictions for the total moles of nitrous oxide in the draining tank as a function of time, for parameter values as set in Section 6-1 for the launch scenario.

62
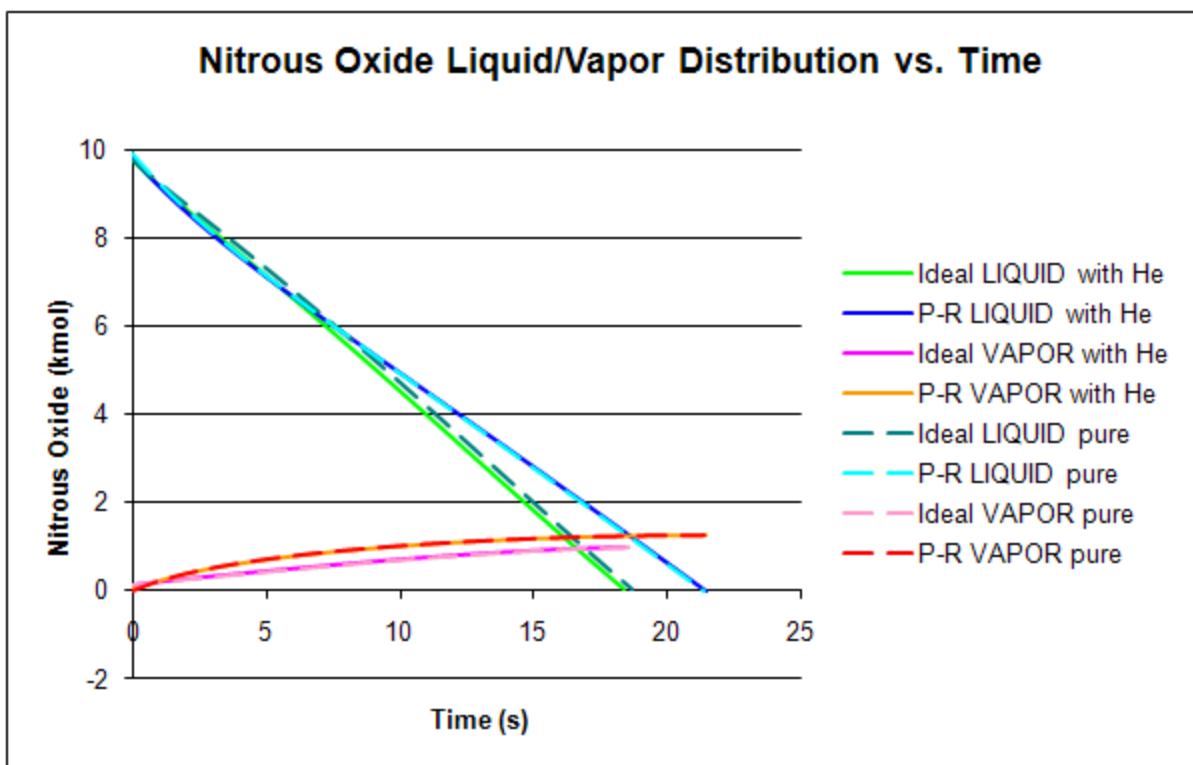
Figure 6.2e: Theoretical (ideal, non-ideal) predictions for the moles of nitrous oxide liquid and vapor in the draining tank as a function of time, for parameter values as set in Section 6-1 for the launch scenario.

6-3   Discussion

The amount of helium needed to bring the total tank pressure up to 850 psia is small, and so the drain histories for the pure nitrous oxide and helium-augmented histories are extremely close and almost indistinguishable on the plots. The effect of helium addition is mostly seen in the pressure histories (Figures 6.2b,c) at the beginning of the drain. Note, however, that it takes a different amount of helium in each model to pressurize the oxidizer tank up to 850 psia. For the ideal model, 0.8472 moles of helium are added, whereas 5.579 moles were added for the Peng-Robinson model. Interaction between nitrous oxide and helium included in the non-ideal Peng-Robinson model is likely the primary reason for the discrepancy between the amounts of helium added for each model. In addition, there is an approximately 1-2% error in the Peng-Robinson calculation of the pure-component vapor pressure (Figure 6.2c) which probably also plays a small role in this discrepancy. The initial nitrous oxide mole fraction, y_2, in the gas phase is 0.955657 for the ideal model, whereas it is 0.978618 for the Peng-Robinson model.

Of particular interest is the divergence between the ideal and non-ideal models, resulting in an approximate three second difference in drain time (Figure 6.2e). These results indicate that the ideal model cannot be used for accurate draining predictions, assuming the non-ideal model will agree with experiment. Note that the data is consistent with results in the sensitivity study where the ideal and non-ideal model predictions start to diverge at lower fill levels (Figure 6.2d,e). The reason for this is as follows. The largest differences between the ideal and non-ideal model predictions occur in the gas phase due to the inherently high gas compressibility. On the other hand, the liquid is much less compressible, and the Peng-Robinson predictions for the liquid are not nearly as affected by the non-ideal behavior. Because of the large molar volume of the gas compared with the liquid, the number of moles of nitrous oxide in the gas phase is typically very small compared with that in the liquid when the volume constraint is satisfied. As a result, the large discrepancy in molar volumes in the gas phase does not show up in the draining history at higher fill levels because the liquid molar volumes are fairly close between the ideal and non-ideal models. It is only when the nitrous oxide liquid level is low that the discrepancy between the models can really be seen, as the gas moles become a significant volume of the total moles in the container. When the tank drains over a long period of time as in the study above, this discrepancy persists over a relatively long time, and the divergence between the ideal and non-ideal model draining histories continually increases. At shorter drain times, the models begin to diverge, but the discrepancy is not as large (compare results in Figure 6.2d to those in Figures 4.1-4b).

An important observation in the pressure history above (Figures 6.2b,c) is that the oxidizer tank pressure is initially dropping at a steeper rate, but then picks up the decreasing trend of the exit pressure for the remainder of the drain. Such coupling is also seen in Tests 2 and 3 of Zilliac and Karabeyoglu (2005) (Figures 4.2.2a and 4.2.3a). This would suggest that, initially, the difference in pressure between the oxidizer tank and the combustion chamber is defining the flow rate; however, there comes a certain point where the flow rate is then dictating the pressure history upstream such that the flow rate remains constant. While it is understood that the pressure difference and the flow rate are always coupled, a thorough examination of this behavior should be assessed in future work. Additional sensitivity studies introducing different pressure differences and different exit pressure trends will likely elucidate this coupling phenomenon.

The most interesting observation, however, is in the Peng-Robinson pure nitrous oxide history. The initial condition was calculated to yield a negative amount of nitrous oxide in the gas phase. This is because the liquid molar volume predicted by the Peng-Robinson equation-of-state is approximately 9% greater than the experimental molar volume (taken from correlation in *Perry's Chemical Engineers' Handbook* (1997)), resulting in a tank that is over 100% full of liquid. The correct molar volume is present in the ideal model since the handbook correlation is used to calculate the nitrous oxide liquid molar volume as a function of temperature. Therefore, the non-ideal prediction of the pure nitrous oxide history begins in a non-real physical state, but becomes physical (a positive number of moles of nitrous oxide vapor, n_{2v}) after 0.165 seconds of draining. A quick calculation was done in order to assess the Peng-Robinson error in molar volume over a range of temperatures seen in this pure drain data set. The results showed a gradual increase in error at increasing temperatures, with ~1% error at 276 K, ~4% error at 286 K and ~9.3% error at 297.1 K. Therefore, for this launch scenario with an initial temperature within 15 K of the nitrous oxide critical point and a high fill-level of approximately 92%, the Peng-Robinson model will have more error due to its reduced accuracy of extracting the correct thermodynamic properties of pure nitrous oxide. Predictions of the Peng-Robinson equation-of-state can be improved by utilizing corrections to the equation-of-state specifically meant for accuracy at temperatures close to the critical point. Zilliac (personal communication, 2009) has found one such correction available in the literature which can be implemented into this model in future work.

Note that despite this significant error in the liquid molar volume, the drain time predicted by the Peng-Robinson model for the helium-augmented system is 21.45 seconds, which is approximately the expected drain time. The time scale for the non-physical moles of nitrous oxide vapor is very small compared with the total drain time, and so the initially poor predictions do not largely affect the longer time predictions. There is a significant divergence of the ideal and Peng-Robinson model predictions (approximate 14% difference in drain time), again indicating that the non-ideal model should be used. The predicted Peng-Robinson drain time is very close to the expected drain time, suggesting that the non-ideal model may be capable of predicting the drain histories to within the desired accuracy. However, the predicted drain time may be fortuitous considering the errors cited above, and future work should focus on further comparisons between theory and experiment. It is worth

the effort to seek out the necessary corrections to the Peng-Robinson equation-of-state to more accurately predict properties near the critical temperature and to see how these improved predictions affect the draining history.

CHAPTER 7

CONCLUSIONS AND RECOMMENDATIONS

The results from the experimental data comparison (Chapter 4), the sensitivity studies (Chapter 5), and the theoretical launch scenario (Chapter 6) indicate that the non-ideal Peng-Robinson model is superior to the ideal model in describing the self-pressurization behavior of a draining oxidizer tank with or without a pressurant used. One of the main assumptions for the ideal model is that the molecules do not interact, and this can only happen at low pressure. According to Felder and Rousseau (1978), the ideal gas model predicts gas behavior to within 1% accuracy for non-diatomic gases when the molar volume is greater than 20 L/mol. However, in this high pressure system, the gas phase molar volumes fall well below this value. Note that in the nitrous oxide drain histories in general, the ideal and non-ideal models start to diverge at lower fill levels. This trend is further accentuated when the drain time increases. This is likely due to differences in the behavior of the gas phase equation-of-state, which becomes more evident as the gas phase becomes a larger percentage of the total tank contents and thus has more effect on the draining behavior.

There are properties in the Peng-Robinson model that are still unverified, which could improve the accuracy of the model if the information is located or measured in the future. The first is that the correlation of molar heat capacity for nitrous oxide liquid pulled from *Perry's Chemical Engineers' Handbook* (1997) has a cited temperature range outside those found in these tests. Also, the Peng-Robinson binary interaction parameter for a nitrous oxide/helium mixture is an experimentally determined parameter that has not, to date, been found in the literature. The sensitivity study results in Chapter 5 indicate that this parameter has a relatively small effect on the results over the range of variations examined. Nevertheless, this parameter depends on the mixture properties and should be formally measured to verify its effect is small. It is also important to find corrections to the Peng-Robinson equation-of-state in order to more accurately extract the thermodynamic properties of pure nitrous oxide near the critical point. In all these cases, error is introduced to the model simply because of limitations on the availability of published data.

Another important step to take in future work is to verify the accuracy of the Peng-Robinson equation-of-state in predicting the thermodynamic properties of pure nitrous oxide.

If the desired accuracy cannot be attained, even after the above-stated corrections have been implemented, perhaps a different or adjusted cubic equation-of-state could provide the needed accuracy.

Future experiments that utilize the helium-augmented pressurization method are needed not only to verify the theoretical models of nitrous oxide/helium mixture drain histories but also Peng-Robinson accuracy for nitrous oxide/helium mixtures. Refer to Appendix G for a proposed testing procedure for future work. In addition, in order to assess the accuracy of an equilibrium model, a third model that incorporates heat and mass transfer coupled at the oxidizer liquid-vapor interface can be completed for the purposes of examining the relative importance of the heat and mass transfer resistances on the draining behavior. If it can be shown conclusively that the purely equilibrium-based model used in this study is insufficient to predict the pressurization behavior to within the desired accuracy, then the coupled heat and mass transfer model would be the next model to implement and study.

Comparisons of the non-ideal models with experimental data for pure nitrous oxide systems provide guidance on the design of future experiments involving helium-augmented systems. The sensitivity studies have shed light on the most important features of the hybrid delivery system that need to be controlled. For instance, the "error" sensitivity study reveals that slight changes in fill-level, initial temperature, and discharge coefficient make significant changes in drain time. This study thus indicates that accurate measurements of fill level, initial temperature, and discharge coefficient are important to meet the goal of predictive modeling to within 5% of experiment.

The main benefit of attaining an accurate model is the ability to use it to extrapolate beyond the verified experimental parameter range. This is necessary to scale propellant delivery systems for a rocket regardless of its size. The non-ideal model presented in this thesis shows strong potential to be used in future hybrid rocket design and scale-up. A major finding of this study is that the non-ideal model that uses the Peng-Robinson equation-of-state predicts that the flow rate of the oxidizer will be approximately constant despite the changing thermodynamic state of the oxidizer tank contents and the combustion chamber pressure. This is very desirable behavior that could not be anticipated due to the highly nonlinear nature of the underlying physics. This study thus reveals that a pressure-fed

propellant delivery system is a strong candidate to provide a reasonably constant flow rate without the use of pumps or other means of flow rate control in a hybrid rocket.

REFERENCES

Abdalla, K. L., Frysinger, T. C., & Andracchio, C. R. (1965). Pressure-Rise Characteristics for a Liquid-Hydrogen Dewar for Homogeneous, Normal-Gravity Quiescent, and Zero-Gravity Tests (NASA TM X-1134). Cleveland, OH: Lewis Research Center.

Abramowitz, M., & Stegun, I. A. (1972). Handbook of Mathematical Functions. New York: Dover Publications.

Arnett, R. W., & Millhiser, D. R. (1965). A Theoretical Model for Predicting Thermal Stratification and Self Pressurization of a Fluid Container. In Conference on Propellant Tank Pressurization and Stratification, Volume 2 (pp. 1-20). Huntsville, AL: Marshall Space Flight Center.

Arnett, R. W., & Voth, R. O. (1972). A Computer Program for the Calculation of Thermal Stratification and Self-Pressurization in a Liquid Hydrogen Tank (NASA CR-2026). Boulder, CO: National Bureau of Standards.

Aydelott, J. C. (1967a). Normal Gravity Self-Pressurization of 9-inch- (23 cm) Diameter Spherical Liquid Hydrogen Tankage (NASA TN D-4171). Cleveland, OH: Lewis Research Center.

Aydelott, J. C. (1967b). Effect of Gravity on Self-Pressurization of Spherical Liquid-Hydrogen Tankage (NASA TN D-4286). Cleveland, OH: Lewis Research Center.

Aydelott, J. C., & Spuckler, C. M. (1969). Effect of Size on Normal-Gravity Self-Pressurization of Spherical Liquid Hydrogen Tankage (NASA TN D-5196). Cleveland, OH: Lewis Research Center.

Barakat, H. Z. (1965). Transient Laminar Free Convection Heat and Mass Transfer in Two-Dimensional Closed Containers Containing Distributed Heat Source. In Conference on Propellant Tank Pressurization and Stratification, Volume 2 (pp. 87-117). Huntsville, AL: Marshall Space Flight Center.

Barsi, S., & Kassemi, M. (2007). Validation of Tank Self-Pressurization Models in Normal Gravity. In 45th AIAA Aerospace Sciences Meeting, 17 (pp. 11550-11562). Reno, NV: American Institute of Aeronautics and Astronautics.

Barsi, S., Kassemi, M., Panzarella, C. H., & Alexander, J. I. D. (2005). A Tank Self-Pressurization Experiment Using a Model Fluid in Normal Gravity. In 43rd AIAA Aerospace Sciences Meeting and Exhibit (AIAA 2005-1143, pp. 495-507). Reno, NV: American Institute of Aeronautics and Astronautics.

Bornhorst, W. J., Hatsopoulos, G. N. (1967, December). Analysis of a Liquid Vapor Phase Change by the Methods of irreversible Thermodynamics. Journal of Applied Mechanics, 34(4). 840-846.

Cabaas, A., Menduia, C., Pando, C., & Renuncio, J. A. R. (1998). Excess Molar Enthalpies of Nitrous Oxide/Hexane Mixtures in the Liquid and Supercritical Regions. Industrial & Engineering Chemistry Research, 37(8), 3036-3042.

Clark, J. A., & Barakat, H. Z. (1965). Transient, Laminar, Free-Convection Heat and Mass Transfer in Closed, Partially Filled, Liquid Containers. In Conference on Propellant Tank Pressurization and Stratification, Volume 2 (pp. 119-189). Huntsville, AL: Marshall Space Flight Center.

Felder, R. M., & Rousseau, R.W. (1978). Elementary Principles of Chemical Processes. New York: John Wiley & Sons.

Giordano, D., & De Serio, M. (2002, April-June). Thermodynamic Model of Hydrazine that Accounts for Liquid-Vapor Phase Change. Journal of Thermophysics and Heat Transfer, 16(2), 261-272.

Grayson, G. D. (1995, October). Coupled Thermodynamic-Fluid-Dynamic Solution for a Liquid-Hydrogen Tank. Journal of Spacecraft and Rockets, 32(5), 918-921.

Grayson, G. D., Watts, D. A., & Jurns, J. M. (1997). Thermo-Fluid-Dynamic Modeling of a Contained Liquid in Variable Heating and Acceleration Environments. In 1997 ASME Fluids Engineering Division Summer Meeting, Part 16 (FEDSM97-3567). Vancouver, Canada: American Society of Mechanical Engineers.

Greer (1999, July). Cryogenic Fuel Tank Draining Analysis Model [WWW Document]. URL http://www.nasa.gov/centers/dryden/pdf/88643main_H-2344.pdf (visited 2009, July 22).

Hasan, M. M., Lin, C. S., & Van Dresar, N. T. (1991). Self Pressurization of a Flightweight Liquid Hydrogen Storage Tank Subjected to Low Heat Flux (NASA TM 103804). Minneapolis, MN: ASME/AIChE National Heat Transfer Conference.

Holt, K., Majumdar, A., Streadman, T., & Hedayat, A. (2000). Numerical Modeling and Test Data Comparison of Propulsion Test Article Helium Pressurization System. In 36th AIAA/ASME/SAE/ASEE Joint Propulsion Conference and Exhibit (AIAA 2000-3719). Huntsville, AL: American Institute of Aeronautics and Astronautics.

Kumar, V., Danov, K. D., & Durst, F. (2003). Extended Statistical Rate Theory for Liquid Evaporation. KONWIHR-Quartl.

Lemmon, E. W., & Span, R. (2006). Short Fundamental Equations of State for 20 Industrial Fluids. Journal of Chemical & Engineering Data, 51(3), 785-850.

Liebenberg, D. H., & Edeskuty, F. J. (1965). Pressurization Analysis of a Large-Scale Liquid-Hydrogen Dewar. International Advances in Cryogenic Engineering, 10, 284-289.

Lin, C. S., Van Dresar, N. T., & Hasan, M. M. (2004, May-June). Pressure Control Analysis of Cryogenic Storage Systems. Journal of Propulsion and Power, 20(3), 480-485.

Majumdar, A., & Steadman, T. (2001, March-April). Numerical Modeling of Pressurization of a Propellant Tank. Journal of Propulsion and Power, 17(2), 385-390.

Martin, J. J., & Hou, Y. (1955, June). Development of an Equation of State for Gases. American Institute of Chemical Engineers Journal, 1(2), 142-151.

Nein, M. E., & Thompson, Jr., J. F. (1965). Experimental and Analytical Studies of Cryogenic Propellant Tank Pressurization. In Conference on Propellant Tank Pressurization and Stratification, Volume 1 (pp. 29-54). Huntsville, AL: Marshall Space Flight Center.

O'Loughlin, J. R. (1965). Dimensionless Mass Transfer Alignment Chart for Suddenly Pressurized Liquid-Vapor Systems. In Conference on Propellant Tank Pressurization and Stratification, Volume 1 (pp. 143-155). Huntsville, AL: Marshall Space Flight Center.

O'Loughlin, J. R., & Glenn, H. (1965). Bulk Liquid Interfacial Mass Transfer with Variable Ullage Pressure. In Conference on Propellant Tank Pressurization and Stratification, Volume 1 (pp. 125-142). Huntsville, AL: Marshall Space Flight Center.

Otto, E. W. (1966). Static and Dynamic Behavior of the Liquid-Vapor Interface During Weightlessness. Chemical Engineering Progress Symposium Series, 62(61), 158-177.

Panzarella, C. H., & Kassemi, M. (2003). On the Validity of Purely Thermodynamic Descriptions of Two-Phase Cryogenic Fluid Storage. Journal of Fluid Mechanics, 484, 41-68.

Pasley, G. F. (1970, December). Optimization of Stored Pressurant Supply for Liquid Propulsion Systems. Journal of Spacecraft and Rockets, 7(12), 1478-1480.

Peng, D., & Robinson, D. B. (1976). A New Two-Constant Equation of State. Industrial and Engineering Chemistry Fundamentals, 15(1), 59-64.

Perry, R. H., & Green, D. W. (Eds.). (1997). Perry's Chemical Engineers' Handbook (7th Edition). McGraw-Hill.

Redlich, O., & Kwong, J. N. S. (1948). On the Thermodynamics of Solutions. Chemical Reviews, 44, 233-244.

Roudebush, W. H., & Mandell, D. A. (1965). Analytical Investigation of Some Important Parameters in the Pressurized Liquid Hydrogen Tank Outflow Problem. In Conference on Propellant Tank Pressurization and Stratification, Volume 1 (pp. 3-27). Huntsville, AL: Marshall Space Flight Center.

Sandler, S. I. (2006). <u>Chemical, Biochemical, and Engineering Thermodynamics</u>. 4th edition. John Wiley & Sons, Inc.

Smithson, J. C., & Scott, W. R. (1965). A Cryogenic Helium Pressurization System for the Lunar Excursion Module. In <u>Conference on Propellant Tank Pressurization and Stratification, Volume 1</u> (pp. 109-123). Huntsville, AL: Marshall Space Flight Center.

Span, R., & Wagner, W. (2003, January). Equations of State for Technical Applications. I. Simultaneously Optimized Functional forms for Nonpolar and Polar Fluids. <u>International Journal of Thermodynamics, 24</u>(1), 1-39.

Tyler, J. S. (1965). Cryogenic Storage of Helium for Propellant Tank Pressurization. In <u>Conference on Propellant Tank Pressurization and Stratification, Volume 1</u> (pp. 327-342). Huntsville, AL: Marshall Space Flight Center.

Van Dresar, N. T. (1997, November-December). Prediction of Pressurant Mass Requirements for Axisymmetric Liquid Hydrogen Tanks. <u>Journal of Propulsion and Power, 13</u>(6), 796-799.

Van Dresar, N. T., Lin, C. S., & Hasan, M. M. (1992). <u>Self-Pressurization of a Flightweight Liquid Hydrogen Tank: Effects of Fill Level at Low Wall Heat Flux</u> (NASA TM 105411). Reno, NV: 30th Aerospace Sciences Meeting and Exhibit.

Ward, C.A., & Fang, G. (1999, January). Expression for predicting liquid evaporation flux: Statistical rate theory approach. <u>Physical Review E, 59</u>(1), 429-440.

Wisniak, J., & Golden, M. (1998, February). Predicting Saturation Curve of a Pure Substance Using Maxwell's Rule. <u>Journal of Chemical Education, 75</u>(2), 200-203.

Zilliac, G., & Karabeyoglu, M. A. (2005). Modeling of Propellant Tank Pressurization. In <u>41st AIAA/ASME/ASEE Joint Propulsion Conference</u> (AIAA 2005-3549). Tucson, AZ: American Institute of Aeronautics and Astronautics.

APPENDIX A

IDEAL MODEL DERIVATION

The problem statement associated with the derivation presented in this appendix has been provided in Chapter 3. The temperature range in which current experiments have been carried out (near the critical point of nitrous oxide) as well as the presence of helium in the system indicate that the resulting oxidizer tank pressure will exceed that for which the ideal gas assumption is valid. Nevertheless, an ideal analysis is useful as it reveals the mathematical structure of the solution while keeping the governing equations relatively simple, and it lays the groundwork for more sophisticated non-ideal models.

The analysis of the draining liquid system proceeds by partitioning the tank into three control volumes: the gas, liquid, and interfacial regions, as shown in Figure A.1. The liquid control volume is examined first. Note that the liquid control volume is drawn in the liquid alone, but a negligible distance away from the tank walls and interface. There are no chemical reactions occurring, and kinetic and potential energy variations are neglected in the control volume. It is convenient to use molar balances instead of mass balances, as gas equations-of-state and phase equilibrium constraints are based on moles, and not mass.
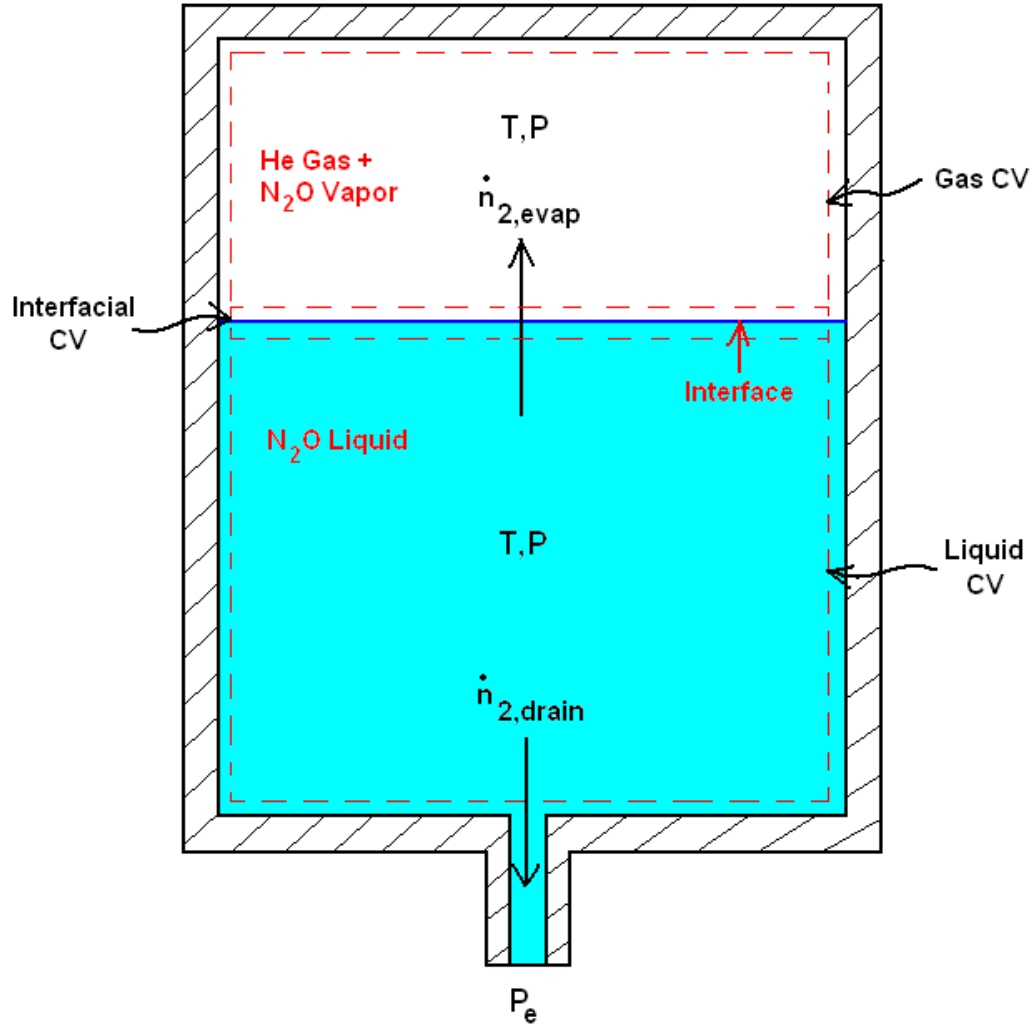
Figure A.1: Draining Tank Schematic with Three Control Volumes (CV)

A molar balance on the liquid control volume is given by

$$\frac{dn_{2l}}{dt} = -\dot{n}_{2,evap} - \dot{n}_{2,drain} \tag{A.1}$$

where n_{2l} is the number of moles in the liquid, and $\dot{n}_{2,evap}$ and $\dot{n}_{2,drain}$ are the molar rates of evaporation and liquid draining, respectively.

An energy balance on the liquid control volume is given by

$$\frac{d}{dt}\left(n_{2l}\hat{U}_{2l}\right) = -\hat{H}_{2l}\left(\dot{n}_{2,evap} + \dot{n}_{2,drain}\right) - \dot{Q}_{2l} - P\frac{dV_l}{dt} \tag{A.2}$$

where $\hat{U}_{2l}$ and $\hat{H}_{2l}$ are the internal energy and enthalpy per mole of liquid, respectively. This balance has been written under the assumptions that potential and kinetic energy

changes are negligible, and the only work being done on the control volume is flow work that is accounted for in the enthalpy term and moving boundary work that is accounted for in the $P\left(\dfrac{dV_l}{dt}\right)$ term. There can be heat loss from the liquid into the gas, $\dot{Q}_{2l}$ (>0), but the tank walls are assumed to be adiabatic.

In order to induce liquid flow out of the tank, there must be a pressure difference between the oxidizer tank and the downstream combustion chamber which is given by the following relation:

$$\dot{n}_{2,drain} = C_D A_{injector} \sqrt{\frac{2(P - P_e)}{(MW)_2 \hat{V}_{2l}}} \tag{A.3}$$

In Equation A.3, C_D is the discharge coefficient (empirically determined by Zilliac and Karabeyoglu (2005) for different feed systems used in testing), $A_{injector}$ is the cross-sectional area of the injector into the combustion chamber, P is the total pressure in the tank, P_e is the pressure in the combustion chamber, $(MW)_2$ is the molecular weight of component 2 (the nitrous oxide), and $\hat{V}_{2l}$ is its molar volume, a correlated function of temperature found in *Perry's Chemical Engineers' Handbook* (1997). When $P = P_e$, the tank will stop draining. Note that this equation is only valid during the liquid portion of the drain. This equation is strictly valid for the flow across the injector, but in the absence of other losses in the tank and pipeline out of the tank, it is a good approximation for the flow rate dependence on pressure. Additionally, it is assumed that gravitational head in the tank is negligible as well. This assumption is certainly reasonable for a ground test firing, but thrust forces during launch may contribute a significant amount of effective pressure to the oxidizer tank exit. These could be easily added to the model, but this complication was not included due to its preliminary nature.

A molar balance and energy balance on the gas phase control volume yields:

$$\frac{dn_g}{dt} = \dot{n}_{2,evap} \tag{A.4}$$

$$\frac{d}{dt}\left(n_g \hat{U}_g\right) = \dot{n}_{2,evap} \hat{H}_{2v} - \dot{Q}_g - P\frac{dV_g}{dt} \tag{A.5}$$

where $\dot{Q}_g$ (>0) is heat loss from the gas into the liquid, $\hat{U}_g$ is the internal energy per mole of the gas phase, and $\hat{H}_{2v}$ is the enthalpy per mole of the nitrous oxide vapor. The total number of moles in the gas phase at any instant, n_g, is defined as the sum of the moles of nitrous oxide vapor, n_{2v}, and the constant moles of helium gas, n_{1_o}:

$$n_g = n_{2v} + n_{1_O} \tag{A.6}$$

The gas behavior is assumed to be ideal, with R defined as the universal gas constant:

$$PV_g = n_g RT \tag{A.7}$$

The system is assumed to be in quasi-phase equilibrium throughout the draining process. This means that as the liquid in the tank drains, liquid also evaporates to saturate the gas phase instantaneously. The equilibrium equation used for ideal gases is Raoult's Law, which is given for the system examined as:

$$Py_2 = P_2^*\big|_T \tag{A.8}$$

$$y_2 = \frac{n_{2v}}{n_{1_O} + n_{2v}} \tag{A.9}$$

Equations A.8 and A.9 state that the partial pressure of nitrous oxide is equal to the vapor pressure of nitrous oxide P_2^* at a given temperature T (the mole fraction of nitrous oxide in the liquid phase is assumed to be 1, meaning the liquid is assumed to be pure nitrous oxide), which is also equal to the overall pressure in the tank P times the mole fraction y_2 of the nitrous oxide in the gas phase. The equation for vapor pressure of nitrous oxide as a function of temperature, P_2^*, is available in *Perry's Chemical Engineers' Handbook* (1997). Combining Equations A.6 and A.7 and combining Equations A.8 and A.9 yields two equations for pressure in the tank, P. The equations can then be set equal to each other in order to eliminate the pressure as an explicit variable. As can be seen in the ideal gas law, pressure can be expressed explicitly in terms of T, n_{2l}, and n_{2v}. Therefore, pressure can be

extracted from the solution for these parameters once they are obtained (See Equation A.16c below).

An interfacial control volume lies between the gas and liquid phase control volumes. This control volume is infinitesimally thin, and it hugs the interface with its top surface in the gas and its bottom surface in the liquid. Since the control volume is so thin, the number of moles in the control volume is negligible. Therefore, there is also no internal energy in the interfacial energy balance, given as:

$$\dot{Q}_{2l} + \dot{Q}_g = \dot{n}_{2,evap}\left(\hat{H}_{2v} - \hat{H}_{2l}\right) = \dot{n}_{2,evap}\Delta\hat{H}_{2v} \qquad (A.10)$$

The heat of vaporization, $\Delta\hat{H}_{2v}$, has now been introduced to the model through the heat exchange at the interface. The heat of vaporization for nitrous oxide is also available from *Perry's Chemical Engineers' Handbook* (1997) as a function of reduced temperature.

An alternative way of looking at the tank, instead of as three separate control volumes, is to view the entire tank as a single control volume, as shown in Figure A.2. Note that the tank itself has been added to the control volume which will affect the energy balance of the system.
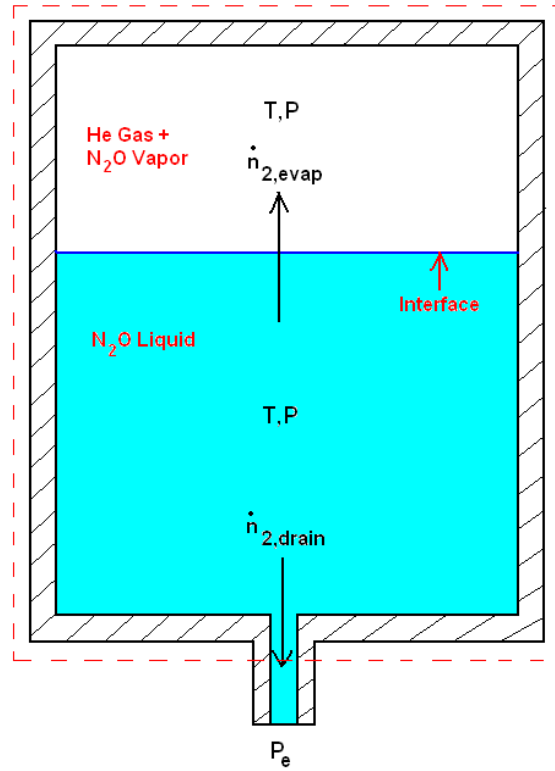
Figure A.2: Draining Tank Schematic with One Control Volume

The total internal volume of the tank, V, is defined as the sum of the gas phase volume, V_g, and the liquid phase volume, V_l:

$$V = V_g + V_l = V_g + n_{2l}\hat{V}_{2l} \tag{A.11}$$

A molar balance on the entire tank gives the following in equation A.12:

$$\frac{d}{dt}\left(n_g + n_{2l}\right) = -\dot{n}_{2,drain} \tag{A.12}$$

An energy balance is quite simple for the entire control volume because there is neither heat being transferred nor moving boundary work being done on the control volume; there is only flow work being done to drain the tank. The tank itself is assumed to be in thermal equilibrium with the tank contents, and thus its internal energy has been added to the energy balance. The energy equation is as follows:

$$\frac{d}{dt}\left(m_T\overline{U}_T + n_{2l}\hat{U}_{2l} + n_g\hat{U}_g\right) = -\dot{n}_{2,drain}\hat{H}_{2l} \tag{A.13}$$

where m_T is the mass of the tank and $\overline{U}_T$ is the specific internal energy of the tank. It can be shown that combining the results from the three control volumes results in the identical equations for the entire tank control volume, Equations A.12 and A.13, except for the tank internal energy term included in the new energy equation. Using chain rule to expand the stored terms in the energy equation, the following equation is obtained:

$$
\begin{aligned}
& m_T\frac{d\overline{U}_T}{dt} + n_{2l}\frac{d\hat{U}_{2l}}{dt} + n_{2v}\frac{d\hat{U}_{2v}}{dt} + n_{1o}\frac{d\hat{U}_{1o}}{dt} = \\
& = \frac{dn_{2v}}{dt}\left(\hat{H}_{2l} - \hat{U}_{2v}\right) + \frac{dn_{2l}}{dt}\left(\hat{H}_{2l} - \hat{U}_{2l}\right)
\end{aligned}
\tag{A.14}
$$

The right hand side of Equation A.14 can be simplified as follows. The liquid enthalpy is related to heat of vaporization as, $\hat{H}_{2v} - \hat{H}_{2l} = \Delta\hat{H}_{2v}$; the nitrous oxide vapor enthalpy is related to the internal energy and pressure as, $\hat{H}_{2v} = \hat{U}_{2v} + P\hat{V}_{2v}$; and the ideal gas law is the P-V-T relationship, $P\hat{V}_{2v} = RT$. Substituting these into Equation A.14 yields:

$$m_T \frac{d\bar{U}_T}{dt} + n_{2l} \frac{d\hat{U}_{2l}}{dt} + n_{2v} \frac{d\hat{U}_{2v}}{dt} + n_{1_o} \frac{d\hat{U}_{1_o}}{dt} =$$

$$= \frac{dn_{2v}}{dt}\left[RT - \Delta\hat{H}_{2v}\right] + \frac{dn_{2l}}{dt}\left(P\hat{V}_{2l}\right) \tag{A.15}$$

The rate of change of specific (or molar) internal energy with respect to time for an ideal gas is simply the heat capacity at constant volume multiplied by the rate of change of temperature with respect to time. All heat capacities at constant pressure are available in *Perry's Chemical Engineers' Handbook* (1997). Using the ideal gas relation $C_V = C_P - R$ and the fact that $\dfrac{d\bar{U}_T}{dt} \approx \dfrac{d\bar{H}_T}{dt} = \bar{C}_{P_T} \dfrac{dT}{dt}$ for a solid material, the energy equation now becomes:

$$\left(m_T \bar{C}_{P_T} + n_{2l}\hat{C}_{V_{2l}} + n_{2v}\hat{C}_{V_{2v}} + n_{1_o}\hat{C}_{V_{1_o}}\right)\frac{dT}{dt} =$$

$$= \frac{dn_{2v}}{dt}\left[RT - \Delta\hat{H}_{2v}\right] + \frac{dn_{2l}}{dt}\left(P\hat{V}_{2l}\right) \tag{A.16a}$$

Equation A.16a is the first of three equations needed to solve the problem. Now, if the total molar balance equation is combined with the flow relation from the liquid control volume, the second equation needed for the solution is produced:

$$\frac{dn_{2v}}{dt} + \frac{dn_{2l}}{dt} = -C_D A_{injector}\sqrt{\frac{2(P - P_e)}{(MW)_2 \hat{V}_{2l}}} \tag{A.16b}$$

The third and final equation is acquired by combining Raoult's Law (Equation A.8), the ideal gas law (Equation A.7), and the volume constraint (Equation A.11), and then taking the derivative of the entire equation with respect to time:

$$-\hat{V}_{2l}\frac{dn_{2l}}{dt}P_2^* + \left(V - n_{2l}\hat{V}_{2l}\right)\frac{dP_2^*}{dT}\frac{dT}{dt} = R\left(T\frac{dn_{2v}}{dt} + n_{2v}\frac{dT}{dt}\right) \tag{A.16c}$$

The system A.16 provides three equations and three unknowns: temperature, *T*, moles of nitrous oxide liquid, n_{2l}, and moles of nitrous oxide gas, n_{2v}. Total tank pressure, *P*, is a function of these three unknowns and can be extracted (from either Raoult's Law or by combining the volume constraint and the ideal gas law) once the solution is obtained.

The system A.16 can be arranged to facilitate numerical solution. Equations A.16a-c are rewritten respectively as Equations A.17a-c as follows:

$$a\frac{dT}{dt} = b\frac{dn_{2l}}{dt} + e\frac{dn_{2v}}{dt} \tag{A.17a}$$

$$\frac{dn_{2v}}{dt} + \frac{dn_{2l}}{dt} = f \tag{A.17b}$$

$$j\frac{dn_{2l}}{dt} + k\frac{dT}{dt} = m\frac{dn_{2v}}{dt} + q\frac{dT}{dt} \tag{A.17c}$$

Then, solving the system of three equations in the three unknown derivatives, the result is:

$$\frac{dn_{2v}}{dt} = \frac{-f[-ja + (q-k)b]}{[a(m+j) + (q-k)(e-b)]} = Z \tag{A.18a}$$

$$\frac{dn_{2l}}{dt} = \frac{-Z[ma + (q-k)e]}{[-ja + (q-k)b]} = W \tag{A.18b}$$

$$\frac{dT}{dt} = \frac{bW + eZ}{a} \tag{A.18c}$$

These equations are thus in the following form:

$$\begin{bmatrix} \dfrac{dT}{dt} \\ \dfrac{dn_{2l}}{dt} \\ \dfrac{dn_{2v}}{dt} \end{bmatrix} = \begin{bmatrix} f_1(T, n_{2l}, n_{2v}) \\ f_2(T, n_{2l}, n_{2v}) \\ f_3(T, n_{2l}, n_{2v}) \end{bmatrix} \tag{A.19}$$

The Matlab code implementing the above solution is located in Appendix H. A set of initial conditions is required to make the system A.18 well posed. An initial temperature, total moles of helium in the tank, total initial moles of nitrous oxide in the tank, density of nitrous oxide liquid (available in *Perry's Chemical Engineers' Handbook* (1997)), and the tank volume are specified. The initial equilibrium state can be calculated using Raoult's law, the ideal gas law, and an equation specifying that the total number of nitrous oxide moles is the sum of the liquid and vapor nitrous oxide moles. The result is:

$$n_{2l_o} = \frac{n_{2T} R T_o - P_2^*\big|_{T_o} V}{R T_o - P_2^*\big|_{T_o} \hat{V}_{2l}}$$

(A.20a)

$$n_{2v_o} = \frac{P_2^*\big|_{T_o} \left(V - n_{2T} \hat{V}_{2l}\right)}{R T_o - P_2^*\big|_{T_o} \hat{V}_{2l}}$$

(A.20b)

where the subscript 'o' denotes initial, and n_{2T} is the total moles of nitrous oxide initially loaded into the tank. As can be seen in the two equations, the presence of helium has no effect on the distribution of nitrous oxide into liquid or gas. This is because Raoult's law specifies that the partial pressure of a component of the system is only dependent on the *pure* component's vapor pressure. Raoult's law is only valid for systems where the ideal gas assumption is valid.

APPENDIX B

NON-IDEAL MODEL DERIVATION

B-1   Time History Calculation

In this appendix, the governing equations and solution procedure to solve for the draining tank time history including non-ideal behavior are outlined. The problem to be solved is stated explicitly in Chapter 3. The equations which constrain the tank draining problem at hand are the same as that for the ideal model as shown in Appendix A, except those which reflect the non-ideal equation-of-state. One important aspect of the problem is that the non-ideal equation-of-state will not only describe the P-V-T behavior of the gas and liquid phases, but also affects the form of the equilibrium constraint.

Choosing a control volume that encompasses all of the liquid and gas in the tank as well as the tank itself, as indicated in Figure A.2, the following equations arise. Note that component 1 is a non-condensable pressurant (helium), and component 2 is a self-pressurizing oxidizer (nitrous oxide). All notation is identical to that in Appendix A, except for any additional notation needed to describe the non-ideal behavior. A complete list of notation is also available in the Nomenclature section.

Molar Conservation:

$$\frac{d}{dt}\left(n_g + n_{2l}\right) = \frac{d}{dt}\left(n_{2v} + n_{2l}\right) = -\dot{n}_{2,drain} \tag{B.1a}$$

Energy Conservation:

$$\frac{d}{dt}\left(m_T \overline{U}_T + n_{2l}\hat{U}_{2l} + n_g \hat{U}_g\right) = -\dot{n}_{2,drain}\hat{H}_{2l} \tag{B.1b}$$

Flow Relation:

$$\dot{n}_{2l} = \frac{C_D A_{injector}}{(MW)_2}\sqrt{\frac{2(MW)_2\left(P - P_e\right)}{\hat{V}_{2l}}} \tag{B.1c}$$

Vapor-Liquid Equilibrium:

$$\phi_{2l} = y_2 \phi_{2v}$$
$$\phi_{2l} = \phi_{2l}(T, P, Z_{2l})$$
$$\phi_{2v} = \phi_{2v}(T, P, Z_g, y_2)$$

(B.1d,e,f)

Liquid Equation-of-State (Pure 2):

$$P\hat{V}_{2l} = Z_{2l}RT$$
$$Z_{2l} = Z_{2l}(T, P)$$

(B.1g,h)

Gas Equation-of-State (Mixture of 1 and 2 vapor):

$$P\hat{V}_g = Z_g RT$$
$$Z_g = Z_g(T, P, y_2)$$

(B.1i,j)

Volume Constraint:

$$V = V_g + V_l = V_g + n_{2l}\hat{V}_{2l}$$

(B.1k)

Refer to Appendix D for the full forms of Equations B.1e,f,h,g.

Once boundary conditions are provided, system B.1 is well-posed to determine the time history in the tank. Ultimately, the above system of equations can be manipulated into a set of four equations with four unknown derivatives in time: T, P, n_{2l}, and n_{2v}. The derivation to achieve this result proceeds below.

The chain rule can be used to expand the left-hand-side of Equation B1.b as:

$$\frac{d}{dt}\left(m_T \overline{U}_T + n_{2l}\hat{U}_{2l} + n_g \hat{U}_g\right) =$$
$$= \frac{dm_T}{dt}\overline{U}_T + m_T \frac{d\overline{U}_T}{dt} + \frac{dn_{2l}}{dt}\hat{U}_{2l} + n_{2l}\frac{d\hat{U}_{2l}}{dt} + \frac{dn_g}{dt}\hat{U}_g + n_g \frac{d\hat{U}_g}{dt}$$

(B.2)

The following simplification set B.3 can be applied to Equation B.2:

$$\frac{dm_T}{dt} = 0 \tag{B.3a}$$

$$\frac{dn_g}{dt} = \frac{dn_{2v}}{dt} \tag{B.3b}$$

$$\overline{U}_T \approx \overline{H}_T \text{ (solid)} \tag{B.3c}$$

$$\left.\begin{array}{l} \hat{H}_{2l} = \hat{U}_{2l} + P\hat{V}_{2l} \\ P\hat{V}_{2l} = Z_{2l}RT \end{array}\right\} \Rightarrow \hat{U}_{2l} = \hat{H}_{2l} - Z_{2l}RT \tag{B.3d}$$

$$\left.\begin{array}{l} \hat{H}_g = \hat{U}_g + P\hat{V}_g \\ P\hat{V}_g = Z_g RT \end{array}\right\} \Rightarrow \hat{U}_g = \hat{H}_g - Z_g RT \tag{B.3e}$$

The resulting energy equation can be written as follows:

$$m_T \frac{d\overline{H}_T}{dt} + \left(\hat{H}_{2l} - Z_{2l}RT\right)\frac{dn_{2l}}{dt} + n_{2l}\left[\frac{d\hat{H}_{2l}}{dt} - \frac{d}{dt}\left(Z_{2l}RT\right)\right]$$

$$+ \left(\hat{H}_g - Z_g RT\right)\frac{dn_{2v}}{dt} + n_g\left[\frac{d\hat{H}_g}{dt} - \frac{d}{dt}\left(Z_g RT\right)\right] = -\dot{n}_{2,drain}\hat{H}_{2l} \tag{B.4}$$

The first three terms on the left-hand-side of Equation B.4 may be rewritten in a form more suitable for solution as follows. The first term in the energy equation can be simplified as follows:

$$m_T \frac{d\overline{H}_T}{dt} = m_T \overline{C}_{P_T} \frac{dT}{dt} \tag{B.5a}$$

The liquid enthalpy, $\hat{H}_{2l}$, can be expressed as:

$$\hat{H}_{2l} = \hat{H}_{2l}^*(T) + \hat{H}_{2l,excess}\left(Z_{2l}(T,P),T,P\right) \tag{B.5b}$$

In Equation B.5b, $\hat{H}_{2l}^{*}(T)$ is the ideal liquid molar enthalpy at low pressures, and $\hat{H}_{2l,excess}$ is the non-ideal correction to this quantity at high pressures. $\hat{H}_{2l,excess} \to 0$ as $P \to 0$. The form of $\hat{H}_{2l,excess}$ is given in Appendix D. The derivative of the liquid enthalpy can be expressed as:

$$\frac{d\hat{H}_{2l}}{dt} = \frac{\partial \hat{H}_{2l}}{\partial T}\bigg|_{P} \frac{dT}{dt} + \frac{\partial \hat{H}_{2l}}{\partial P}\bigg|_{T} \frac{dP}{dt} \tag{B.5c}$$

where

$$\frac{\partial \hat{H}_{2l}}{\partial T}\bigg|_{P} = \frac{d\hat{H}_{2l}^{*}}{dT} + \left(\frac{\partial \hat{H}_{2l,excess}}{\partial Z_{2l}}\bigg|_{T,P} \frac{\partial Z_{2l}}{\partial T}\bigg|_{P} + \frac{\partial \hat{H}_{2l,excess}}{\partial T}\bigg|_{Z_{2l},P} \right) \tag{B.5d}$$

$$\frac{\partial \hat{H}_{2l}}{\partial P}\bigg|_{T} = \frac{\partial \hat{H}_{2l,excess}}{\partial Z_{2l}}\bigg|_{T,P} \frac{\partial Z_{2l}}{\partial P}\bigg|_{T} + \frac{\partial \hat{H}_{2l,excess}}{\partial P}\bigg|_{Z_{2l},T} \tag{B.5e}$$

$$\frac{d\hat{H}_{2l}^{*}}{dT} \equiv \hat{C}_{P_{2l}}^{*} \tag{B.5f}$$

The next derivative in the first square bracket of Equation B.4 can be expanded as follows:

$$\frac{d}{dt}(Z_{2l}RT) = R\left[Z_{2l}\frac{dT}{dt} + T\left(\frac{\partial Z_{2l}}{\partial T}\bigg|_{P}\frac{dT}{dt} + \frac{\partial Z_{2l}}{\partial P}\bigg|_{T}\frac{dP}{dt} \right) \right]$$

$$= R\left(Z_{2l} + T\frac{\partial Z_{2l}}{\partial T}\bigg|_{P} \right)\frac{dT}{dt} + RT\frac{\partial Z_{2l}}{\partial P}\bigg|_{T}\frac{dP}{dt} \tag{B.6}$$

Substituting Equations B.5 and B.6 into the first three terms of Equation B.4 and combining like terms, the following equation is obtained:

$$m_{T}\frac{d\overline{H}_{T}}{dt} + \left(\hat{H}_{2l} - Z_{2l}RT \right)\frac{dn_{2l}}{dt} + n_{2l}\left[\frac{d\hat{H}_{2l}}{dt} - \frac{d}{dt}(Z_{2l}RT) \right]$$

$$= N\frac{dT}{dt} + Q\frac{dP}{dt} + \left(\hat{H}_{2l}^{*} + S \right)\frac{dn_{2l}}{dt} \tag{B.7a}$$

where

$$N(T,P,n_{2l}) = m_T \overline{C}_{P_T} + n_{2l} \left[\begin{array}{c} \hat{C}_{P_{2l}}^* + \left.\dfrac{\partial \hat{H}_{2l,excess}}{\partial Z_{2l}}\right|_{T,P} \left.\dfrac{\partial Z_{2l}}{\partial T}\right|_P \\[4mm] + \left.\dfrac{\partial \hat{H}_{2l,excess}}{\partial T}\right|_{Z_{2l},P} - R\left(Z_{2l} + T \left.\dfrac{\partial Z_{2l}}{\partial T}\right|_P \right) \end{array} \right] \qquad \text{(B.7b)}$$

$$Q(T,P,n_{2l}) = n_{2l} \left\{ \left.\dfrac{\partial \hat{H}_{2l,excess}}{\partial Z_{2l}}\right|_{T,P} \left.\dfrac{\partial Z_{2l}}{\partial P}\right|_T + \left.\dfrac{\partial \hat{H}_{2l,excess}}{\partial P}\right|_{Z_{2l},T} - RT \left.\dfrac{\partial Z_{2l}}{\partial P}\right|_T \right\} \qquad \text{(B.7c)}$$

$$S(T,P) = \hat{H}_{2l,excess} - Z_{2l}RT \qquad \text{(B.7d)}$$

where $\overline{C}_{P_T}$ and $\hat{C}_{P_{2l}}^*$ are correlated functions of temperature found in *Perry's Chemical Engineers' Handbook* (1997).

The remaining terms of the left-hand-side of Equation B.4 are rewritten below. The gas mixture enthalpy derivative in the fifth term can be expanded as follows:

$$\hat{H}_g = (1 - y_2)\hat{H}_{1g}^*(T) + y_2 \hat{H}_{2v}^*(T) + \hat{H}_{g,excess}(Z_g, T, P, y_2) \qquad \text{(B.8a)}$$

$$
\frac{d\hat{H}_g}{dt} = \left\{ \begin{array}{l} \left(1 - y_2\right)\frac{d\hat{H}^*_{1g}}{dT} + y_2\,\frac{d\hat{H}^*_{2v}}{dT} + \left.\frac{\partial\hat{H}_{g,excess}}{\partial Z_g}\right|_{T,P,y_2} \left.\frac{\partial Z_g}{\partial T}\right|_{P,y_2} \\[3ex] + \left.\frac{\partial\hat{H}_{g,excess}}{\partial T}\right|_{Z_g,P,y_2} \end{array} \right\} \frac{dT}{dt}
$$

$$
+ \left\{ \left.\frac{\partial\hat{H}_{g,excess}}{\partial Z_g}\right|_{T,P,y_2} \left.\frac{\partial Z_g}{\partial P}\right|_{T,y_2} + \left.\frac{\partial\hat{H}_{g,excess}}{\partial P}\right|_{Z_g,T,y_2} \right\} \frac{dP}{dt}
$$

$$
+ \left\{ \begin{array}{l} -\frac{dy_2}{dn_{2v}}\,\hat{H}^*_{1g} + \frac{dy_2}{dn_{2v}}\,\hat{H}^*_{2v} + \left.\frac{\partial\hat{H}_{g,excess}}{\partial Z_g}\right|_{T,P,y_2} \left.\frac{\partial Z_g}{\partial y_2}\right|_{T,P} \frac{dy_2}{dn_{2v}} \\[3ex] + \left.\frac{\partial\hat{H}_{g,excess}}{\partial y_2}\right|_{Z_g,T,P} \frac{dy_2}{dn_{2v}} \end{array} \right\} \frac{dn_{2v}}{dt}
$$

(B.8b)

In Equation B.8, "*" denotes ideal as found in handbooks (at low pressures), and excess quantities are contributions due to the non-ideal equation-of-state. The expression for $\hat{H}_{g,excess}$ is given in Appendix D. The next derivative in the fifth term of the energy equation can be expanded as follows:

$$
\frac{d}{dt}\left(Z_g RT\right) = R\left(Z_g + T\left.\frac{\partial Z_g}{\partial T}\right|_{P,y_2} \right)\frac{dT}{dt} + RT\left.\frac{\partial Z_g}{\partial P}\right|_{T,y_2} \frac{dP}{dt}
$$

$$
+ RT\left.\frac{\partial Z_g}{\partial y_2}\right|_{T,P} \frac{dy_2}{dn_{2v}}\frac{dn_{2v}}{dt}
$$

(B.8c)

Therefore, the fifth term of the energy equation can be written as:

$$
n_g \left[\frac{d\hat{H}_g}{dt} - \frac{d}{dt}\left(Z_g RT \right) \right] =
$$

$$
\left\{ n_{1_o} \frac{d\hat{H}_{1g}^*}{dT} + n_{2v} \frac{d\hat{H}_{2v}^*}{dT} + n_g \left[\begin{array}{c} \dfrac{\partial \hat{H}_{g,excess}}{\partial Z_g}\bigg|_{T,P,y_2} \dfrac{\partial Z_g}{\partial T}\bigg|_{P,y_2} + \dfrac{\partial \hat{H}_{g,excess}}{\partial T}\bigg|_{Z_g,P,y_2} \\[2em] - R\left(Z_g + T\dfrac{\partial Z_g}{\partial T}\bigg|_{P,y_2} \right) \end{array} \right] \right\} \frac{dT}{dt}
$$

$$
+ n_g \left\{ \frac{\partial \hat{H}_{g,excess}}{\partial Z_g}\bigg|_{T,P,y_2} \frac{\partial Z_g}{\partial P}\bigg|_{T,y_2} + \frac{\partial \hat{H}_{g,excess}}{\partial P}\bigg|_{Z_g,T,y_2} - RT\frac{\partial Z_g}{\partial P}\bigg|_{T,y_2} \right\} \frac{dP}{dt}
$$

$$
+ (1 - y_2) \left\{ \begin{array}{c} -\hat{H}_{1g}^* + \hat{H}_{2v}^* + \dfrac{\partial \hat{H}_{g,excess}}{\partial Z_g}\bigg|_{T,P,y_2} \dfrac{\partial Z_g}{\partial y_2}\bigg|_{T,P} \\[2em] + \dfrac{\partial \hat{H}_{g,excess}}{\partial y_2}\bigg|_{Z_g,T,P} - RT\dfrac{\partial Z_g}{\partial y_2}\bigg|_{T,P} \end{array} \right\} \frac{dn_{2v}}{dt}
$$

$$
\hspace{13cm} \text{(B.8d)}
$$

Note that:

$$
\frac{d\hat{H}_{1g}^*}{dT} \equiv C_{P_{1g}}^* \tag{B.9a}
$$

$$
\frac{d\hat{H}_{2v}^*}{dT} \equiv C_{P_{2v}}^* \tag{B.9b}
$$

where $C_{P_{1g}}^*$ and $C_{P_{2v}}^*$ are ideal heat capacities at low pressures, both correlated with

temperature in *Perry's Chemical Engineers' Handbook* (1997). The fourth and fifth terms of

the energy equation B.4 can thus be rewritten using Equations B.8 and B.9 as:

$$\left(\hat{H}_g - Z_g RT\right)\frac{dn_{2v}}{dt} + n_g\left[\frac{d\hat{H}_g}{dt} - \frac{d}{dt}\left(Z_g RT\right)\right] =$$

$$D\frac{dT}{dt} + E\frac{dP}{dt} + \left(\hat{H}_{2v}^* + M\right)\frac{dn_{2v}}{dt} \tag{B.10a}$$

where

$$D(T, P, n_{2v}) = n_{1_O} C_{P_{1g}}^* + n_{2v} C_{P_{2v}}^*$$

$$+ n_g\left[\frac{\partial \hat{H}_{g,excess}}{\partial Z_g}\bigg|_{T,P,y_2} \frac{\partial Z_g}{\partial T}\bigg|_{P,y_2} + \frac{\partial \hat{H}_{g,excess}}{\partial T}\bigg|_{Z_g,P,y_2} - R\left(Z_g + T\frac{\partial Z_g}{\partial T}\bigg|_{P,y_2}\right)\right]$$

$$E(T, P, n_{2v}) = n_g\left\{\frac{\partial \hat{H}_{g,excess}}{\partial Z_g}\bigg|_{T,P,y_2} \frac{\partial Z_g}{\partial P}\bigg|_{T,y_2} + \frac{\partial \hat{H}_{g,excess}}{\partial P}\bigg|_{Z_g,T,y_2} - RT\frac{\partial Z_g}{\partial P}\bigg|_{T,y_2}\right\}$$

$$M(T, P, n_{2v}) = \hat{H}_{g,excess} - Z_g RT + (1 - y_2)\left[\begin{array}{c}\dfrac{\partial \hat{H}_{g,excess}}{\partial Z_g}\bigg|_{T,P,y_2} \dfrac{\partial Z_g}{\partial y_2}\bigg|_{T,P} \\[2ex] + \dfrac{\partial \hat{H}_{g,excess}}{\partial y_2}\bigg|_{Z_g,T,P} - RT\dfrac{\partial Z_g}{\partial y_2}\bigg|_{T,P}\end{array}\right]$$

$$\text{(B.10b,c,d)}$$

Combining Equations B.4, B.7, and B.10, the energy equation can now be written as:

$$(N + D)\frac{dT}{dt} + (Q + E)\frac{dP}{dt} + \left(\hat{H}_{2l}^* + S\right)\frac{dn_{2l}}{dt} + \left(\hat{H}_{2v}^* + M\right)\frac{dn_{2v}}{dt} = -\dot{n}_{2l}\hat{H}_{2l} \tag{B.11}$$

From the molar conservation equation:

$$-\dot{n}_{2,drain} = \frac{d}{dt}\left(n_{2v} + n_{2l}\right) = \frac{dn_{2v}}{dt} + \frac{dn_{2l}}{dt} \tag{B.12a}$$

and thus:

$$-\dot{n}_{2,drain}\hat{H}_{2l} = \left(\frac{dn_{2v}}{dt} + \frac{dn_{2l}}{dt}\right)\left[\hat{H}_{2l}^* + \hat{H}_{2l,excess}\right] \tag{B.12b}$$

Using the molar conservation equation, Equation B.1a, the definition of heat of vaporization, $\hat{H}_{2l}^* - \hat{H}_{2v}^* = -\Delta\hat{H}_{2v}$, and the following substitutions, Equations B.13, the energy equation can be written in its final form:

$$X\frac{dT}{dt} + W\frac{dP}{dt} + Y\frac{dn_{2l}}{dt} + \zeta\frac{dn_{2v}}{dt} = 0 \tag{B.13a}$$

where:

$$X = D + N \tag{B.13b}$$

$$W = E + Q \tag{B.13c}$$

$$Y = S - \hat{H}_{2l,excess} \tag{B.13d}$$

$$\zeta = \Delta\hat{H}_{2v} + M - \hat{H}_{2l,excess} \tag{B.13e}$$

Equation set B.13 the first of four equations that is required for solution of the unknowns T, P, n_{2l}, and n_{2v}. The second equation comes from combining the flow relation and the liquid equation-of-state with the molar balance to obtain the following equation:

$$\frac{dn_{2v}}{dt} + \frac{dn_{2l}}{dt} = -K \tag{B.14a}$$

where

$$K = C_D A_{injector}\sqrt{\frac{2P(P-P_e)}{(MW)_2 Z_{2l} RT}} \tag{B.14b}$$

The volume constraint can be combined with both liquid and gas equations-of-state to obtain the following equation:

$$P = \frac{RT}{V}\left(Z_g n_g + Z_{2l} n_{2l}\right)$$

(B.15a)

Ultimately, the derivatives of T, P, n_{2l}, and n_{2v} with respect to time will be solved for explicitly; therefore, it is convenient for later computer implementation to take the time derivative of the above equation to express it in terms of derivatives:

$$\frac{dP}{dt} = \left.\frac{\partial P}{\partial Z_g}\right|_{n_g,Z_{2l},n_{2l},T} \frac{dZ_g}{dt} + \left.\frac{\partial P}{\partial n_g}\right|_{Z_g,Z_{2l},n_{2l},T} \frac{dn_g}{dt} + \left.\frac{\partial P}{\partial Z_{2l}}\right|_{Z_g,n_g,n_{2l},T} \frac{dZ_{2l}}{dt}$$
$$+ \left.\frac{\partial P}{\partial n_{2l}}\right|_{Z_g,n_g,Z_{2l},T} \frac{dn_{2l}}{dt} + \left.\frac{\partial P}{\partial T}\right|_{Z_g,n_g,Z_{2l},n_{2l}} \frac{dT}{dt}$$

(B.15b)

Expanding Equation B.15b yields:

$$\beta \frac{dT}{dt} + \gamma \frac{dP}{dt} + Z_{2l}\frac{dn_{2l}}{dt} + \delta \frac{dn_{2v}}{dt} = 0$$

(B.16a)

where

$$\beta = n_g \left.\frac{\partial Z_g}{\partial T}\right|_{P,y_2} + n_{2l} \left.\frac{\partial Z_{2l}}{\partial T}\right|_{P} + \frac{1}{T}\left(Z_g n_g + Z_{2l} n_{2l}\right)$$

(B.16b)

$$\gamma = n_g \left.\frac{\partial Z_g}{\partial P}\right|_{T,y_2} + n_{2l} \left.\frac{\partial Z_{2l}}{\partial P}\right|_{T} - \frac{V}{RT}$$

(B.16c)

$$\delta = \left(1 - y_2\right)\left.\frac{\partial Z_g}{\partial y_2}\right|_{T,P} + Z_g$$

(B.16d)

Equation B.16 is the third equation to solve for the derivatives. The final equation needed to solve for the derivatives comes from taking the time derivative of the equilibrium constraint, Equation B1.d. Like Equation B.15a, the time derivative of Equation B1.d was taken in order to express it in terms of the four unknown derivatives.

$$\frac{d}{dt}\left(n_g\phi_{2l} - n_{2v}\phi_{2v}\right) = 0$$

After this equation is expanded, the final form of this equation (the fourth required to solve for the time derivatives) is written as follows:

$$\theta\frac{dT}{dt} + \lambda\frac{dP}{dt} + \psi\frac{dn_{2v}}{dt} = 0 \tag{B.17a}$$

where

$$\theta = n_g\left(\left.\frac{\partial\phi_{2l}}{\partial Z_{2l}}\right|_{T,P}\left.\frac{\partial Z_{2l}}{\partial T}\right|_P + \left.\frac{\partial\phi_{2l}}{\partial T}\right|_{Z_{2l},P}\right) - n_{2v}\left(\left.\frac{\partial\phi_{2v}}{\partial Z_g}\right|_{T,P,y_2}\left.\frac{\partial Z_g}{\partial T}\right|_{P,y_2} + \left.\frac{\partial\phi_{2v}}{\partial T}\right|_{Z_g,P,y_2}\right)$$

$$\lambda = n_g\left(\left.\frac{\partial\phi_{2l}}{\partial Z_{2l}}\right|_{T,P}\left.\frac{\partial Z_{2l}}{\partial P}\right|_T + \left.\frac{\partial\phi_{2l}}{\partial P}\right|_{Z_{2l},T}\right) - n_{2v}\left(\left.\frac{\partial\phi_{2v}}{\partial Z_g}\right|_{T,P,y_2}\left.\frac{\partial Z_g}{\partial P}\right|_{T,y_2} + \left.\frac{\partial\phi_{2v}}{\partial P}\right|_{Z_g,T,y_2}\right)$$

$$\psi = \phi_{2l} - \phi_{2v} - y_2\left(1-y_2\right)\left(\left.\frac{\partial\phi_{2v}}{\partial Z_g}\right|_{T,P,y_2}\left.\frac{\partial Z_g}{\partial y_2}\right|_{T,P} + \left.\frac{\partial\phi_{2v}}{\partial y_2}\right|_{Z_g,T,P}\right)$$

$$(B.17b,c,d)$$

In summary, the final set of equations to solve is given by B.13, B.14, B.16, and B.17, rewritten here for convenience:

$$X\frac{dT}{dt} + W\frac{dP}{dt} + Y\frac{dn_{2l}}{dt} + \zeta\frac{dn_{2v}}{dt} = 0 \tag{B.18a}$$

$$\frac{dn_{2l}}{dt} + \frac{dn_{2v}}{dt} = -K \tag{B.18b}$$

$$\beta\frac{dT}{dt} + \gamma\frac{dP}{dt} + Z_{2l}\frac{dn_{2l}}{dt} + \delta\frac{dn_{2v}}{dt} = 0 \tag{B.18c}$$

$$\theta \frac{dT}{dt} + \lambda \frac{dP}{dt} + \psi \frac{dn_{2v}}{dt} = 0 \qquad\qquad\qquad \text{(B.18d)}$$

The system B.18 can easily be solved in the form:

$$
\begin{bmatrix}
X & W & Y & \zeta \\
0 & 0 & 1 & 1 \\
\beta & \gamma & Z_{2l} & \delta \\
\theta & \lambda & 0 & \psi
\end{bmatrix}
\begin{bmatrix}
\dfrac{dT}{dt} \\[4pt]
\dfrac{dP}{dt} \\[4pt]
\dfrac{dn_{2l}}{dt} \\[4pt]
\dfrac{dn_{2v}}{dt}
\end{bmatrix}
=
\begin{bmatrix}
0 \\
-K \\
0 \\
0
\end{bmatrix}
\qquad\qquad \text{(B.19)}
$$

The above system B.19 requires an initial condition to make the system well posed. This is considered in the next section.

B-2   Initial Condition Calculation

For the problem presented in Chapter 3, the only initial quantities known for the tank before it drains are the tank's internal volume, its temperature, and the amount of nitrous oxide and helium placed in the tank. The pressure and distribution of nitrous oxide between the liquid and gas phases are not known. However, all of these quantities need to be known to start the draining calculation. Thus, the initial state of the material in the tank needs to be fully determined before the draining time history can be found.

The initial condition calculation uses many of the same equations as for the draining tank derivation in Section B-1. However, in this case the time derivatives are not necessary because the tank is not yet draining. It is assumed that all the helium is in the gas phase, and therefore the nitrous oxide liquid is pure. When there is no helium in the tank, the calculation should *output* a pressure corresponding to the vapor pressure of pure nitrous oxide at the given temperature, which can be checked against any handbook value, for instance *Perry's Chemical Engineers' Handbook* (1997). This is also a helpful check to see how accurately the Peng-Robinson equation-of-state describes pure nitrous oxide properties, such as vapor pressure.

The following are the equations that govern the initial state of the tank contents:

Molar Conservation:

$$n_{2T} = n_{2v} + n_{2l}$$
$$n_g = n_{1_o} + n_{2v}$$

(B.20a,b)

Vapor-Liquid Equilibrium Relation:

$$\phi_{2l} = y_2 \phi_{2v}$$
$$\phi_{2l} = \phi_{2l}(T, P, Z_{2l})$$
$$\phi_{2v} = \phi_{2v}(T, P, Z_g, y_2)$$

(B.20c)

Liquid Equation-of-State (Pure 2):

$$P\hat{V}_{2l} = Z_{2l}RT$$
$$Z_{2l} = Z_{2l}(T, P)$$

(B.20d)

Gas Equation-of-State (Mixture of 1 and 2 vapor):

$$P\hat{V}_g = Z_g RT$$
$$Z_g = Z_g(T, P, y_2)$$

(B.20e)

Volume Constraint:

$$V = V_g + V_l = n_g \hat{V}_g + n_{2l}\hat{V}_{2l}$$

(B.20f)

The desired output is three initial conditions (P, n_{2v}, n_{2l}) with respect to four inputs: V, T, n_{2T}, and n_{1_o}. The nitrous oxide liquid, n_{2l}, can be expressed explicitly in terms of the total number of moles of nitrous oxide placed in the tank and that in the gas phase, given by n_{2T} and n_{2v}, respectively, using the conservation equation B.20a. This allows the explicit appearance of n_{2l} to be eliminated from the system of equations, leaving two unknowns: P and n_{2v}. By combining the volume constraint with the equations-of-state and the molar conservation equation, the following equation is obtained:

$$V = \frac{RT}{P}\left[\left(n_{1_o} + n_{2v}\right)Z_g + \left(n_{2T} - n_{2v}\right)Z_{2l}\right]$$ (B.21)

This equation and the vapor-liquid equilibrium relation (B.20c) are the two equations, both in terms of P and n_{2v}, needed to solve for the initial conditions. They can be rewritten in the form:

$$F_1(P, n_{2v}) = \left(n_{1_o} + n_{2v}\right)\phi_{2l} - n_{2v}\phi_{2v}$$ (B.22a)

$$F_2(P, n_{2v}) = \left(n_{1_o} + n_{2v}\right)Z_g + \left(n_{2T} - n_{2v}\right)Z_{2l} - \frac{PV}{RT}$$ (B.22b)

The solution of B.22 is achieved when the two functions, F_1 and F_2, equal zero. This is attained by iteration using Newton's method. The calculation sequence goes as follows:

1) Initial guesses:

    a. Use an initial estimate for y_2 to determine guess for n_{2v}:

$$n_{2v} = \frac{y_2 n_{1_o}}{1 - y_2}$$

    b. Give initial guess for P according to Raoult's Law, where $P_2^*(T)$ is from correlation:

$$P = \frac{P_2^*(T)}{y_2}$$

2) Calculate compressibilities: $Z_{2l} = Z_{2l}(T, P)$ and $Z_g = Z_g(T, P, y_2)$

$$Z^3 - (1 - B)Z^2 + \left(A - 3B^2 - 2B\right)Z - \left(AB - B^2 - B^3\right) = 0$$

$$a_2 = -(1 - B)$$

$$a_1 = \left(A - 3B^2 - 2B\right)$$

$$a_0 = -\left(AB - B^2 - B^3\right)$$

$$\Rightarrow Z^3 + a_2 Z^2 + a_1 Z + a_0 = 0$$

Note: Only real roots are of interest. When there are three real roots (Z_1, Z_2, Z_3):

$$Z_g = \max(Z_1, Z_2, Z_3)$$

$$Z_{2l} = \min(Z_1, Z_2, Z_3)$$

Solution to a cubic equation can be found in Abramowitz and Stegun (1972), and is given as follows:

$$q = \frac{1}{3}a_1 - \frac{1}{9}a_2^2$$

$$r = \frac{1}{6}(a_1 a_2 - 3a_0) - \frac{1}{27}a_2^3$$

Case 1: $q^3 + r^2 > 0$, one real root and two complex conjugate roots:

$$s_1 = \left[r + \sqrt{q^3 + r^2} \right]^{1/3}$$

$$s_2 = \left[r - \sqrt{q^3 + r^2} \right]^{1/3}$$

$$Z = s_1 + s_2 - \frac{a_2}{3}$$

Case 2: $q^3 + r^2 = 0$, Three real roots where at least two are equal:

$$s_1 = s_2 = r^{1/3}$$

$$Z_1 = s_1 + s_2 - \frac{a_2}{3}$$

$$Z_2 = Z_3 = -\frac{1}{2}(s_1 + s_2) - \frac{a_2}{3}$$

Case 3: $q^3 + r^2 < 0$, three real and distinct roots

(Note that the following case is said to be "non-reducible" in Abramowitz and Stegun (1972). The explicit solution via complex variables shown below was found by S. Weinstein.)

$$\sqrt{q^3 + r^2} = i\sqrt{\left| q^3 + r^2 \right|}$$

Let $\alpha = \sqrt{\left| q^3 + r^2 \right|}$

$\Rightarrow \sqrt{q^3 + r^2} = i\alpha$

$s_1 = (r + i\alpha)^{1/3}$

$s_2 = (r - i\alpha)^{1/3}$

Let $r + i\alpha = \rho e^{i\theta}$

Let $r - i\alpha = \rho e^{-i\theta}$

$\rho = \sqrt{r^2 + \alpha^2}$

$\theta = \begin{cases} \tan^{-1}\left(\dfrac{\alpha}{r}\right), & r > 0 \\[4mm] \pi - \tan^{-1}\left(\dfrac{\alpha}{|r|}\right), & r < 0 \end{cases}$

$\rho e^{\pm i\theta} = \rho \cos\theta \pm i\rho \sin\theta$

$\Rightarrow s_1 = \left(\rho e^{i\theta}\right)^{1/3}$

$\Rightarrow s_2 = \left(\rho e^{-i\theta}\right)^{1/3}$

$Z_1 = s_1 + s_2 - \dfrac{a_2}{3} = 2\rho^{1/3}\cos\left(\dfrac{\theta}{3}\right) - \dfrac{a_2}{3}$

$Z_2 = -\dfrac{1}{2}(s_1 + s_2) - \dfrac{a_2}{3} + \dfrac{i\sqrt{3}}{2}(s_1 - s_2) = \rho^{1/3}\left[-\cos\left(\dfrac{\theta}{3}\right) + \sqrt{3}\sin\left(\dfrac{\theta}{3}\right)\right] - \dfrac{a_2}{3}$

$Z_3 = -\dfrac{1}{2}(s_1 + s_2) - \dfrac{a_2}{3} - \dfrac{i\sqrt{3}}{2}(s_1 - s_2) = \rho^{1/3}\left[-\cos\left(\dfrac{\theta}{3}\right) - \sqrt{3}\sin\left(\dfrac{\theta}{3}\right)\right] - \dfrac{a_2}{3}$

3) Evaluate $F_1(P, n_{2v})$ and $F_2(P, n_{2v})$

4) Update guesses for P and n_{2v} using Newton's Method:

$$\begin{pmatrix} n_{2v} \\ P \end{pmatrix}_{k+1} = \begin{pmatrix} n_{2v} \\ P \end{pmatrix}_{k} - \underline{\underline{JAC}}\Big|_{k}^{-1} \begin{bmatrix} F_1 \\ F_2 \end{bmatrix}_{k}$$

$$\underline{\underline{JAC}}\Big|_{k} = \begin{bmatrix} \dfrac{\partial F_1}{\partial n_{2v}} & \dfrac{\partial F_1}{\partial P} \\ \dfrac{\partial F_2}{\partial n_{2v}} & \dfrac{\partial F_2}{\partial P} \end{bmatrix}_{k}$$

$$\underline{\underline{JAC}}\Big|_{k}^{-1} = \dfrac{\begin{bmatrix} \dfrac{\partial F_2}{\partial P} & -\dfrac{\partial F_1}{\partial P} \\ -\dfrac{\partial F_2}{\partial n_{2v}} & \dfrac{\partial F_1}{\partial n_{2v}} \end{bmatrix}_{k}}{\dfrac{\partial F_1}{\partial n_{2v}}\dfrac{\partial F_2}{\partial P} - \dfrac{\partial F_1}{\partial P}\dfrac{\partial F_2}{\partial n_{2v}}}$$

$$\dfrac{\partial F_i}{\partial P} = \dfrac{F_i\left(P + \dfrac{\Delta P}{2}\right) - F_i\left(P - \dfrac{\Delta P}{2}\right)}{\Delta P}$$

$$\dfrac{\partial F_i}{\partial n_{2v}} = \dfrac{F_i\left(n_{2v} + \dfrac{\Delta n_{2v}}{2}\right) - F_i\left(n_{2v} - \dfrac{\Delta n_{2v}}{2}\right)}{\Delta n_{2v}}$$

5) Check errors (norms)

$$\left\| \delta_{k+1} \right\| = \sqrt{\left(n_{2v}\big|_{k+1} - n_{2v}\big|_{k}\right)^2 + \left(P\big|_{k+1} - P\big|_{k}\right)^2}$$

$$\left\| F \right\| = \sqrt{F_1^2 + F_2^2}$$

Let $norm = \max\left(\left\| \delta_{k+1} \right\|, \left\| F \right\|\right)$

6) If norm > tolerance

   a. Calculate $y_2\big|_{k+1} = \dfrac{n_{2v}\big|_{k+1}}{n_{2v}\big|_{k+1} + n_{1_o}}$

b. Repeat steps 2 through 6 using updated P and n_{2v} guesses.

7) If norm < tolerance, then the solution has converged.

B-3   Summary

To solve the draining tank problem, the initial conditions are first determined according to the process set out in Section B-2. This provides T, P, n_{2l}, and n_{2v} at $t = 0$. Then the system B.19 derived in Section B-1 is solved, subject to these initial conditions. The numerical procedure used to solve these equations is discussed in Chapter 3. The Matlab code implementing this solution is located in Appendix I.

APPENDIX C

PENG-ROBINSON EQUATION-OF-STATE

This appendix contains the mathematical form of the Peng-Robinson equation-of-state, which falls into the class of cubic equations-of-state (Sandler, 2006). Cubic equations-of-state in the form shown below can be rewritten as cubic in the molar volume, $\hat{V}$, or alternatively the compressibility, Z.

$$P = \frac{RT}{\hat{V}-b} - \frac{a(T)}{\hat{V}(\hat{V}+b)+b(\hat{V}-b)} \tag{C.1}$$

where P is the total tank pressure, T is the temperature, and R is the universal gas constant. The constants a and b are functions of the critical temperatures and pressures, T_C and P_C respectively, of the tank contents (nitrous oxide and helium in this case). Recall from Chapter 3 that component 1 is the pressurant, and component 2 is the oxidizer. The subscripts "m" and "g" denote mixture quantities of the gas phase. Alternatively, Equation C.1 may be rewritten in terms of the compressibility, Z, by using the definition $P\hat{V}=ZRT$ to yield:

$$Z_{2l}{}^3 - (1-B_2)Z_{2l}{}^2 + (A_2 - 3B_2^2 - 2B_2)Z_{2l} - (A_2B_2 - B_2^2 - B_2^3) = 0$$

$$Z_g{}^3 - (1-B_m)Z_g{}^2 + (A_m - 3B_m^2 - 2B_m)Z_g - (A_mB_m - B_m^2 - B_m^3) = 0$$

where

$$A_2 = \frac{a_2 P}{R^2 T^2}$$

$$B_2 = \frac{b_2 P}{RT}$$

$$A_m = \frac{a_m P}{R^2 T^2}$$

$$B_m = \frac{b_m P}{RT}$$

$$a_1 = 0.45724 \frac{R^2 T_{C_1}^2}{P_{C_1}} \alpha_1$$

$$a_2 = 0.45724 \frac{R^2 T_{C_2}^2}{P_{C_2}} \alpha_2$$

$$b_1 = 0.0778 \frac{RT_{C_1}}{P_{C_1}}$$

$$b_2 = 0.0778 \frac{RT_{C_2}}{P_{C_2}}$$

$$a_m = (1 - y_2)^2 a_1 + 2 y_2 (1 - y_2) a_{21} + y_2^2 a_2$$

$$b_m = (1 - y_2) b_1 + y_2 b_2$$

$$a_{21} = \sqrt{a_1 a_2} (1 - k_{12})$$

$$\sqrt{\alpha_1} = 1 + \kappa \left(1 - \sqrt{\frac{T}{T_{C_1}}} \right)$$

$$\sqrt{\alpha_2} = 1 + \kappa \left(1 - \sqrt{\frac{T}{T_{C_2}}} \right)$$

$$\kappa_1 = 0.37464 + 1.54226 \omega_1 - 0.26992 \omega_1^2$$

$$\kappa_2 = 0.37464 + 1.54226 \omega_2 - 0.26992 \omega_2^2$$

$$y_2 = \frac{n_{2v}}{n_{2v} + n_{1o}}$$

Note that as $\hat{V}$ increases, the Peng-Robinson Equation C.1 yields predictions in accordance with the ideal gas law. This can be seen by inspection, since $\hat{V} \gg b$, and the term including $a(T)$ is small compared with the first term on the right-hand-side of Equation C.1.

APPENDIX D

PENG-ROBINSON ENTHALPIES AND FUGACITY COEFFICIENTS

The following are equations for the enthalpies and fugacity coefficients corresponding to the Peng-Robinson equation-of-state which are used in the energy conservation equation and the equilibrium constraint. All variable definitions and equations are provided in the Nomenclature section and in Appendix C, respectively. The equations listed below have been derived by Sandler (2006).

$$\hat{H}_{2l,excess} = RT(Z_{2l} - 1) + \frac{T\frac{da_2}{dT} - a_2}{2\sqrt{2}b_2} \ln\left[\frac{Z_{2l} + (1 + \sqrt{2})B_2}{Z_{2l} + (1 - \sqrt{2})B_2}\right] \tag{D.1}$$

$$\hat{H}_{g,excess} = RT(Z_g - 1) + \frac{T\frac{da_m}{dT} - a_m}{2\sqrt{2}b_m} \ln\left[\frac{Z_m + (1 + \sqrt{2})B_m}{Z_m + (1 - \sqrt{2})B_m}\right] \tag{D.2}$$

$$\ln\phi_{2l} = (Z_{2l} - 1) - \ln(Z_{2l} - B_2) - \frac{A_2}{2\sqrt{2}B_2} \ln\left[\frac{Z_{2l} + (1 + \sqrt{2})B_2}{Z_{2l} + (1 - \sqrt{2})B_2}\right] \tag{D.3}$$

$$\ln\phi_{2v} = \frac{B_2}{B_m}(Z_g - 1) - \ln(Z_g - B_m)$$
$$- \frac{A_m}{2\sqrt{2}B_m}\left[\frac{2\{(1 - y_2)A_{21} + y_2 A_2\}}{A_m} - \frac{B_2}{B_m}\right]\ln\left[\frac{Z_m + (1 + \sqrt{2})B_m}{Z_m + (1 - \sqrt{2})B_m}\right] \tag{D.4}$$

$$A_{21} = \frac{a_{21}P}{R^2 T^2} \tag{D.5}$$

APPENDIX E

PENG ROBINSON DERIVATIVES

The following are analytical derivatives used in the non-ideal tank draining model outlined in Chapter 3, and whose mathematical details are provided in Appendix B. All variables are defined in these sections in addition to the Nomenclature section, and all variable equations are located in Appendix C.

$$\left.\begin{array}{l} \phi_{2l} = \phi_{2l}(Z_{2l}, T, P) \\ Z_{2l} = Z_{2l}(T, P) \\ A_2, B_2 = A_2, B_2(T, P) \end{array}\right\} \Rightarrow$$

$$\frac{d\phi_{2l}}{dt} = \left.\frac{\partial \phi_{2l}}{\partial Z_{2l}}\right|_{T,P} \left(\left.\frac{\partial Z_{2l}}{\partial T}\right|_P \frac{dT}{dt} + \left.\frac{\partial Z_{2l}}{\partial P}\right|_T \frac{dP}{dt} \right) + \left.\frac{\partial \phi_{2l}}{\partial T}\right|_{Z_{2l},P} \frac{dT}{dt} + \left.\frac{\partial \phi_{2l}}{\partial P}\right|_{Z_{2l},T} \frac{dP}{dt}$$

$$\left.\frac{\partial \phi_{2l}}{\partial Z_{2l}}\right|_{T,P} = \phi_{2l}\left\{ 1 - \frac{1}{Z_{2l} - B_2} + \frac{A_2}{\left[Z_{2l} + \left(1 + \sqrt{2}\right)B_2\right]\left[Z_{2l} + \left(1 - \sqrt{2}\right)B_2\right]} \right\}$$

$$\left.\frac{\partial \phi_{2l}}{\partial T}\right|_{Z_{2l},P} = \phi_{2l}\left\{\begin{array}{l}\dfrac{\dfrac{\partial B_2}{\partial T}}{Z_{2l}-B_2} - \dfrac{1}{2\sqrt{2}}\left(\dfrac{\dfrac{\partial A_2}{\partial T}B_2 - A_2\dfrac{\partial B_2}{\partial T}}{B_2^2}\right)\ln\left[\dfrac{Z_{2l}+\left(1+\sqrt{2}\right)B_2}{Z_{2l}+\left(1-\sqrt{2}\right)B_2}\right] \\[2em] -\dfrac{A_2}{B_2}\dfrac{\partial B_2}{\partial T}\dfrac{Z_{2l}}{\left[Z_{2l}+\left(1+\sqrt{2}\right)B_2\right]\left[Z_{2l}+\left(1-\sqrt{2}\right)B_2\right]}\end{array}\right\}$$

$$\left.\frac{\partial \phi_{2l}}{\partial P}\right|_{Z_{2l},T} = \phi_{2l}\left\{\begin{array}{l}\dfrac{\dfrac{\partial B_2}{\partial P}}{Z_{2l}-B_2} - \dfrac{1}{2\sqrt{2}}\left(\dfrac{\dfrac{\partial A_2}{\partial P}B_2 - A_2\dfrac{\partial B_2}{\partial P}}{B_2^2}\right)\ln\left[\dfrac{Z_{2l}+\left(1+\sqrt{2}\right)B_2}{Z_{2l}+\left(1-\sqrt{2}\right)B_2}\right] \\[2em] -\dfrac{A_2}{B_2}\dfrac{\partial B_2}{\partial P}\dfrac{Z_{2l}}{\left[Z_{2l}+\left(1+\sqrt{2}\right)B_2\right]\left[Z_{2l}+\left(1-\sqrt{2}\right)B_2\right]}\end{array}\right\}$$

$$\left.\begin{array}{l}\phi_{2v} = \phi_{2v}\left(Z_g,T,P,y_2\right) \\[0.5em] Z_g = Z_g\left(T,P,y_2\right) \\[0.5em] y_2 = y_2\left(n_{2v}\right) \\[0.5em] A_2,B_2,A_{21} = A_2,B_2,A_{21}\left(T,P\right) \\[0.5em] A_m,B_m = A_m,B_m\left(T,P,y_2\right)\end{array}\right\} \Rightarrow$$

$$\frac{d\phi_{2v}}{dt} = \left.\frac{\partial\phi_{2v}}{\partial Z_g}\right|_{T,P,y_2}\left(\left.\frac{\partial Z_g}{\partial T}\right|_{P,y_2}\frac{dT}{dt} + \left.\frac{\partial Z_g}{\partial P}\right|_{T,y_2}\frac{dP}{dt} + \left.\frac{\partial Z_g}{\partial y_2}\right|_{T,P}\frac{dy_2}{dn_{2v}}\frac{dn_{2v}}{dt}\right)$$

$$+ \left.\frac{\partial\phi_{2v}}{\partial T}\right|_{Z_g,P,y_2}\frac{dT}{dt} + \left.\frac{\partial\phi_{2v}}{\partial P}\right|_{Z_g,T,y_2}\frac{dP}{dt} + \left.\frac{\partial\phi_{2v}}{\partial y_2}\right|_{Z_g,T,P}\frac{dy_2}{dn_{2v}}\frac{dn_{2v}}{dt}$$

$$\left.\frac{\partial\phi_{2v}}{\partial Z_g}\right|_{T,P,y_2} = \phi_{2v}\left\{\frac{B_2}{B_m} - \frac{1}{Z_g - B_m} + \left[\frac{2\{(1-y_2)A_{21} + y_2A_2\}}{A_m} - \frac{B_2}{B_m}\right]\frac{A_m}{\left[Z_g + \left(1+\sqrt{2}\right)B_m\right]\left[Z_g + \left(1-\sqrt{2}\right)B_m\right]}\right\}$$

$$\left.\frac{\partial \phi_{2v}}{\partial T}\right|_{Z_g,P,y_2} = \phi_{2v}\left\{ \begin{array}{l} \left(Z_g - 1\right)\left(\dfrac{\dfrac{\partial B_2}{\partial T} B_m - B_2 \dfrac{\partial B_m}{\partial T}}{B_m^2}\right) + \dfrac{\dfrac{\partial B_m}{\partial T}}{Z_g - B_m} \\[2em] -\dfrac{1}{2\sqrt{2}}\left\{ \begin{array}{l} \left(\dfrac{\dfrac{\partial A_m}{\partial T} B_m - A_m \dfrac{\partial B_m}{\partial T}}{B_m^2}\right)\left[\dfrac{2\{(1-y_2)A_{21} + y_2 A_2\}}{A_m} - \dfrac{B_2}{B_m}\right] + \\[2em] \dfrac{A_m}{B_m}\left[\dfrac{2\left\{(1-y_2)\dfrac{\partial A_{21}}{\partial T} + y_2\dfrac{\partial A_2}{\partial T}\right\}A_m - 2\{(1-y_2)A_{21} + y_2 A_2\}\dfrac{\partial A_m}{\partial T}}{A_m^2} - \left(\dfrac{\dfrac{\partial B_2}{\partial T} B_m - B_2 \dfrac{\partial B_m}{\partial T}}{B_m^2}\right)\right] \end{array} \right\} \\[4em] \ln\left[\dfrac{Z_g + \left(1+\sqrt{2}\right)B_m}{Z_g + \left(1-\sqrt{2}\right)B_m}\right] - \dfrac{A_m}{B_m}\dfrac{\partial B_m}{\partial T}\left[\dfrac{2\{(1-y_2)A_{21} + y_2 A_2\}}{A_m} - \dfrac{B_2}{B_m}\right]\dfrac{Z_m}{\left[Z_g + \left(1+\sqrt{2}\right)B_m\right]\left[Z_g + \left(1-\sqrt{2}\right)B_m\right]} \end{array} \right\} *$$

$$\left.\frac{\partial \phi_{2v}}{\partial P}\right|_{Z_g,T,y_2} = \phi_{2v}\left\{ (Z_g-1)\left(\frac{\dfrac{\partial B_2}{\partial P}B_m - B_2\dfrac{\partial B_m}{\partial P}}{B_m^2}\right) + \frac{\dfrac{\partial B_m}{\partial P}}{Z_g - B_m} \right.$$

$$-\frac{1}{2\sqrt{2}}\left\{ \left(\frac{\dfrac{\partial A_m}{\partial P}B_m - A_m\dfrac{\partial B_m}{\partial P}}{B_m^2}\right)\left[\frac{2\{(1-y_2)A_{21}+y_2 A_2\}}{A_m} - \frac{B_2}{B_m}\right] + \right.$$

$$\left. \frac{A_m}{B_m}\left[\frac{2\left\{(1-y_2)\dfrac{\partial A_{21}}{\partial P}+y_2\dfrac{\partial A_2}{\partial P}\right\}A_m - 2\{(1-y_2)A_{21}+y_2 A_2\}\dfrac{\partial A_m}{\partial P}}{A_m^2} - \left(\frac{\dfrac{\partial B_2}{\partial P}B_m - B_2\dfrac{\partial B_m}{\partial P}}{B_m^2}\right)\right]\right\}$$

$$\left. \ln\left[\frac{Z_g+(1+\sqrt{2})B_m}{Z_g+(1-\sqrt{2})B_m}\right] - \frac{A_m}{B_m}\frac{\partial B_m}{\partial P}\left[\frac{2\{(1-y_2)A_{21}+y_2 A_2\}}{A_m} - \frac{B_2}{B_m}\right]\frac{Z_m}{[Z_g+(1+\sqrt{2})B_m][Z_g+(1-\sqrt{2})B_m]} \right\}*$$

$$\frac{\partial \phi_{2v}}{\partial y_2}\bigg|_{Z_g,T,P} = \phi_{2v}\left\{ \begin{array}{l} \left(Z_g-1\right)\left(-\frac{B_2}{B_m^2}\right)\frac{\partial B_m}{\partial y_2}+\frac{\dfrac{\partial B_m}{\partial y_2}}{Z_g-B_m}-\frac{1}{2\sqrt{2}}\left\{ \begin{array}{l} \left(\dfrac{\dfrac{\partial A_m}{\partial y_2}B_m-A_m\dfrac{\partial B_m}{\partial y_2}}{B_m^2}\right)\left[\dfrac{2\{(1-y_2)A_{21}+y_2A_2\}}{A_m}-\dfrac{B_2}{B_m}\right]+ \\[4ex] \dfrac{A_m}{B_m}\left[2\left\{\dfrac{(-A_{21}+A_2)A_m-\{(1-y_2)A_{21}+y_2A_2\}\dfrac{\partial A_m}{\partial y_2}}{A_m^2}\right\}+\dfrac{B_2}{B_m^2}\dfrac{\partial B_m}{\partial y_2}\right] \end{array}\right\}* \\[8ex] \ln\left[\dfrac{Z_g+\left(1+\sqrt{2}\right)B_m}{Z_g+\left(1-\sqrt{2}\right)B_m}\right]-\dfrac{A_m}{B_m}\dfrac{\partial B_m}{\partial y_2}\left[\dfrac{2\{(1-y_2)A_{21}+y_2A_2\}}{A_m}-\dfrac{B_2}{B_m}\right]\dfrac{Z_m}{\left[Z_g+\left(1+\sqrt{2}\right)B_m\right]\left[Z_g+\left(1-\sqrt{2}\right)B_m\right]} \end{array}\right\}$$

$$\frac{dy_2}{dn_{2v}} = \frac{n_{1_o}}{\left(n_{2v}+n_{1_o}\right)^2}$$

$$\left.\begin{array}{l} \hat{H}_{2l,excess} = \hat{H}_{2l,excess}\left(Z_{2l},T,P\right) \\[1ex] Z_{2l} = Z_{2l}\left(T,P\right) \\[1ex] B_2 = B_2\left(T,P\right) \\[1ex] a_2,\dfrac{da_2}{dT} = a_2,\dfrac{da_2}{dT}\left(T\right) \end{array}\right\} \Rightarrow$$

$$\left.\frac{\partial \hat{H}_{2l,excess}}{\partial Z_{2l}}\right|_{T,P} = RT - \left(\frac{T\dfrac{da_2}{dT} - a_2}{b_2}\right)\frac{B_2}{\left[Z_{2l} + \left(1+\sqrt{2}\right)B_2\right]\left[Z_{2l} + \left(1-\sqrt{2}\right)B_2\right]}$$

$$\left.\frac{\partial \hat{H}_{2l,excess}}{\partial T}\right|_{Z_{2l},P} = R(Z_{2l} - 1) + \frac{T\dfrac{d^2a_2}{dT^2}}{2\sqrt{2}b_2}\ln\left[\frac{Z_{2l} + \left(1+\sqrt{2}\right)B_2}{Z_{2l} + \left(1-\sqrt{2}\right)B_2}\right] + \left(\frac{T\dfrac{da_2}{dT} - a_2}{b_2}\right)\frac{\partial B_2}{\partial T}\frac{Z_{2l}}{\left[Z_{2l} + \left(1+\sqrt{2}\right)B_2\right]\left[Z_{2l} + \left(1-\sqrt{2}\right)B_2\right]}$$

$$\left.\frac{\partial \hat{H}_{2l,excess}}{\partial P}\right|_{Z_{2l},T} = \left(\frac{T\dfrac{da_2}{dT} - a_2}{b_2}\right)\frac{\partial B_2}{\partial P}\frac{Z_{2l}}{\left[Z_{2l} + \left(1+\sqrt{2}\right)B_2\right]\left[Z_{2l} + \left(1-\sqrt{2}\right)B_2\right]}$$

$$\left.\begin{aligned}
\hat{H}_{g,excess} &= \hat{H}_{g,excess}\left(Z_g, T, P\right)\\
Z_g &= Z_g\left(T, P, y_2\right)\\
B_m &= B_m\left(T, P, y_2\right)\\
a_m, \frac{\partial a_m}{\partial T} &= a_m, \frac{\partial a_m}{\partial T}\left(T, y_2\right)\\
b_m &= b_m\left(y_2\right)
\end{aligned}\right\} \Rightarrow$$

$$\frac{\partial \hat{H}_{g,excess}}{\partial Z_{2l}}\bigg|_{T,P,y_2} = RT - \left(\frac{T\frac{\partial a_m}{\partial T} - a_m}{b_m}\right)\frac{B_m}{\left[Z_g + \left(1+\sqrt{2}\right)B_m\right]\left[Z_g + \left(1-\sqrt{2}\right)B_m\right]}$$

$$\frac{\partial \hat{H}_{g,excess}}{\partial T}\bigg|_{Z_g,P,y_2} = R\left(Z_g - 1\right) + \frac{T\frac{\partial^2 a_m}{\partial T^2}}{2\sqrt{2}b_m}\ln\left[\frac{Z_g + \left(1+\sqrt{2}\right)B_m}{Z_g + \left(1-\sqrt{2}\right)B_m}\right] + \left(\frac{T\frac{\partial a_m}{\partial T} - a_m}{b_m}\right)\frac{\partial B_m}{\partial T}\frac{Z_g}{\left[Z_g + \left(1+\sqrt{2}\right)B_m\right]\left[Z_g + \left(1-\sqrt{2}\right)B_m\right]}$$

$$\frac{\partial \hat{H}_{g,excess}}{\partial P}\bigg|_{Z_g,T,y_2} = \left(\frac{T\frac{\partial a_m}{\partial T} - a_m}{b_m}\right)\frac{\partial B_m}{\partial P}\frac{Z_g}{\left[Z_g + \left(1+\sqrt{2}\right)B_m\right]\left[Z_g + \left(1-\sqrt{2}\right)B_m\right]}$$

$$\left.\frac{\partial \hat{H}_{g,excess}}{\partial y_2}\right|_{Z_g,T,P} = \left[\frac{\left(T\frac{\partial^2 a_m}{\partial T \partial y_2} - \frac{\partial a_m}{\partial y_2}\right)2\sqrt{2}b_m - \left(T\frac{\partial a_m}{\partial T} - a_m\right)2\sqrt{2}\frac{db_m}{dy_2}}{8b_m^2}\right]\ln\left[\frac{Z_g + \left(1+\sqrt{2}\right)B_m}{Z_g + \left(1-\sqrt{2}\right)B_m}\right]$$

$$+\left(\frac{T\frac{\partial a_m}{\partial T} - a_m}{b_m}\right)\frac{\partial B_m}{\partial y_2}\frac{Z_g}{\left[Z_g + \left(1+\sqrt{2}\right)B_m\right]\left[Z_g + \left(1-\sqrt{2}\right)B_m\right]}$$

$$\left.\frac{\partial Z_{2l}}{\partial T}\right|_P = \frac{\left(-Z_{2l}^2 + 6B_2 Z_{2l} + 2Z_{2l} + A_2 - 2B_2 - 3B_2^2\right)\left.\frac{\partial B_2}{\partial T}\right|_P + \left(-Z_{2l} + B_2\right)\left.\frac{\partial A_2}{\partial T}\right|_P}{3Z_{2l}^2 - 2(1-B_2)Z_{2l} + A_2 - 3B_2^2 - 2B_2}$$

$$\left.\frac{\partial Z_{2l}}{\partial P}\right|_T = \frac{\left(-Z_{2l}^2 + 6B_2 Z_{2l} + 2Z_{2l} + A_2 - 2B_2 - 3B_2^2\right)\left.\frac{\partial B_2}{\partial P}\right|_T + \left(-Z_{2l} + B_2\right)\left.\frac{\partial A_2}{\partial P}\right|_T}{3Z_{2l}^2 - 2(1-B_2)Z_{2l} + A_2 - 3B_2^2 - 2B_2}$$

$$\left.\frac{\partial Z_g}{\partial T}\right|_{P,y_2} = \frac{\left(-Z_g^2 + 6B_m Z_g + 2Z_g + A_m - 2B_m - 3B_m^2\right)\left.\frac{\partial B_m}{\partial T}\right|_{P,y_2} + \left(-Z_g + B_m\right)\left.\frac{\partial A_m}{\partial T}\right|_{P,y_2}}{3Z_g^2 - 2(1-B_m)Z_g + A_m - 3B_m^2 - 2B_m}$$

$$\left.\frac{\partial Z_g}{\partial P}\right|_{T,y_2} = \frac{\left(-Z_g^2 + 6B_m Z_g + 2Z_g + A_m - 2B_m - 3B_m^2\right)\left.\frac{\partial B_m}{\partial P}\right|_{T,y_2} + \left(-Z_g + B_m\right)\left.\frac{\partial A_m}{\partial P}\right|_{T,y_2}}{3Z_g^2 - 2(1 - B_m)Z_g + A_m - 3B_m^2 - 2B_m}$$

$$\left.\frac{\partial Z_g}{\partial y_2}\right|_{T,P} = \frac{\left(-Z_g^2 + 6B_m Z_g + 2Z_g + A_m - 2B_m - 3B_m^2\right)\left.\frac{\partial B_m}{\partial y_2}\right|_{T,P} + \left(-Z_g + B_m\right)\left.\frac{\partial A_m}{\partial y_2}\right|_{T,P}}{3Z_g^2 - 2(1 - B_m)Z_g + A_m - 3B_m^2 - 2B_m}$$

$$\left.\frac{\partial A_2}{\partial T}\right|_P = \frac{P}{R^2}\left(\frac{1}{T^2}\frac{da_2}{dT} - \frac{2a_2}{T^3}\right)$$

$$\left.\frac{\partial A_2}{\partial P}\right|_T = \frac{a_2}{R^2 T^2}$$

$$\left.\frac{\partial B_2}{\partial T}\right|_P = -\frac{b_2 P}{RT^2}$$

$$\left.\frac{\partial B_2}{\partial P}\right|_T = \frac{b_2}{RT}$$

$$\left.\frac{\partial A_m}{\partial T}\right|_{P,y_2} = \frac{P}{R^2}\left(\frac{1}{T^2}\left.\frac{\partial a_m}{\partial T}\right|_{y_2} - \frac{2a_m}{T^3}\right)$$

$$\left.\frac{\partial A_m}{\partial P}\right|_{T,y_2} = \frac{a_m}{R^2 T^2}$$

$$\left.\frac{\partial A_m}{\partial y_2}\right|_{T,P} = \frac{P}{R^2 T^2}\left.\frac{\partial a_m}{\partial y_2}\right|_T$$

$$\left.\frac{\partial a_m}{\partial y_2}\right|_T = -2(1-y_2)a_1 + 2a_{21}(1-2y_2) + 2y_2 a_2$$

$$\left.\frac{\partial B_m}{\partial T}\right|_{P,y_2} = -\frac{b_m P}{RT^2}$$

$$\left.\frac{\partial B_m}{\partial P}\right|_{T,y_2} = \frac{b_m}{RT}$$

$$\left.\frac{\partial B_m}{\partial y_2}\right|_{T,P} = \frac{P}{RT}\frac{db_m}{dy_2}$$

$$\frac{db_m}{dy_2} = -b_1 + b_2$$

$$\frac{da_2}{dT} = -0.45724 \frac{R^2 T_{C_2}^2}{P_{C_2}} \kappa_2 \sqrt{\frac{\alpha_2}{TT_{C_2}}}$$

$$\frac{d^2 a_2}{dT^2} = -0.45724 \frac{R^2 T_{C_2}^2}{P_{C_2}} \frac{\kappa_2}{2} \left(\frac{\alpha_2}{TT_{C_2}}\right)^{-\frac{1}{2}} \left[\frac{-\kappa_2 \sqrt{\alpha_2 TT_{C_2}} - \alpha_2 T_{C_2}}{\left(TT_{C_2}\right)^2}\right]$$

$$\left.\frac{\partial a_m}{\partial T}\right|_{y_2} = (1-y_2)^2 \frac{da_1}{dT} + 2y_2(1-y_2)\frac{da_{21}}{dT} + y_2^2 \frac{da_2}{dT}$$

$$\left.\frac{\partial^2 a_m}{\partial T^2}\right|_{y_2} = (1-y_2)^2 \frac{d^2 a_1}{dT^2} + 2y_2(1-y_2)\frac{d^2 a_{21}}{dT^2} + y_2^2 \frac{d^2 a_2}{dT^2}$$

$$\frac{da_1}{dT} = -0.45724 \frac{R^2 T_{C_1}^2}{P_{C_1}} \kappa_1 \sqrt{\frac{\alpha_1}{TT_{C_1}}}$$

$$\frac{d^2 a_1}{dT^2} = -0.45724 \frac{R^2 T_{C_1}^2}{P_{C_1}} \frac{\kappa_1}{2} \left(\frac{\alpha_1}{TT_{C_1}}\right)^{-\frac{1}{2}} \left[\frac{-\kappa_1 \sqrt{\alpha_1 TT_{C_1}} - \alpha_1 T_{C_1}}{\left(TT_{C_1}\right)^2}\right]$$

$$\frac{da_{21}}{dT} = 0.45724R^2\left(1-k_{12}\right)\sqrt{\frac{T_{C_1}^2 T_{C_2}^2}{P_{C_1}P_{C_2}}}\left(-\frac{\kappa_2}{2}\sqrt{\frac{\alpha_1}{TT_{C_2}}} - \frac{\kappa_1}{2}\sqrt{\frac{\alpha_2}{TT_{C_1}}}\right)$$

$$\frac{d^2 a_{21}}{dT^2} = 0.45724R^2\left(1-k_{12}\right)\sqrt{\frac{T_{C_1}^2 T_{C_2}^2}{P_{C_1}P_{C_2}}}\left(-\frac{\kappa_2}{4\sqrt{\alpha_1 TT_{C_2}}} + \frac{\kappa_2}{4}\sqrt{\frac{\alpha_1}{T^3 T_{C_2}}} - \frac{\kappa_1}{4\sqrt{\alpha_2 TT_{C_1}}} + \frac{\kappa_1}{4}\sqrt{\frac{\alpha_2}{T^3 T_{C_1}}}\right)$$

$$\frac{d^2 a_m}{dTdy_2} = -2\left(1-y_2\right)\frac{da_1}{dT} + 2\left(1-2y_2\right)\frac{da_{21}}{dT} + 2y_2\frac{da_2}{dT}$$

$$\left.\frac{\partial A_{21}}{\partial T}\right|_P = \frac{P}{R^2}\left(\frac{1}{T^2}\frac{da_{21}}{dT} - \frac{2a_{21}}{T^3}\right)$$

$$\left.\frac{\partial A_{21}}{\partial P}\right|_T = \frac{a_{21}}{R^2 T^2}$$

APPENDIX F

ADDITIONAL "ERROR" SENSITIVITY STUDY PLOTS

F-1   Introduction

This appendix contains the remaining plots from the error sensitivity study discussed in Chapter 5. The specific inputs for these data sets are also in Chapter 5. Recall that for the error sensitivity studies, only the non-ideal model was assessed.

F-2   Binary Interaction Parameter Study Plots

For this study, zero was chosen as the nominal case since this is what is assumed for a nitrous oxide/helium mixture in the Peng-Robinson model. The maximum and minimum values of k_{12} were chosen from Table 9.4-1 in Sandler (2006, p. 424) based on the extreme values measured for other binary mixtures; no data was available for the mixture of nitrous oxide and helium. The minimum value, $k_{12} = -0.02$, is for a mixture of CO_2 and N_2. The maximum value, $k_{12} = 0.136$, is for a mixture of SO_2 and CH_4. The only detectible difference was a small difference in the nitrous oxide vapor history.

Note that the inputs for this study are as stated in Chapter 5 except that there is 0.01 kmol of helium in the tank. A pure nitrous oxide system will not invoke the mixing rule that uses the binary interaction parameter.
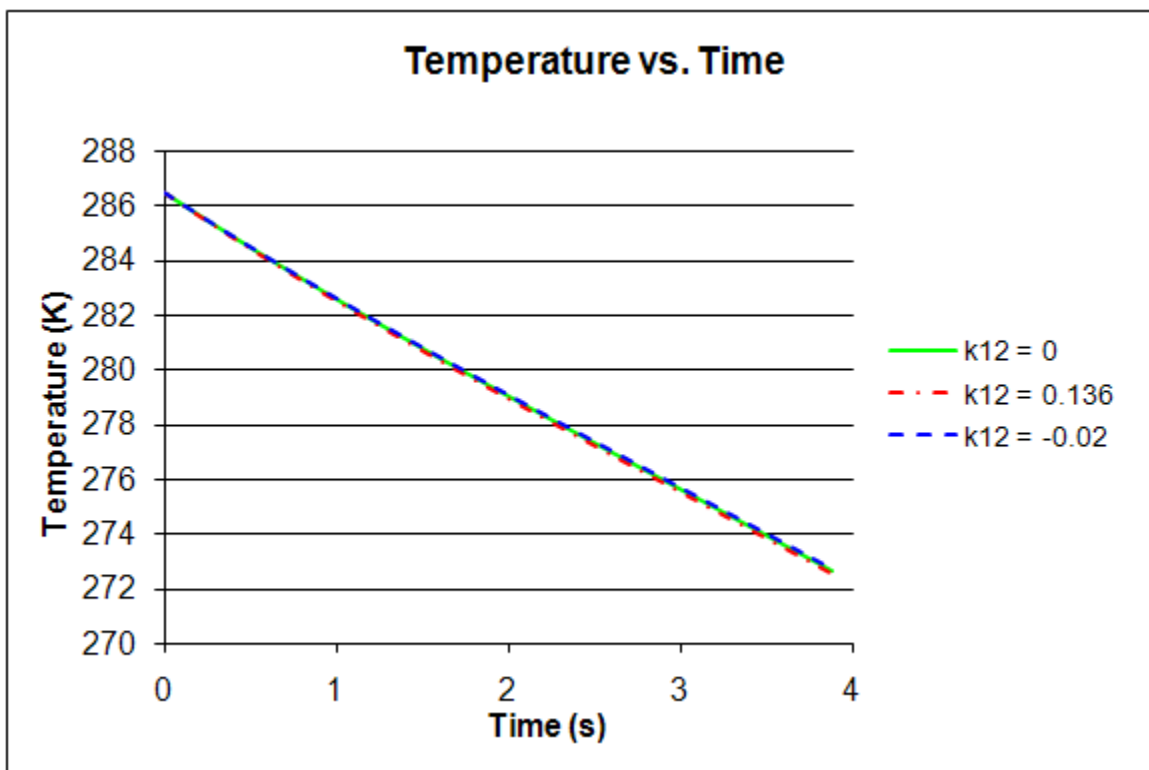
Figure F.2a: Theoretical (non-ideal) predictions for the temperature in the draining tank as a function of time, for parameter values as set in Section 5-3 for the binary interaction parameter "error" sensitivity study.
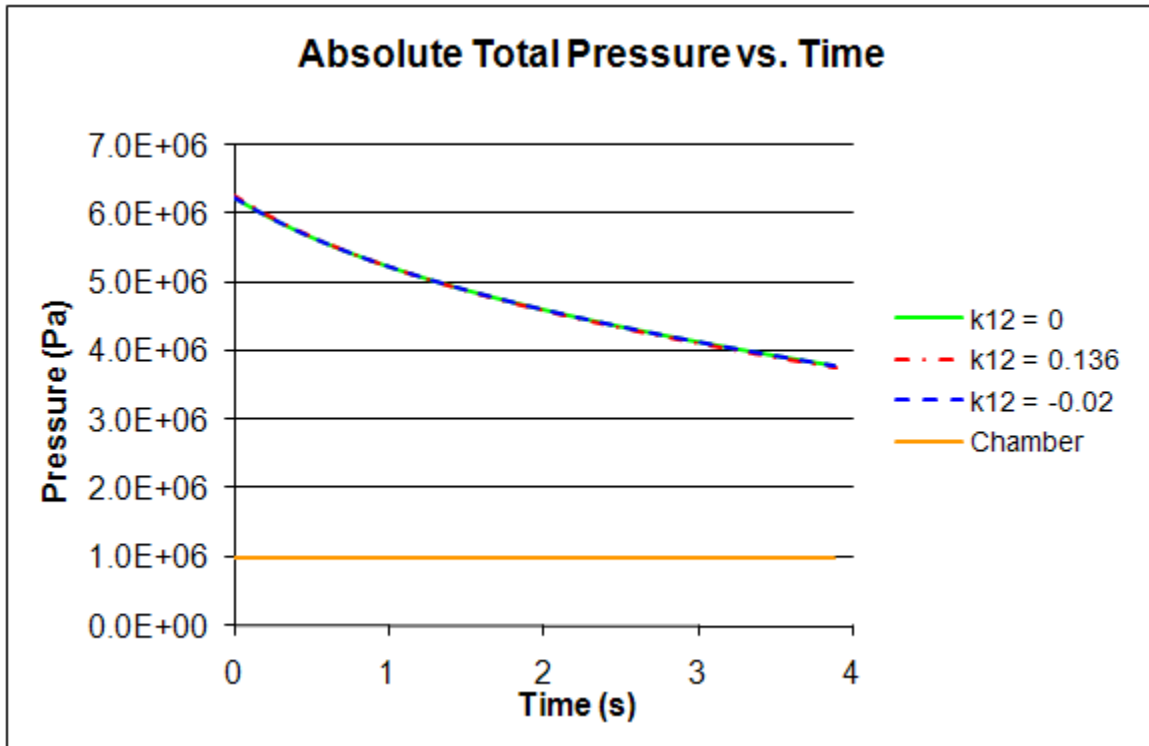
Figure F.2b: Theoretical (non-ideal) predictions for the absolute total pressure in the draining tank as a function of time, for parameter values as set in Section 5-3 for the binary interaction parameter "error" sensitivity study.
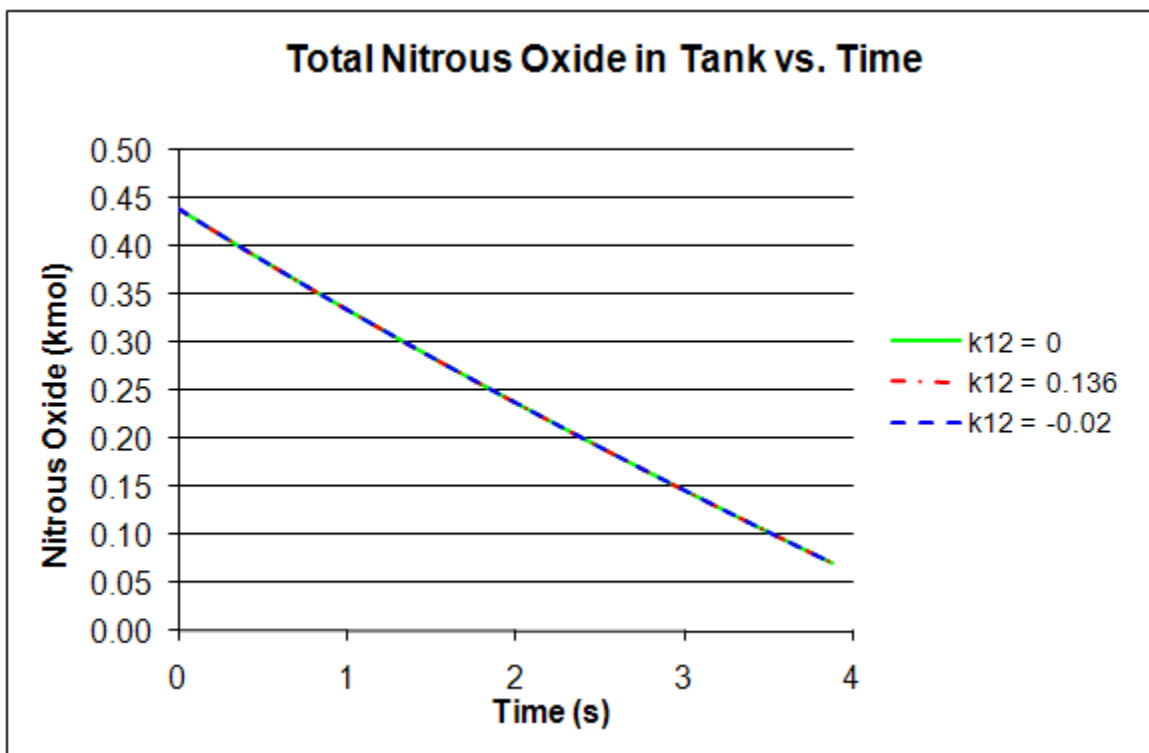
Figure F.2c: Theoretical (non-ideal) predictions for the total moles of nitrous oxide in the draining tank as a function of time, for parameter values as set in Section 5-3 for the binary interaction parameter "error" sensitivity study.
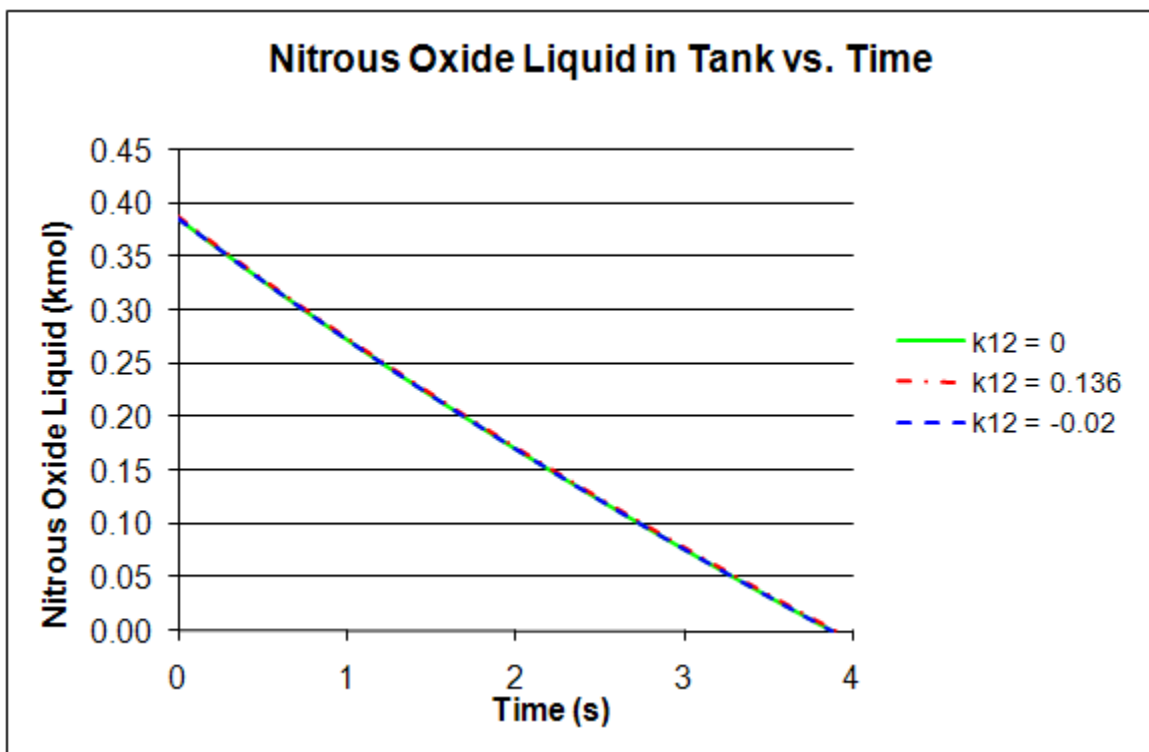
Figure F.2d: Theoretical (non-ideal) predictions for the moles of nitrous oxide liquid in the draining tank as a function of time, for parameter values as set in Section 5-3 for the binary interaction parameter "error" sensitivity study.
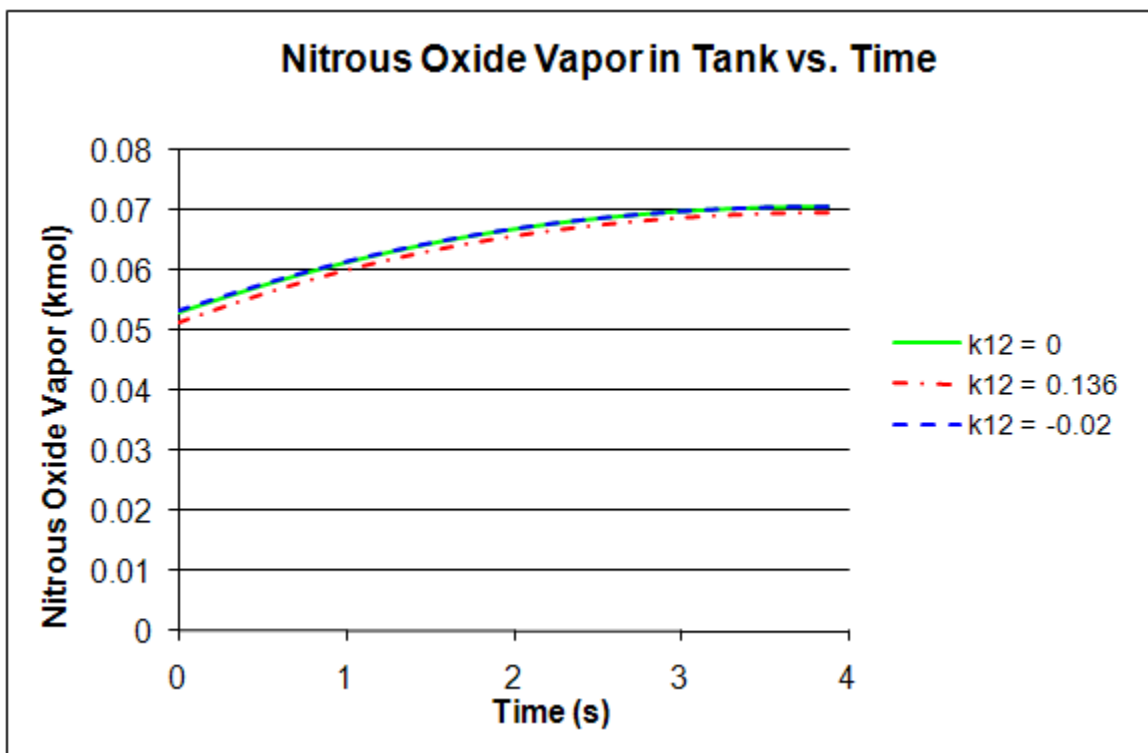
Figure F.2e: Theoretical (non-ideal) predictions for the moles of nitrous oxide vapor in the draining tank as a function of time, for parameter values as set in Section 5-3 for the binary interaction parameter "error" sensitivity study.

F-3   Critical Constant Study Plots

For this study, the values of critical temperature, critical pressure, and acentric factor for both nitrous oxide and helium were compared from two different references: Sandler's (2006) mixture vapor-liquid equilibrium code on a CD accompanying his textbook and *Perry's Chemical Engineers' Handbook* (1997). Two cases were run for each set of properties: a pure nitrous oxide case, and a case with 0.01 kmol of helium added to the tank. While the different sets of properties from each source do make a small but detectible difference in the drain histories, the most significant difference is in the nitrous oxide vapor history.

Table F.1 shows the two sets of critical constants used in this sensitivity study: the critical temperature of helium, T_{C1}, the critical temperature of nitrous oxide, T_{C2}, the critical pressure of helium, P_{C1}, the critical pressure of nitrous oxide, P_{C2}, the acentric factor for helium, w_1, and the acentric factor for nitrous oxide, w_2. Note that the inputs for this study

120

are as stated in Chapter 5 except for the case with 0.01 kmol of helium in the tank included in addition to the pure nitrous oxide case.

Critical Constant	Sandler (2006)	Perry's Handbook (1997)
T_{C1} (K)	5.19	5.2
T_{C2} (K)	309.6	309.57
P_{C1} (Pa)	2.27E+05	2.30E+05
P_{C2} (Pa)	7.24E+06	7.28E+06
w_1	-0.365	-0.388
w_2	0.165	0.143

Table F.1: Critical Constants for Sensitivity Study
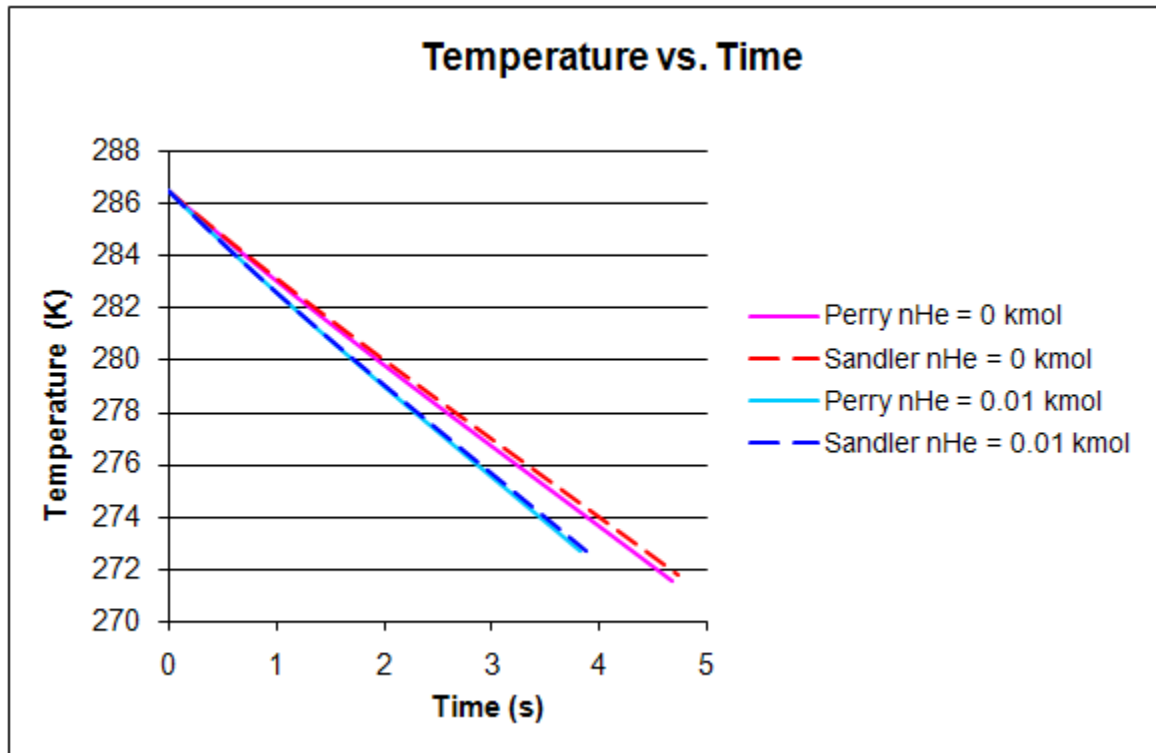
Figure F.3a: Theoretical (non-ideal) predictions for the temperature in the draining tank as a function of time, for parameter values as set in Section 5-3 for the critical constants "error" sensitivity study.
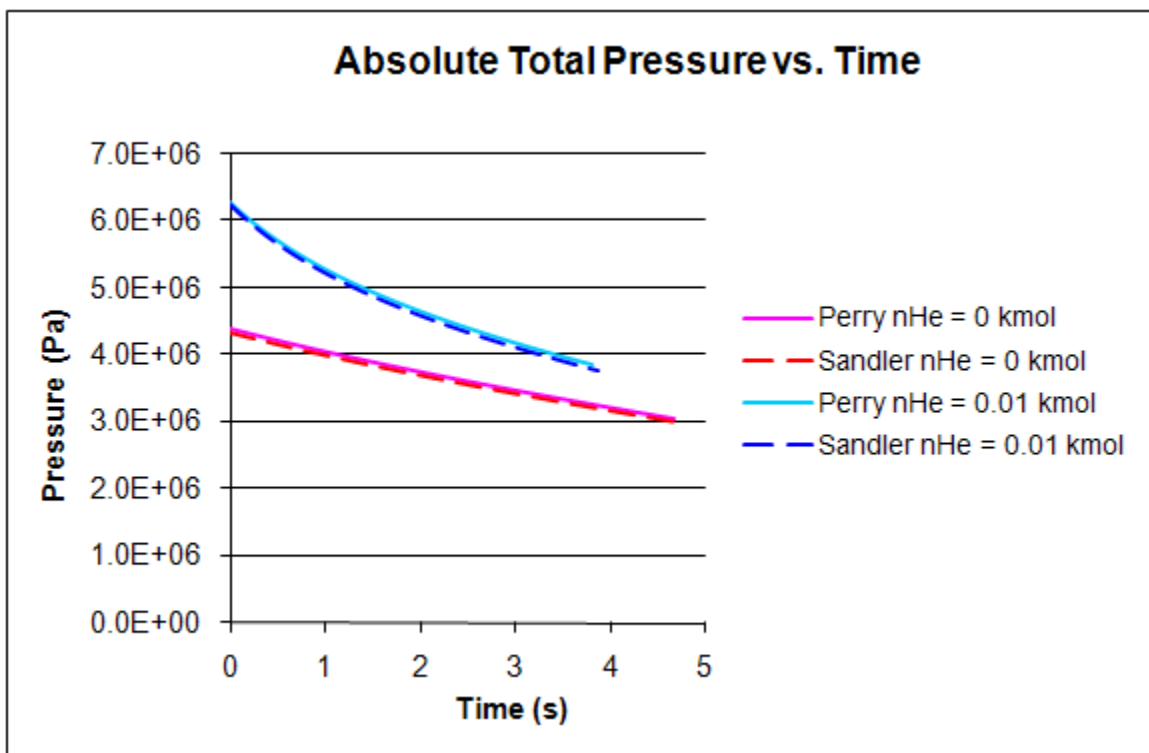
Figure F.3b: Theoretical (non-ideal) predictions for the absolute total pressure in the draining tank as a function of time, for parameter values as set in Section 5-3 for the critical constants "error" sensitivity study.
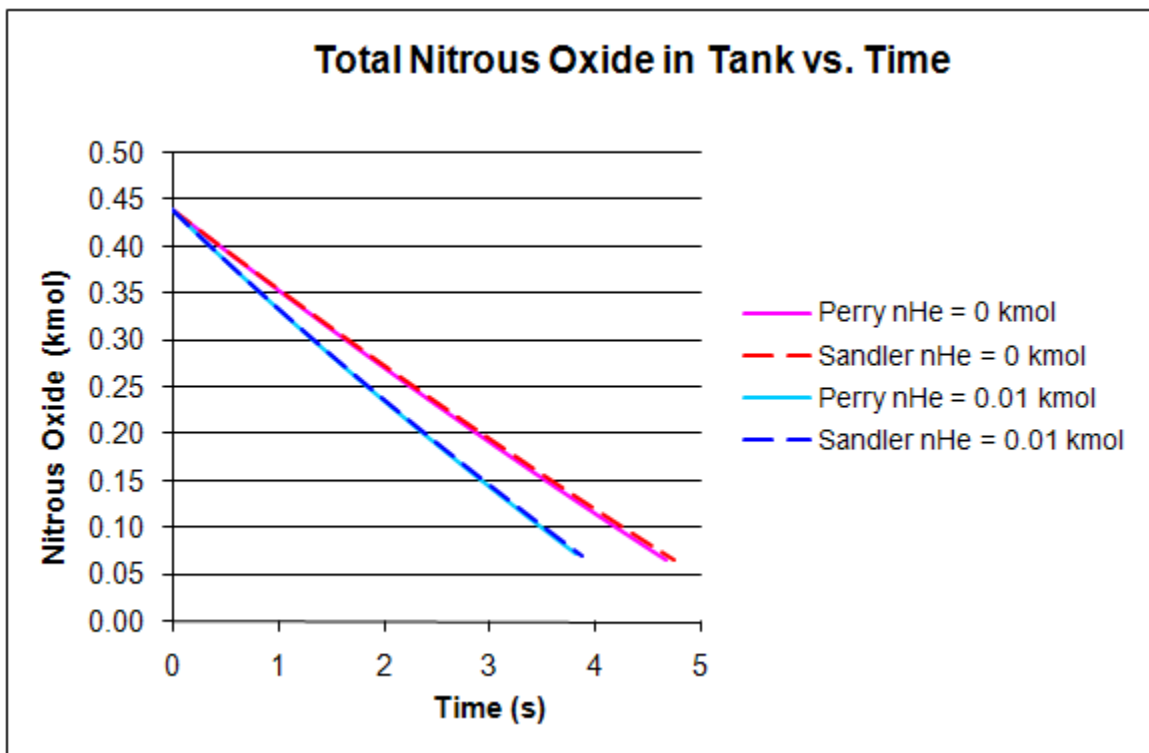
Figure F.3c: Theoretical (non-ideal) predictions for the total moles of nitrous oxide in the draining tank as a function of time, for parameter values as set in Section 5-3 for the critical constants "error" sensitivity study.
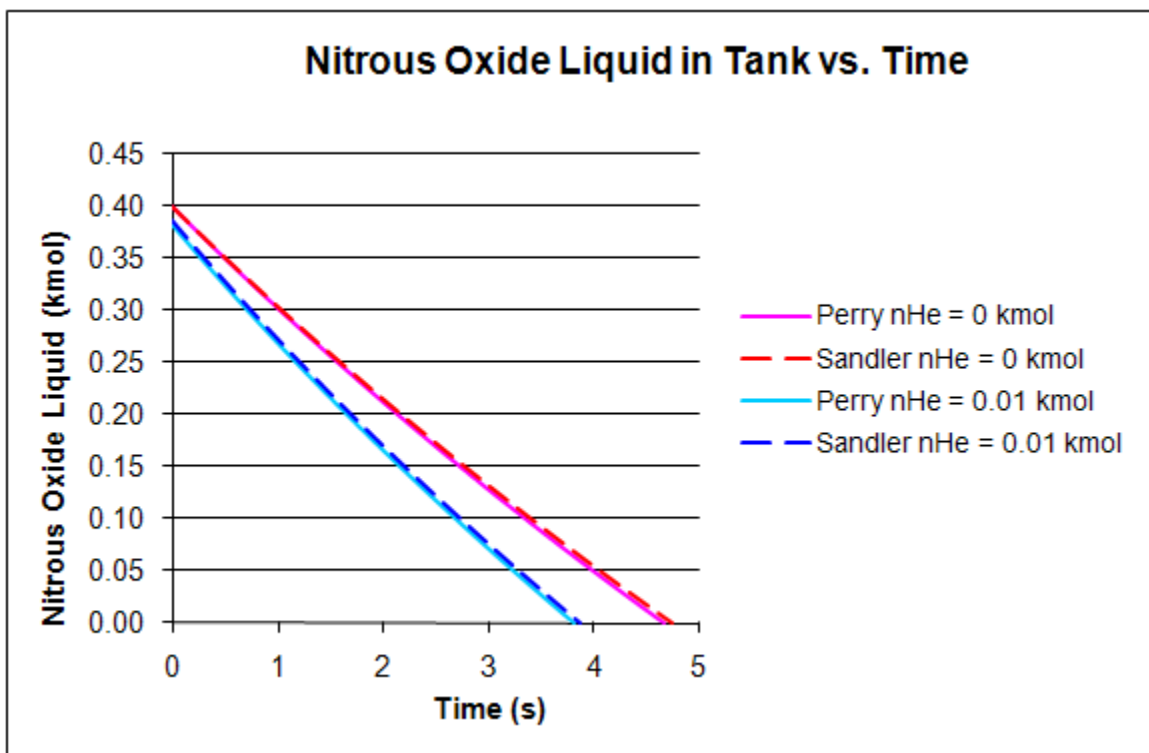
Figure F.3d: Theoretical (non-ideal) predictions for the moles of nitrous oxide liquid in the draining tank as a function of time, for parameter values as set in Section 5-3 for the critical constants "error" sensitivity study.
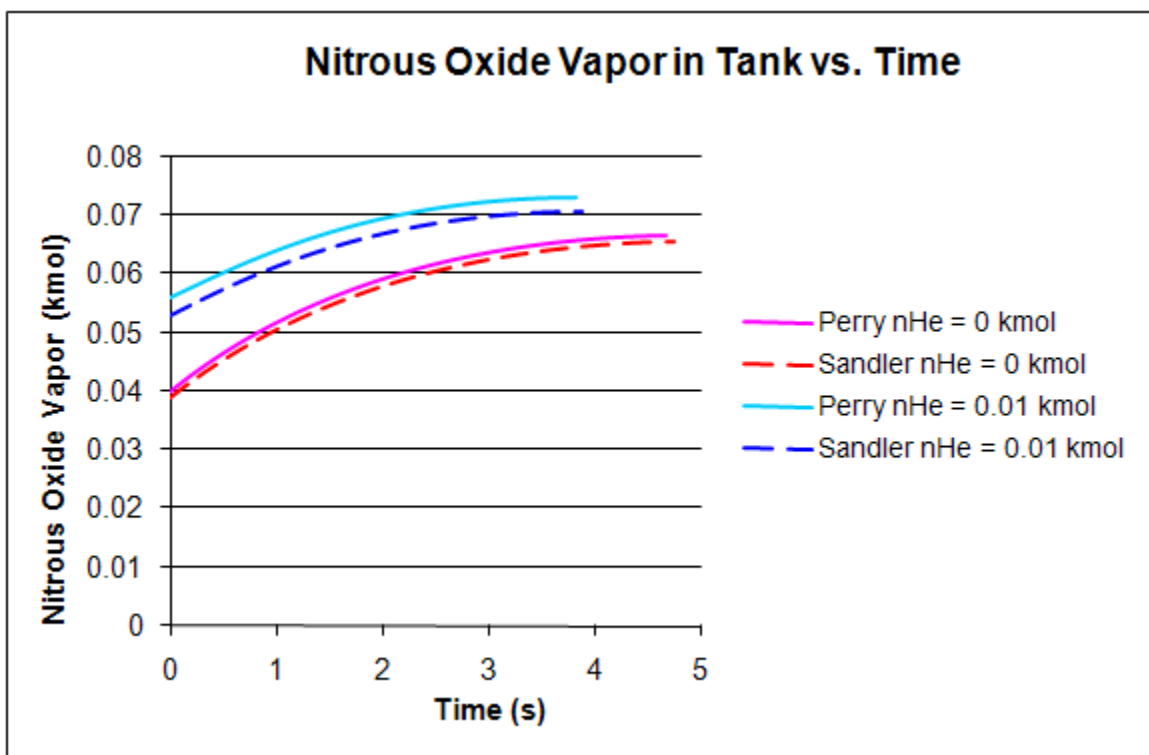
Figure F.3e: Theoretical (non-ideal) predictions for the moles of nitrous oxide vapor in the draining tank as a function of time, for parameter values as set in Section 5-3 for the critical constants "error" sensitivity study.

APPENDIX G

PROPOSED EXPERIMENTS TO VALIDATE DRAINING TANK MODEL

G-1   Overview

Since the primary focus of the joint NASA Ames and Stanford University research is to characterize the hybrid combustion processes, characterization of the propellant delivery system is a secondary concern. Thus, the four tests discussed in Chapter 4 were not carried out for the purposes of studying the oxidizer tank draining process. While the data is useful for an initial assessment of the theoretical models developed in this thesis, it was determined that the pertinent parameters related to the oxidizer delivery system were not sufficiently controlled. Since each experiment had a different set of initial conditions, and none of the tests were repeated, experimental variability cannot be determined. Therefore, the quantitative assessment of agreement between theory and experiment (desired to be within 5% at the onset of the study) cannot be made. In this appendix, additional experiments targeting the study of the propellant delivery system are proposed for future work.

G-2   1st Line of Testing: Equation-of-State

Seeing that the model requires knowledge of the P-V-T behavior of both a pure nitrous oxide and a nitrous oxide/helium mixture two-phase system, the following options are available to incorporate that information into the model: 1) develop a set of tabulated data from measurements and use curve fits to incorporate into code, 2) find the most accurate equation-of-state that captures the behavior of both a pure nitrous oxide and nitrous oxide/helium mixture two-phase systems, or 3) find the most accurate equation-of-state that is also easily implemented into the model. The error in all three of these options would be known assuming that highly accurate nitrous oxide/helium data is collected at different temperatures, fill-levels, and concentrations. This testing would seek to answer questions such as: 1) At a given N_2O/He mass added to the tank, are there two phases present? 2) How does the mass distribute between the two phases? 3) What is the composition of each phase?

Even though this is the logical first step in this model, the testing would be highly tedious and expensive. Therefore, it is more practical to assume that the pure nitrous oxide and nitrous oxide/helium mixture two-phase systems obey an existing equation-of-state. In

124

this case, Peng-Robinson was specified, and all properties are known except the binary interaction parameter. A sensitivity study has been introduced for this parameter using the model already implemented (see Chapter 5 and Appendix F). However, a set of P-V-T data can be collected (within the temperature, fill-level, and concentration ranges of interest) from the next set of testing that would allow the assessment of how much Peng-Robinson deviates from the actual pure and/or mixture P-V-T behavior of the system.

G-3   2nd Line of Testing: Helium-Augmented System

This testing is meant to assess the pure and mixed behavior of nitrous oxide and helium as well as the draining behavior of a helium-augmented pressurization system. It entails collecting data for a tank of pure nitrous oxide, then adding helium in specified increments to attain different mixture concentrations, and then draining the tank. The experiment would be set up as follows:

a) Testing the Peng-Robinson equation-of-state under equilibrium conditions:

Two tanks would be present, one with pure nitrous oxide and the other with pure helium. Ideally, there would be at least one pressure and temperature measurement in the ullage (gas phase at the top of the tank), and also in the liquid (bottom of the tank). The mass of nitrous oxide and helium in their respective tanks would be measured by weighing. The best way to control the temperature of the system is to immerse the nitrous oxide tank in a bath of fixed temperature (also measured). Since the only helium parameter needed for the helium-augmented system is the incremental mass of helium added to the nitrous oxide tank, it is not necessary to control the helium tank temperature in a similar manner, but it may help with controlling the amount added at an increment. The temperature of the bath would remain constant throughout an entire test, but could be varied from test to test as desired.

The nitrous oxide tank would be immersed in the bath long enough to come to equilibrium. This will give pure nitrous oxide P-V-T data. Then helium is added to the nitrous oxide tank. After adding the helium, both the nitrous oxide tank and the helium tank should be weighed to confirm how much helium mass was added to the

nitrous oxide tank. (Note: if precise measurement of the changes in mass due to helium addition is difficult, the helium tank conditions should be more controlled, and the amount of helium added will be measured using some other technique. For instance, helium tank temperature and pressure measurements could be helpful for backing out the mass left in the helium tank, assuming the pressurized helium follows a known equation-of-state. In addition, a flow meter could measure the flow rate of helium into the nitrous oxide tank). The nitrous oxide tank should then be allowed to come back to equilibrium at the bath temperature. This process of adding helium in increments can be repeated as many times as desired to get several different tank pressures and concentrations. This will give nitrous oxide/helium mixture P-V-T data.

b) Draining the tank:

After the final amount of helium has been added, and the tank returns to equilibrium, the tank can then be drained to completion. The feed system details would be handled in the same fashion as was done in Zilliac and Karabeyoglu (2005). The discharge coefficient would need to be derived or experimentally determined. The exit pressure would also need to be measured, and ideally kept constant. There should also be a way of detecting whether or not there is cavitation in the feedline, as this may compromise the accuracy of the measurements.

This experiment can be done for a series of different temperatures, closed tank concentrations, and draining concentrations. For example, a set of experiments at the same temperature and fill-level but at different draining concentrations would verify or disprove the result found in the helium "big picture" sensitivity study (see Figure 5.2.3e) indicating that more helium added to the tank will cause more nitrous oxide to evaporate. High- and low-speed data collection would also be useful: low-speed for getting equilibrium measurements, and high-speed for draining and filling measurements. After the helium-augmented data has been collected, the experiment could easily be updated for helium inflow testing if desired.

APPENDIX H

IDEAL MODEL MATLAB CODE

```matlab
% Masters Thesis
% Ideal Model
% Explicit Method - Forward Difference


clear all
clc

% Given constants
n_He = 0;                % helium gas [kmol]
m_loaded = 19.32933;     % N2O mass initially loaded into tank [kg]: Test 1
% m_loaded = 16.23298;     % Test 2
% m_loaded = 14.10076;     % Test 3
% m_loaded = 23.62427;     % Test 4
Ti = 286.5;              % initial temperature [K]: Test 1
% Ti = 278.5;              % Test 2
% Ti = 271.5;              % Test 3
% Ti = 291.3;              % Test 4
R = 8314.3 ;             % universal gas constant [J/(kmol*K)]
Cd = 0.425;              % discharge coefficient: Test 1
% Cd = 0.365;              % Test 2 and 3
% Cd = 0.09;               % Test 4
Ainj = 0.0001219352;     % injector area [m^2]
MW2 = 44.013;            % molecular weight of N2O
V = 0.0354 ;             % total tank volume [m^3]
m_T = 6.4882;            % tank mass [kg]


% Perry's Chemical Engineers' Handbook Property Equations
G1 = 96.512 ;          % vapor pressure of N2O [Pa] coefficients
G2 = -4045 ;           % valid for Temp range [182.3 K - 309.57 K]
G3 = -12.277 ;
G4 = 2.886e-5 ;
G5 = 2 ;
```

```
Tc = 309.57 ;          % critical temperature of N2O [K]
J1 = 2.3215e7 ;        % heat of vaporization of N2O [J/kmol] coefficients
J2 = 0.384 ;           % valid for Temp range [182.3 K - 309.57 K]
J3 = 0 ;
J4 = 0 ;


C1 = 0.2079e5 ;        % heat capacity of He at constant pressure [J/(kmol*K)] coefficients
C2 = 0 ;               % valid for Temp range [100 K - 1500 K]
C3 = 0 ;
C4 = 0 ;
C5 = 0 ;


D1 = 0.2934e5 ;        % heat capacity of N2O gas at constant pressure [J/(kmol*K)] coefficients
D2 = 0.3236e5 ;        % valid for Temp range [100 K - 1500 K]
D3 = 1.1238e3 ;
D4 = 0.2177e5 ;
D5 = 479.4 ;


E1 = 6.7556e4 ;        % heat capacity of N2O liquid at constant pressure [J/(kmol*K)] coefficients
E2 = 5.4373e1 ;        % valid for Temp range [182.3 K - 200 K]
E3 = 0 ;
E4 = 0 ;
E5 = 0 ;


Q1 = 2.781;            % molar specific volume of liquid N2O [m^3/kmol] coefficients
Q2 = 0.27244;
Q3 = 309.57;
Q4 = 0.2882;


% Initial Conditions
n_to = m_loaded/MW2;                                  % initial total N2O in tank [kmol]
Vhat_li = Q2^(1+(1-Ti/Q3)^Q4)/Q1;                    % molar volume of liquid N2O [m^3/kmol]
To = Ti ;                                            % initial temperature [K]
P_sato = exp(G1 + G2/To + G3*log(To) + G4*To^G5);    % initial vapor pressure of N20 [Pa]
n_go = P_sato*(V - Vhat_li*n_to) / (-P_sato*Vhat_li + R*To);   % initial N2O gas [kmol]
n_lo = (n_to*R*To - P_sato*V) / (-P_sato*Vhat_li + R*To);      % initial N2O liquid [kmol]


% Forward Difference Time Loop
```

```matlab
tf=100;         % final time [s]
tstep=0.0005;   % time step [s]
i_i=0;
i_f=tf/tstep;

for i=i_i:i_f;
    t = i*tstep;
    % Curve fitted combustion chamber pressure [Pa]:
    Pe = -2924.42*t^6 + 46778.07*t^5 - 285170.63*t^4 + 813545.02*t^3 - ...
        1050701.53*t^2 + 400465.85*t + 1175466.2;                        % Test 1
    % Pe = 95.92*t^6 - 2346.64*t^5 + 21128.78*t^4 - 87282.73*t^3 + ...
    %    186675.17*t^2 - 335818.91*t + 3029190.03;                       % Test 2
    % Pe = 58.06*t^6 - 1201.90*t^5 + 8432.11*t^4 - 22175.67*t^3 + ...
    %    21774.66*t^2 - 99922.82*t + 2491369.68;                         % Test 3
    % Pe = -4963.73*t + 910676.22;                                       % Test 4


    % Given functions of temperature:
    Vhat_l = Q2^(1+(1-To/Q3)^Q4)/Q1;
        %molar specific volume of liquid N2O [m^3/kmol]
    CVhat_He = C1 + C2*To + C3*To^2 + C4*To^3 + C5*To^4 - R;
        %specific heat of He at constant volume [J/(kmol*K)]
    CVhat_g = D1 + D2*((D3/To)/sinh(D3/To))^2 + D4*((D5/To)/cosh(D5/To))^2 - R;
        %specific heat of N2O gas at constant volume [J/(kmol*K)]
    CVhat_l = E1 + E2*To + E3*To^2 + E4*To^3 + E5*To^4;
        %specific heat of N2O liquid at constant volume, approx. same as at constant pressure [J/(kmol*K)]
    Tr = To/Tc;                                         % reduced temperature
    delta_Hv = J1*(1 - Tr) ^ (J2 + J3*Tr + J4*Tr^2);    % heat of vaporization of N2O [J/kmol]
    P_sat = exp(G1 + G2/To + G3*log(To) + G4*To^G5);    % vapor pressure of N20 [Pa]
    dP_sat = (-G2/(To^2) + G3/To + G4*G5*To^(G5-1)) * exp(G1 + G2/To + G3*log(To) + G4*To^G5);
        %derivative of vapor pressure with respect to temperature
    Cp_T = (4.8 + 0.00322*To)*155.239;                  % specific heat of tank, Aluminum [J/(kg*K)]


    % Simplified expression definitions for solution
    P = (n_He + n_go)*R*To / (V - n_lo*Vhat_l) ;
    a = m_T*Cp_T + n_He*CVhat_He + n_go*CVhat_g + n_lo*CVhat_l;
    b = P*Vhat_l;
    e = -delta_Hv + R*To;
    f = -Cd*Ainj*sqrt(2/MW2)*sqrt((P-Pe)/Vhat_l);
    j = -Vhat_l*P_sat;
```

129

```matlab
        k = (V - n_lo*Vhat_l)*dP_sat;
        m = R*To;
        q = R*n_go;


        Z=(-f*(-j*a + (q-k)*b)) / (a*(m+j) + (q-k)*(e-b));
        W=(-Z*(m*a + (q-k)*e)) / (-j*a + (q-k)*b);


        % Derivative Functions
        dT = (b*W+e*Z)/a ;
        dn_g = Z;
        dn_l = W;


        % Record variables for each time step in an array
        T(i+1,1) = t;
        T(i+1,2) = To;
        n_g(i+1,1) = t;
        n_g(i+1,2) = n_go;
        n_l(i+1,1) = t;
        n_l(i+1,2) = n_lo;
        Pres(i+1,1) = t;
        Pres(i+1,2) = P;
        PE(i+1,1) = t;
        PE(i+1,2) = Pe;


        % Forward Difference Method
        To = To + dT*tstep;
        n_go = n_go + dn_g*tstep;
        n_lo = n_lo + dn_l*tstep;


        % Physical stops to kick out of loop
        if Pe>=P
            break
        end
        if n_lo<=0
            break
        end
    end
end
```

```
% Plot results
figure(1), plot(T(:,1),T(:,2),'r','LineWidth',2),grid, ...
    title('Temperature vs. Time'),...
    xlabel('Time [s]'),...
    ylabel('Temperature [K]');
figure(2), plot(n_g(:,1),n_g(:,2),'b',n_l(:,1),n_l(:,2),'g','LineWidth',2),grid, ...
    title('kmol of N20 vs. Time'),...
    xlabel('Time [s]'),...
    ylabel('kmol of N2O [kmol]'),...
    legend('kmol of N2O gas','kmol of N2O liquid',1);
figure(3), plot(Pres(:,1),Pres(:,2),'m',PE(:,1),PE(:,2),'c','LineWidth',2),grid, ...
    title('Pressure vs. Time'),...
    xlabel('Time [s]'),...
    ylabel('Pressure [Pa]');
    legend('tank pressure','chamber pressure',1);
```

APPENDIX I

NON-IDEAL MODEL MATLAB CODE

Initial Condition Code (Model2_IC.m)

```
% Masters Thesis
% Non-Ideal (Peng-Robinson), High Pressure Equilibrium Model
% Initial Conditions Calculation


function [P_eq,n2v_eq,n2l_eq,y2_eq] = Model2_IC(y2guess,n_He,n_T,T_sur,V)


R = 8314.3;            % universal gas constant [J/(kmol*K)]


G1 = 96.512 ;         % vapor pressure of N2O [Pa] coefficients
G2 = -4045 ;          % valid for Temp range [182.3 K - 309.57 K]
G3 = -12.277 ;
G4 = 2.886e-5 ;
G5 = 2 ;


Q1 = 2.781;           % liquid molar volume of N2O [m^3/kmol] coefficients
Q2 = 0.27244;
Q3 = 309.57;
Q4 = 0.2882;


Vhat_l = Q2^(1+(1-T_sur/Q3)^Q4)/Q1;     % liquid molar volume of N2O [m^3/kmol]
Psat = exp(G1 + G2/T_sur + G3*log(T_sur) + G4*T_sur^G5);
    % Ideal correlation of pure N2O vapor pressure [Pa]
n2vo = Psat*(V - Vhat_l*n_T) / (-Psat*Vhat_l + R*T_sur);
    % Guess initial N2O vapor [kmol] based on ideal correlation
presso = Psat/y2guess;
    % Guess initial pressure in tank [Pa] based on ideal assumption (Raoult's Law)


% Step sizes for numerical derivative calculation
deltan2v = 1e-8;                    % small change in n2v [kmol]
deltaP = 1e-8;                      % small change in pressure P [Pa]
```

```
Pscale = 10^6;                          % scaling factor for Jacobian calculation


% Critical constants and acentric factors from Perry's Handbook
% Tc1 = 5.2;        % He critical temperature [K]
% Tc2 = 309.57;     % N20 critical temperature [K]
% Pc1 = 0.23e6;     % He critical pressure [Pa]
% Pc2 = 7.28e6;     % N2O critical pressure [Pa]
% w1 = -0.388;      % He acentric factor
% w2 = 0.143;       % N2O acentric factor
% Critical Constants and acentricd factors from Sandler's code
Tc1 = 5.19;
Tc2 = 309.6;
Pc1 = 0.227e6;
Pc2 = 7.24e6;
w1 = -0.365;
w2 = 0.165;


% Peng-Robinson parameters
kappa1 = 0.37464 + 1.54226*w1 - 0.26992*w1^2;    % Sandler p.250
kappa2 = 0.37464 + 1.54226*w2 - 0.26992*w2^2;
alpo1 = (1 + kappa1*(1-sqrt(T_sur/Tc1)))^2;
alpo2 = (1 + kappa2*(1-sqrt(T_sur/Tc2)))^2;
a1 = 0.45724*R^2*Tc1^2*alpo1/Pc1;                % Sandler p.250
a2 = 0.45724*R^2*Tc2^2*alpo2/Pc2;
b1 = 0.0778*R*Tc1/Pc1;
b2 = 0.0778*R*Tc2/Pc2;


% Store values from each iteration
% kth row = iteration number
Y2 = zeros(100,1);            % blank matrix to store y2 values
n2v = zeros(100,1);           % blank matrix to store n_2v values
press = zeros(100,1);         % blank matrix to store P values
pbar = zeros(100,1);          % blank matrix to store Pbar values


Y2(1,1) = y2guess;
n2v(1,1) = n2vo;
press(1,1) = presso;
pbar(1,1) = presso/Pscale;
```

```matlab
for k = 1:100     % iteration number
    for n = 1:5
        if n==1
            P = press(k,1);
            n_2v = n2v(k,1);
        elseif n==2
            P = press(k,1) + deltaP/2;
            n_2v = n2v(k,1);
        elseif n==3
            P = press(k,1) - deltaP/2;
            n_2v = n2v(k,1);
        elseif n==4
            P = press(k,1);
            n_2v = n2v(k,1) + deltan2v/2;
        else
            P = press(k,1);
            n_2v = n2v(k,1) - deltan2v/2;
        end

        y2 = Y2(k,1);

        % Liquid - Pure
        % Z_2l^3 + c2*Z_2l^2 + c1*Z_2l + c0 = 0

        A2 = P*a2/(R*T_sur)^2;                  % Sandler p.251
        B2 = P*b2/(R*T_sur);

        c2 = -(1-B2);
        c1 = (A2 - 3*B2^2 - 2*B2);
        c0 = -(A2*B2 - B2^2 - B2^3);

        ql = c1/3 - c2^2/9;
        rl = (c1*c2 - 3*c0)/6 - c2^3/27;
        qrl = ql^3 + rl^2;

        % loop for finding Z_2l
        if qrl > 0                              % Case 1: 1 real root
```

134

```matlab
        rpqrl = rl + qrl^0.5;
        rmqrl = rl - qrl^0.5;
        if rpqrl>=0
            s1 = rpqrl^(1/3);
        else
            s1 = -(abs(rpqrl)^(1/3));
        end
        if rmqrl>=0
            s2 = rmqrl^(1/3);
        else
            s2 = -(abs(rmqrl)^(1/3));
        end
        Z_2l = s1 + s2 - c2/3;
    elseif qrl == 0                         % Case 2: 3 real roots, at least 2 equal
        if rl >= 0
            s1 = rl^(1/3);
            s2 = rl^(1/3);
        else
            s1 = -(abs(rl))^(1/3);
            s2 = -(abs(rl))^(1/3);
        end
        Z_2l_1 = s1 + s2 - c2/3;
        Z_2l_2 = -0.5*(s1 + s2) - c2/3;
        Z_2l = min([Z_2l_1 Z_2l_2]);
    else                                    % Case 3: 3 real, distinct roots
        alpha = (abs(qrl))^0.5;
        if rl > 0
            th1 = atan(alpha/rl);
        else
            th1 = pi - atan(alpha/abs(rl));
        end
        th2 = atan2(alpha,rl);              % double check angle with Matlab atan2 code
        if abs(th1 - th2) < 1e-14
            th = th1;
        else
            disp('Liquid Thetas do not match');
            pause;
        end
        rho = (rl^2 + alpha^2)^0.5;
```

```matlab
        Z_2l_1 = 2*rho^(1/3)*cos(th/3) - c2/3;
        Z_2l_2 = -rho^(1/3)*cos(th/3) - c2/3 - sqrt(3)*rho^(1/3)*sin(th/3);
        Z_2l_3 = -rho^(1/3)*cos(th/3) - c2/3 + sqrt(3)*rho^(1/3)*sin(th/3);
        Z_2l = min([Z_2l_1 Z_2l_2 Z_2l_3]);
end


% Gas - Mixture
% Z_m^3 + d2*Z_m^2 + d1*Z_m + d0 = 0

k12 = 0;                                % binary interaction parameter (He/N2O mix)
a21 = sqrt(a1*a2)*(1-k12);              % Sandler p.423
am = (1-y2)^2*a1 + 2*y2*(1-y2)*a21 + y2^2*a2;
bm = (1-y2)*b1 + y2*b2;


Am = P*am/(R*T_sur)^2;                  % Sandler p.425
Bm = P*bm/(R*T_sur);
A21 = P*a21/(R*T_sur)^2;


d2 = -(1-Bm);
d1 = (Am - 3*Bm^2 - 2*Bm);
d0 = -(Am*Bm - Bm^2 - Bm^3);


qm = d1/3 - d2^2/9;
rm = (d1*d2 - 3*d0)/6 - d2^3/27;
qrm = qm^3 + rm^2;


% loop for finding Z_m
if qrm > 0                              % Case 1: 1 real root
    rpqrm = rm + qrm^0.5;
    rmqrm = rm - qrm^0.5;
    if rpqrm>=0
        s1m = rpqrm^(1/3);
    else
        s1m = -(abs(rpqrm)^(1/3));
    end
    if rmqrm>=0
        s2m = rmqrm^(1/3);
    else
```

```matlab
            s2m = -(abs(rmqrm)^(1/3));
        end
        Z_m = s1m + s2m - d2/3;
    elseif qrm == 0                             % Case 2: 3 real roots, at least 2 equal
        if rm >= 0
            s1m = rm^(1/3);
            s2m = rm^(1/3);
        else
            s1m = -(abs(rm))^(1/3);
            s2m = -(abs(rm))^(1/3);
        end
        Z_m_1 = s1m + s2m - d2/3;
        Z_m_2 = -0.5*(s1m + s2m) - d2/3;
        Z_m = max([Z_m_1 Z_m_2]);
    else                                        % Case 3: 3 real, distinct roots
        alpham = (abs(qrm))^0.5;
        if rm > 0
            th1m = atan(alpham/rm);
        else
            th1m = pi - atan(alpham/abs(rm));
        end
        th2m = atan2(alpham,rm);                % double check angle with Matlab atan2 code
        if abs(th1m - th2m) < 1e-14
            thm = th1m;
        else
            disp('Mixture Thetas do not match');
            pause;
        end
        rhom = (rm^2 + alpham^2)^0.5;
        Z_m_1 = 2*rhom^(1/3)*cos(thm/3) - d2/3;
        Z_m_2 = -rhom^(1/3)*cos(thm/3) - d2/3 - sqrt(3)*rhom^(1/3)*sin(thm/3);
        Z_m_3 = -rhom^(1/3)*cos(thm/3) - d2/3 + sqrt(3)*rhom^(1/3)*sin(thm/3);
        Z_m = max([Z_m_1 Z_m_2 Z_m_3]);
    end

% Fugacity Coefficient Calculations
% phi_2l: Sandler p.300
% phi_2v: Sandler p.423
phi_2l = exp((Z_2l-1) - log(Z_2l - B2) - (A2/(2*sqrt(2)*B2))*...
```

```matlab
                log((Z_2l+(1+sqrt(2))*B2)/(Z_2l+(1-sqrt(2))*B2)));
        phi_2v = exp((B2/Bm)*(Z_m-1) - log(Z_m - Bm) - (Am/(2*sqrt(2)*Bm))*...
            ((2*((1-y2)*A21+y2*A2)/Am) - B2/Bm)*...
            log((Z_m+(1+sqrt(2))*Bm)/(Z_m+(1-sqrt(2))*Bm)));

        % Initial Solution Guess Calculation
        f1(k,n) = (n_He + n_2v)*phi_2l - n_2v*phi_2v;
        f2(k,n) = (n_He + n_2v)*Z_m + (n_T - n_2v)*Z_2l - P*V/(R*T_sur);
end

% for derivative calculations
F1   = f1(k,1);                    % F1(n2v,P)
F1pp = f1(k,2);                    % F1(n2v,P+deltaP/2)
F1pm = f1(k,3);                    % F1(n2v,P-deltaP/2)
F1np = f1(k,4);                    % F1(n2v+deltan2v/2,P)
F1nm = f1(k,5);                    % F1(n2v-deltan2v/2,P)
F2   = f2(k,1);                    % F2(n2v,P)
F2pp = f2(k,2);                    % F2(n2v,P+deltaP/2)
F2pm = f2(k,3);                    % F2(n2v,P-deltaP/2)
F2np = f2(k,4);                    % F2(n2v+deltan2v/2,P)
F2nm = f2(k,5);                    % F2(n2v-deltan2v/2,P)


% Update guesses for n_2v and P
Pbar = P/Pscale;
dF1dn = (F1np - F1nm)/deltan2v;
dF1dP = (F1pp - F1pm)/deltaP;
dF1dPb = dF1dP*Pscale;
dF2dn = (F2np - F2nm)/deltan2v;
dF2dP = (F2pp - F2pm)/deltaP;
dF2dPb = dF2dP*Pscale;

JAC_inv = (1/(dF1dn*dF2dPb - dF1dPb*dF2dn))*[dF2dPb -dF1dPb;-dF2dn dF1dn];
F = [F1 F2]';

sol_old = [n_2v Pbar]';           % old guess
sol_new = sol_old - JAC_inv*F;    % new guess
n2v(k+1,1) = sol_new(1,1);
pbar(k+1,1) = sol_new(2,1);
```

```
        press(k+1,1) = sol_new(2,1)*Pscale;
        Y2(k+1,1) = n2v(k+1,1)/(n2v(k+1,1) + n_He);      % update y2

        % Check errors
        del = ((n2v(k+1,1) - n2v(k,1))^2 + (pbar(k+1,1) - pbar(k,1))^2)^0.5;
        delF = (F1^2 + F2^2)^0.5;
        error = max([del delF]);

        % convergence criterion
        if error < 1e-8
            break;
        end
    end
end


P_eq = press(k+1,1);
n2v_eq = n2v(k+1,1);
n2l_eq = n_T - n2v(k+1,1);
y2_eq = Y2(k+1,1);
```

Drain History Code, Run File (Model2_drainA_run.m)

```
% Masters Thesis
% Non-Ideal (Peng-Robinson), High Pressure Equilibrium Model
% Draining Tank Calculation - ODE45 Run File

clear all
clc


% --------------- Get Initial Conditions from Model2_IC.m --------------
y2_guess = 1;                % Guess mol fraction of N2O
nHe = 0;                     % He in tank [kmol]
mloaded = 19.32933;          % mass of N2O initially loaded into tank [kg]: Test 1
% mloaded = 16.23298;          % Test 2
% mloaded = 14.10076;          % Test 3
% mloaded = 23.62427;          % Test 4
MW2 = 44.013;                % molecular weight of N2O [kg/kmol]
```

```matlab
nT = mloaded/MW2;              % total N2O loaded into tank [kmol]
Tsur = 286.5;                  % initial temperature in tank [K]: Test 1
% Tsur = 278.5;                  % Test 2
% Tsur = 271.5;                  % Test 3
% Tsur = 291.3;                  % Test 4
Vol = 0.0354;                  % total volume of tank [m^3]


[Po,n2vo,n2lo,y2o] = Model2_IC(y2_guess,nHe,nT,Tsur,Vol);
% -----------------------------------------------------------------------
% NOTE: if "nHe" or "Vol" are changed above, change them in Model2_drainA_sol.m

IC = [Tsur Po n2lo n2vo]';
time = (0:0.0005:4.8)';


% Matlab ODE: Implicit Solution Method
[t_out,x_out] = ode45(@Model2_drainA_sol,time,IC);


T = x_out(:,1);
P = x_out(:,2);
n2l = x_out(:,3);
n2v = x_out(:,4);


figure(1),plot(t_out,x_out(:,1),'r','LineWidth',2),grid, ...
    title('Temperature vs. Time'),...
    xlabel('Time [s]'),...
    ylabel('Temperature [K]');
figure(2),plot(t_out,x_out(:,2),'m','LineWidth',2),grid, ...
    title('Pressure vs. Time'),...
    xlabel('Time [s]'),...
    ylabel('Pressure [Pa]');
figure(3),plot(t_out,x_out(:,3),'g',t_out,x_out(:,4),'b','LineWidth',2),grid, ...
    title('kmol of N20 vs. Time'),...
    xlabel('Time [s]'),...
    ylabel('kmol of N2O [kmol]'),...
    legend('kmol of N2O liquid','kmol of N2O gas',1);
```

<u>Drain History Code, Solution File</u> (Model2_drainA_sol.m)

```matlab
% Masters Thesis
% Non-Ideal (Peng-Robinson), High Pressure Equilibrium Model
% Draining Tank Calculation - ODE45 Solution File

function dx = Model2_drainA_sol(t,x)


T = x(1) ;
P = x(2);
n2l = x(3) ;
n2v = x(4) ;


% Given constants
nHe = 0;                    % He in tank [kmol]
Vol = 0.0354;               % total volume of tank [m^3]
y2 = n2v/(n2v+nHe);         % mol fraction of N2O
m_T = 6.4882;               % tank mass [kg]
R = 8314.3;                 % universal gas constant [J/(kmol*K)];
C_D = 0.425;                % discharge coefficient: Test 1
% C_D = 0.365;                % Test 2 and 3
% C_D = 0.09;                 % Test 4
A_inj = 0.0001219352;       % injector hole area [m^2]
MW2 = 44.013;               % molecular weight of N2O [kg/kmol]


C1 = 0.2079e5 ;      % heat capacity of He at constant pressure [J/(kmol*K)] coefficients
C2 = 0 ;             % valid for Temp range [100 K - 1500 K]
C3 = 0 ;
C4 = 0 ;
C5 = 0 ;


D1 = 0.2934e5 ;      % heat capacity of N2O gas at constant pressure [J/(kmol*K)] coefficients
D2 = 0.3236e5 ;      % valid for Temp range [100 K - 1500 K]
D3 = 1.1238e3 ;
D4 = 0.2177e5 ;
D5 = 479.4 ;


E1 = 6.7556e4 ;      % heat capacity of N2O liquid at constant pressure [J/(kmol*K)] coefficients
```

```matlab
E2 = 5.4373e1 ;        % valid for Temp range [182.3 K - 200 K]
E3 = 0 ;
E4 = 0 ;
E5 = 0 ;


J1 = 2.3215e7 ;        % heat of vaporization of N2O [J/kmol] coefficients
J2 = 0.384 ;           % valid for Temp range [182.3 K - 309.57 K]
J3 = 0 ;
J4 = 0 ;


% polynomial fit of combustion chamber pressure [Pa]
Pe = -2924.42*t^6 + 46778.07*t^5 - 285170.63*t^4 + 813545.02*t^3 - ...
   1050701.53*t^2 + 400465.85*t + 1175466.2;                          % Test 1
% Pe = 95.92*t^6 - 2346.64*t^5 + 21128.78*t^4 - 87282.73*t^3 + ...
%    186675.17*t^2 - 335818.91*t + 3029190.03;                        % Test 2
% Pe = 58.06*t^6 - 1201.90*t^5 + 8432.11*t^4 - 22175.67*t^3 + ...
%    21774.66*t^2 - 99922.82*t + 2491369.68;                          % Test 3
% Pe = -4963.73*t + 910676.22;                                        % Test 4



% Critical constants and acentric factors from Perry's Handbook
% Tc1 = 5.2;       % He critical temperature [K]
% Tc2 = 309.57;    % N2O critical temperature [K]
% Pc1 = 0.23e6;    % He critical pressure [Pa]
% Pc2 = 7.28e6;    % N2O critical pressure [Pa]
% w1 = -0.388;     % He acentric factor
% w2 = 0.143;      % N2O acentric factor
% Critical constants and acentric factors from Sandler's code
Tc1 = 5.19;
Tc2 = 309.6;
Pc1 = 0.227e6;
Pc2 = 7.24e6;
w1 = -0.365;
w2 = 0.165;


% Peng-Robinson parameters
kappa1 = 0.37464 + 1.54226*w1 - 0.26992*w1^2;    % Sandler p.250
kappa2 = 0.37464 + 1.54226*w2 - 0.26992*w2^2;
```

```matlab
alpo1 = (1 + kappa1*(1-sqrt(T/Tc1)))^2;
alpo2 = (1 + kappa2*(1-sqrt(T/Tc2)))^2;


a1 = 0.45724*R^2*Tc1^2*alpo1/Pc1;                    % Sandler p.250
a2 = 0.45724*R^2*Tc2^2*alpo2/Pc2;
b1 = 0.0778*R*Tc1/Pc1;
b2 = 0.0778*R*Tc2/Pc2;
da1dT = -0.45724*R^2*Tc1^2*kappa1*sqrt(alpo1/(T*Tc1))/Pc1;
da2dT = -0.45724*R^2*Tc2^2*kappa2*sqrt(alpo2/(T*Tc2))/Pc2;
d2a1dT2 = (-0.45724*R^2*Tc1^2/Pc1)*kappa1*0.5*(alpo1/(T*Tc1))^-0.5*...
        ((-kappa1*sqrt(alpo1*T*Tc1)-alpo1*Tc1)/(T*Tc1)^2);
d2a2dT2 = (-0.45724*R^2*Tc2^2/Pc2)*kappa2*0.5*(alpo2/(T*Tc2))^-0.5*...
        ((-kappa2*sqrt(alpo2*T*Tc2)-alpo2*Tc2)/(T*Tc2)^2);


A2 = P*a2/(R*T)^2;                                   % Sandler p.251
B2 = P*b2/(R*T);


c2 = -(1-B2);
c1 = (A2 - 3*B2^2 - 2*B2);
c0 = -(A2*B2 - B2^2 - B2^3);


ql = c1/3 - c2^2/9;
rl = (c1*c2 - 3*c0)/6 - c2^3/27;
qrl = ql^3 + rl^2;


% Liquid - Pure
% Z_2l^3 + c2*Z_2l^2 + c1*Z_2l + c0 = 0


% loop for finding Z_2l
if qrl > 0                              % Case 1: 1 real root
    rpqrl = rl + qrl^0.5;
    rmqrl = rl - qrl^0.5;
    if rpqrl>=0
        s1 = rpqrl^(1/3);
    else
        s1 = -(abs(rpqrl)^(1/3));
    end
    if rmqrl>=0
```

```matlab
            s2 = rmqrl^(1/3);
        else
            s2 = -(abs(rmqrl)^(1/3));
        end
        Z2l = s1 + s2 - c2/3;
    elseif qrl == 0                         % Case 2: 3 real roots, at least 2 equal
        if rl >= 0
            s1 = rl^(1/3);
            s2 = rl^(1/3);
        else
            s1 = -(abs(rl))^(1/3);
            s2 = -(abs(rl))^(1/3);
        end
        Z2l_1 = s1 + s2 - c2/3;
        Z2l_2 = -0.5*(s1 + s2) - c2/3;
        Z2l = min([Z2l_1 Z2l_2]);
    else                                    % Case 3: 3 real, distinct roots
        alpha = (abs(qrl))^0.5;
        if rl > 0
            th1 = atan(alpha/rl);
        else
            th1 = pi - atan(alpha/abs(rl));
        end
        th2 = atan2(alpha,rl);              % double check angle with Matlab atan2 code
        if abs(th1 - th2) < 1e-14
            th = th1;
        else
            disp('Liquid Thetas do not match');
            pause;
        end
        rho = (rl^2 + alpha^2)^0.5;
        Z2l_1 = 2*rho^(1/3)*cos(th/3) - c2/3;
        Z2l_2 = -rho^(1/3)*cos(th/3) - c2/3 - sqrt(3)*rho^(1/3)*sin(th/3);
        Z2l_3 = -rho^(1/3)*cos(th/3) - c2/3 + sqrt(3)*rho^(1/3)*sin(th/3);
        Z2l = min([Z2l_1 Z2l_2 Z2l_3]);
end

% Gas - Mixture
% Z_m^3 + d2*Z_m^2 + d1*Z_m + d0 = 0
```

```matlab
k12 = 0;                                % binary interaction parameter (He/N2O mix)
a21 = sqrt(a1*a2)*(1-k12);              % Sandler p.423
am = (1-y2)^2*a1 + 2*y2*(1-y2)*a21 + y2^2*a2;
bm = (1-y2)*b1 + y2*b2;
da21dT = (1-k12)/2*((a1*a2)^-0.5*(da1dT*a2+a1*da2dT));
d2a21dT2 = (1-k12)/2*(-0.5*(a1*a2)^(-3/2)*(da1dT*a2+a1*da2dT)^2+(a1*a2)^-0.5*...
    (d2a1dT2*a2+2*da1dT*da2dT+a1*d2a2dT2));
damdT = (1-y2)^2*da1dT + 2*y2*(1-y2)*da21dT + y2^2*da2dT;
d2amdT2 = (1-y2)^2*d2a1dT2 + 2*y2*(1-y2)*d2a21dT2 + y2^2*d2a2dT2;
d2amdTdy2 = -2*(1-y2)*da1dT + 2*(1-2*y2)*da21dT + 2*y2*da2dT;
damdy2 = -2*(1-y2)*a1 + 2*a21*(1-2*y2) + 2*y2*a2;    % @T
dbmdy2 = -b1 + b2;


Am = P*am/(R*T)^2;                      % Sandler p.425
Bm = P*bm/(R*T);
A21 = P*a21/(R*T)^2;


d2 = -(1-Bm);
d1 = (Am - 3*Bm^2 - 2*Bm);
d0 = -(Am*Bm - Bm^2 - Bm^3);


qm = d1/3 - d2^2/9;
rm = (d1*d2 - 3*d0)/6 - d2^3/27;
qrm = qm^3 + rm^2;


if qrm > 0                              % Case 1: 1 real root
    rpqrm = rm + qrm^0.5;
    rmqrm = rm - qrm^0.5;
    if rpqrm>=0
        s1m = rpqrm^(1/3);
    else
        s1m = -(abs(rpqrm)^(1/3));
    end
    if rmqrm>=0
        s2m = rmqrm^(1/3);
    else
        s2m = -(abs(rmqrm)^(1/3));
```

```matlab
        end
    Zm = s1m + s2m - d2/3;
elseif qrm == 0                              % Case 2: 3 real roots, at least 2 equal
    if rm >= 0
        s1m = rm^(1/3);
        s2m = rm^(1/3);
    else
        s1m = -(abs(rm))^(1/3);
        s2m = -(abs(rm))^(1/3);
    end
    Zm_1 = s1m + s2m - d2/3;
    Zm_2 = -0.5*(s1m + s2m) - d2/3;
    Zm = max([Zm_1 Zm_2]);
else                                         % Case 3: 3 real, distinct roots
    alpham = (abs(qrm))^0.5;
    if rm > 0
        th1m = atan(alpham/rm);
    else
        th1m = pi - atan(alpham/abs(rm));
    end
    th2m = atan2(alpham,rm);
    if abs(th1m - th2m) < 1e-14
        thm = th1m;
    else
        disp('Mixture Thetas do not match');
        pause;
    end
    rhom = (rm^2 + alpham^2)^0.5;
    Zm_1 = 2*rhom^(1/3)*cos(thm/3) - d2/3;
    Zm_2 = -rhom^(1/3)*cos(thm/3) - d2/3 - sqrt(3)*rhom^(1/3)*sin(thm/3);
    Zm_3 = -rhom^(1/3)*cos(thm/3) - d2/3 + sqrt(3)*rhom^(1/3)*sin(thm/3);
    Zm = max([Zm_1 Zm_2 Zm_3]);
end


H2lex = R*T*(Z2l-1) + (T*da2dT-a2)/(2*sqrt(2)*b2)*log((Z2l+(1+sqrt(2))*B2)/(Z2l+(1-sqrt(2))*B2));
Hgex = R*T*(Zm-1) + (T*damdT-am)/(2*sqrt(2)*bm)*log((Zm+(1+sqrt(2))*Bm)/(Zm+(1-sqrt(2))*Bm));
phi2l = exp((Z2l-1) - log(Z2l - B2) - (A2/(2*sqrt(2)*B2))*log((Z2l+(1+sqrt(2))*B2)/(Z2l+(1-sqrt(2))*B2)));
phi2v = exp((B2/Bm)*(Zm-1) - log(Zm - Bm) - (Am/(2*sqrt(2)*Bm))*((2*((1-y2)*A21+y2*A2)/Am) - B2/Bm)*...
        log((Zm+(1+sqrt(2))*Bm)/(Zm+(1-sqrt(2))*Bm)));
```

```
%%%%%%%%%%%%%%%%%% Analytical Derivatives %%%%%%%%%%%%%%%%%%%%%
dA2dT = (P/R^2)*(da2dT/T^2-2*a2/T^3);    % @P
dA2dP = a2/(R*T)^2;                      % @T
dB2dT = -P*b2/(R*T^2);                   % @P
dB2dP = b2/(R*T);                        % @T
dA21dT = (P/R^2)*(da21dT/T^2-2*a21/T^3);
dA21dP = a21/(R*T)^2;
dAmdT = (P/R^2)*(damdT/T^2-2*am/T^3);    % @P,y2
dAmdP = am/(R*T)^2;                      % @T,y2
dAmdy2 = P/(R*T)^2*damdy2;               % @T,P
dBmdT = -P*bm/(R*T^2);                   % @P,y2
dBmdP = bm/(R*T);                        % @T,y2
dBmdy2 = P/(R*T)*dbmdy2;                 % @T,P


% helpful substitutions
Z2lpB2 = Z2l + (1+sqrt(2))*B2;
Z2lmB2 = Z2l + (1-sqrt(2))*B2;
ZmpBm = Zm + (1+sqrt(2))*Bm;
ZmmBm = Zm + (1-sqrt(2))*Bm;
dABT = (dA2dT*B2 - A2*dB2dT)/B2^2;
dABP = (dA2dP*B2 - A2*dB2dP)/B2^2;
dB2mT = (dB2dT*Bm - B2*dBmdT)/Bm^2;
dB2mP = (dB2dP*Bm - B2*dBmdP)/Bm^2;
dABmT = (dAmdT*Bm - Am*dBmdT)/Bm^2;
dABmP = (dAmdP*Bm - Am*dBmdP)/Bm^2;
dABmy2 = (dAmdy2*Bm - Am*dBmdy2)/Bm^2;
AB21m = 2*((1-y2)*A21+y2*A2)/Am - B2/Bm;
dAB21mT = (2/Am^2)*(((1-y2)*dA21dT+y2*dA2dT)*Am-((1-y2)*A21+y2*A2)*dAmdT) - dB2mT;
dAB21mP = (2/Am^2)*(((1-y2)*dA21dP+y2*dA2dP)*Am-((1-y2)*A21+y2*A2)*dAmdP) - dB2mP;
dAB21my2 = (2/Am^2)*((-A21+A2)*Am-((1-y2)*A21+y2*A2)*dAmdy2) + B2*dBmdy2/Bm^2;
exp2l = exp(Z2l-1-log(Z2l-B2)-(A2/(2*sqrt(2)*B2))*log(Z2lpB2/Z2lmB2));
exp2v = exp((B2/Bm)*(Zm-1)-log(Zm-Bm)-(Am/(2*sqrt(2)*Bm))*AB21m*log(ZmpBm/ZmmBm));


% analytical derivatives [T,P,Z(T,P,y2(n2v)),y2(n2v)]
AdZ2ldT = ((-Z2l^2+6*B2*Z2l+2*Z2l+A2-2*B2-3*B2^2)*dB2dT + ...
    (-Z2l+B2)*dA2dT)/(3*Z2l^2-(1-B2)*2*Z2l+A2-3*B2^2-2*B2);          % @P
AdZ2ldP = ((-Z2l^2+6*B2*Z2l+2*Z2l+A2-2*B2-3*B2^2)*dB2dP + ...
    (-Z2l+B2)*dA2dP)/(3*Z2l^2-(1-B2)*2*Z2l+A2-3*B2^2-2*B2);          % @T
```

147

```
AdZmdT = ((-Zm^2+6*Bm*Zm+2*Zm+Am-2*Bm-3*Bm^2)*dBmdT + ...
    (-Zm+Bm)*dAmdT)/(3*Zm^2-(1-Bm)*2*Zm+Am-3*Bm^2-2*Bm);                          % @P,y2;
AdZmdP = ((-Zm^2+6*Bm*Zm+2*Zm+Am-2*Bm-3*Bm^2)*dBmdP + ...
    (-Zm+Bm)*dAmdP)/(3*Zm^2-(1-Bm)*2*Zm+Am-3*Bm^2-2*Bm);                          % @T,y2;
AdZmdy2 = ((-Zm^2+6*Bm*Zm+2*Zm+Am-2*Bm-3*Bm^2)*dBmdy2 + ...
    (-Zm+Bm)*dAmdy2)/(3*Zm^2-(1-Bm)*2*Zm+Am-3*Bm^2-2*Bm);                         % @T,P;
AdH2ldT = R*(Z2l-1) + (1/(2*sqrt(2)*b2))*(T*d2a2dT2)*log(Z2lpB2/Z2lmB2) + ...
    ((T*da2dT-a2)/b2)*(Z2l/(Z2lpB2*Z2lmB2))*dB2dT;                                % @Z2l,P
AdH2ldP = (T*da2dT-a2)/b2*(Z2l/(Z2lpB2*Z2lmB2))*dB2dP;                            % @Z2l,T
AdH2ldZ2l = R*T + (T*da2dT-a2)/b2*(-B2/(Z2lpB2*Z2lmB2));                          % @T,P
AdHgdT = R*(Zm-1) + (1/(2*sqrt(2)*bm))*(T*d2amdT2)*log(ZmpBm/ZmmBm) + ...
    ((T*damdT-am)/bm)*(Zm/(ZmpBm*ZmmBm))*dBmdT;                                   % @Zm,P,y2
AdHgdP = (T*damdT-am)/bm*(Zm/(ZmpBm*ZmmBm))*dBmdP;                                % @Zm,T,y2
AdHgdy2 = (((T*d2amdTdy2-damdy2)*2*sqrt(2)*bm-(T*damdT-am)*2*sqrt(2)*dbmdy2)/(8*bm^2))*log(ZmpBm/ZmmBm)+...
    ((T*damdT-am)/(2*sqrt(2)*bm))*(ZmmBm/ZmpBm)*(2*sqrt(2)*Zm/ZmmBm^2)*dBmdy2;
AdHgdZm = R*T + (T*damdT-am)/(2*sqrt(2)*bm)*(ZmmBm/ZmpBm)*(-2*sqrt(2)*Bm/ZmmBm^2);   % @T,P,y2
Adphi2ldT = exp2l*(dB2dT/(Z2l-B2)-dABT/(2*sqrt(2))*log(Z2lpB2/Z2lmB2)-...
    (A2/B2)*(Z2l/(Z2lpB2*Z2lmB2))*dB2dT);                                        % @Z2l,P
Adphi2ldP = exp2l*(dB2dP/(Z2l-B2)-dABP/(2*sqrt(2))*log(Z2lpB2/Z2lmB2)-...
    (A2/B2)*(Z2l/(Z2lpB2*Z2lmB2))*dB2dP);                                        % @Z2l,T;
Adphi2ldZ2l = exp2l*(1-1/(Z2l-B2)+A2/(Z2lpB2*Z2lmB2));                           % @T,P
Adphi2vdT = exp2v*((Zm-1)*dB2mT+dBmdT/(Zm-Bm)-(1/(2*sqrt(2)))*(dABmT*AB21m+(Am/Bm)*dAB21mT)*...
    log(ZmpBm/ZmmBm)-(Am/Bm)*(AB21m/ZmpBm)*(Zm*dBmdT/ZmmBm));                     % @Zm,P,y2
Adphi2vdP = exp2v*((Zm-1)*dB2mP+dBmdP/(Zm-Bm)-(1/(2*sqrt(2)))*(dABmP*AB21m+(Am/Bm)*dAB21mP)*...
    log(ZmpBm/ZmmBm)-(Am/Bm)*(AB21m/ZmpBm)*(Zm*dBmdP/ZmmBm));                     % @Zm,T,y2
Adphi2vdy2 = exp2v*((Zm-1)*-B2/Bm^2*dBmdy2+dBmdy2/(Zm-Bm)-(1/(2*sqrt(2)))*...
    (dABmy2*AB21m+(Am/Bm)*dAB21my2)*log(ZmpBm/ZmmBm)-(Am/Bm)*(AB21m/ZmpBm)*(Zm*dBmdy2/ZmmBm));  % @Zm,T,P
Adphi2vdZm = exp2v*(B2/Bm-1/(Zm-Bm)+Am*AB21m/(ZmpBm*ZmmBm));


%%%%%%%%%%%%%%%%%%%%%%%%%%%%%%%%%%%%%%%%%%%%%%%%%%%%%%%%%%%%%%%%%%%
ng = n2v + nHe;
Tr = T/Tc2;
Cp_1g = C1 + C2*T + C3*T^2 + C4*T^3 + C5*T^4;       % specific heat of He at constant volume [J/(kmol*K)]
Cp_2v = D1 + D2*((D3/T)/sinh(D3/T))^2 + D4*((D5/T)/cosh(D5/T))^2;
    % specific heat of N2O gas at constant volume [J/(kmol*K)];
Cp_T = (4.8 + 0.00322*T)*155.239;                  % specific heat of tank, Aluminum 6061-T6 [J/(kg*K)]
Cp_2l = E1 + E2*T + E3*T^2 + E4*T^3 + E5*T^4;
    % specific heat of N2O liquid at constant volume, approx. same as at constant pressure [J/(kmol*K)]
deltaH_2v = J1*(1 - Tr)^(J2 + J3*Tr + J4*Tr^2);    % heat of vaporization of N2O [J/kmol];
```

```matlab
D = nHe*Cp_1g + n2v*Cp_2v + ng*AdHgdZm*AdZmdT + ng*AdHgdT - ng*R*(Zm + T*AdZmdT);
N = m_T*Cp_T + n2l*(Cp_2l + AdH2ldZ2l*AdZ2ldT + AdH2ldT - R*(Z2l+T*AdZ2ldT));
E = ng*(AdHgdZm*AdZmdP + AdHgdP - R*T*AdZmdP);
Q = n2l*(AdH2ldZ2l*AdZ2ldP + AdH2ldP - R*T*AdZ2ldP);
M = Hgex - Zm*R*T + (1-y2)*(AdHgdZm*AdZmdy2 + AdHgdy2 - R*T*AdZmdy2);
K = (C_D*A_inj*sqrt(2/MW2))*sqrt(P*(P-Pe)/(Z2l*R*T));
beta = ng*AdZmdT + n2l*AdZ2ldT + (Zm*ng+Z2l*n2l)/T;
gamma = ng*AdZmdP + n2l*AdZ2ldP - Vol/(R*T);
delta = Zm + (1-y2)*AdZmdy2;
theta = ng*(Adphi2ldZ2l*AdZ2ldT + Adphi2ldT) - n2v*(Adphi2vdZm*AdZmdT + Adphi2vdT);
lamda = ng*(Adphi2ldZ2l*AdZ2ldP + Adphi2ldP) - n2v*(Adphi2vdZm*AdZmdP + Adphi2vdP);
psi = phi2l - phi2v - y2*(1-y2)*(Adphi2vdZm*AdZmdy2 + Adphi2vdy2);


X = D+N;
W = E+Q;
Y = -Z2l*R*T;
Z = deltaH_2v + M - H2lex;


% Solve using Cramer's Rule
Col1 = [X 0 beta theta]';
Col2 = [W 0 gamma lamda]';
Col3 = [Y 1 Z2l 0]';
Col4 = [Z 1 delta psi]';
Col5 = [0 -K 0 0]';


AA = [Col1 Col2 Col3 Col4];
BB = [Col5 Col2 Col3 Col4];
CC = [Col1 Col5 Col3 Col4];
DD = [Col1 Col2 Col5 Col4];
EE = [Col1 Col2 Col3 Col5];


dTdt = det(BB)/det(AA);
dPdt = det(CC)/det(AA);
dn2ldt = det(DD)/det(AA);
dn2vdt = det(EE)/det(AA);


dx(1,1) = dTdt ;
```

```
dx(2,1) = dPdt;
dx(3,1) = dn2ldt;
dx(4,1) = dn2vdt;
```